Determining the role of fluid flow on lens biomechanics

by

Shilpa Gorla

A thesis
presented to the University of Waterloo
in fulfillment of the
thesis requirement for the degree of
Doctor of Philosophy
in
Vision Science and Biology

Waterloo, Ontario, Canada, 2026

© Shilpa Gorla 2026

Examining Committee Membership

The following served on the Examining Committee for this thesis. The decision of the Examining Committee is by majority vote.

External Examiner:	Kevin L. Schey Professor, Department of Biochemistry, Vanderbilt University
Supervisor(s):	Vivian Choh Associate Professor, School of Optometry and Vision Science, University of Waterloo
Internal Member:	William Ngo Assistant Professor, School of Optometry and Vision Science, University of Waterloo
Internal-External Member:	Robin E. Duncan Associate Professor, Kinesiology and Health Sciences, University of Waterloo
Internal Member:	Dale Martin Associate Professor, Department of Biology, University of Waterloo

Author's Declaration

This thesis consists of material all of which I authored or co-authored: see Statement of Contributions included in the thesis. This is a true copy of the thesis, including any required final revisions, as accepted by my examiners.

I understand that my thesis may be made electronically available to the public.

Statement of Contributions

I hereby declare my contributions and those of my co-author, Dr. Vivian Choh, to the research presented in this thesis:

Shilpa Gorla: Conceptualization, methodology, analysis, investigation, data curation, writing original draft, visualization

Dr. Vivian Choh: Conceptualization, funding acquisition, resources, supervision, project administration, visualization, analysis, review, and editing

Abstract

The vertebrate crystalline lens is a highly specialized, avascular, and transparent structure whose primary function is to change shape to refract incident light onto the retina. With increasing age, however, the lens undergoes progressive compaction of the fiber cells and crosslinking of the structural proteins, causing it to lose its elasticity. This age-dependent decline in lens ability to change shape is called presbyopia, an ocular condition affecting approximately 2 billion people worldwide. The lens of the eye relies on a specialized microcirculatory system (MCS) to maintain transparency, nutrient supply, and volume homeostasis in the absence of a blood supply. Given that the MCS plays an essential role in volume homeostasis and there is an age-related decline in the function of MCS, modulating the components of the MCS with agonists and antagonists offers a powerful approach to understanding the precise mechanism of presbyopia and identifying novel therapeutic targets for presbyopia. Using chickens, which can deform their lenses to induce shape changes and naturally develop age-related presbyopia, this study investigated the following objectives:

1. To determine the effect of modulators of aquaporin 0 (AQP0) and sodium-potassium ATPase (NKA) pumps on the lens biomechanics.

2. To determine whether TRPV1 and TRPV4 are present in the chicken crystalline lens and how modulating them affects lens biomechanics and protein expression.

3. To determine the temperature-dependent role of the lens microcirculatory system (MCS) in regulating lens biomechanics.

We found that the chicken model is a robust model for investigating lens biomechanical regulation by the MCS. At room temperature, modulating AQP0, water channels altered lens hydrostatic pressure, whereas NKA modulation affected biomechanics only when ionic or volume homeostasis was disturbed. Western blot analysis confirmed the presence of protein expression of both mechanosensitive TRPV1 and TRPV4 channels in chicken lens tissue, mirroring mammalian expression patterns. TRPV4 modulation altered lens biomechanics exclusively at the physiological temperatures, whereas AQP0 and NKA modulation produced no biomechanical effect at the physiological temperature, highlighting temperature-dependent regulation of the lens microcirculatory system.

Acknowledgements

I would like to extend my sincere appreciation to my supervisor, Dr. Vivian Choh, for her unwavering support throughout my doctoral journey. I am deeply grateful for her constant availability, her invaluable assistance with both my experiments and my pronunciation, and her exceptional mentorship. Thank you as well for introducing me to different cuisines and generously bringing those cheesecakes to the lab. I would also like to thank my committee members, Dr. William Ngo and Dr. Dale Martin, for their continuous evaluation of my work and constructive feedback and insights.

Special thanks go to my friend and fellow doctoral candidate, Nijani Nagaarudkumaran, for setting up and troubleshooting the Western blotting protocol before I began my experiments, which allowed my work to proceed smoothly. Thank you for being a constant pillar of support and a patient listener during stressful times and for being a wonderful research confidante. I also thank Dr. Varadharajan Jayakumar and Dr. Parvin Shokrollahi for their positive energy and encouragement during difficult moments. To my lab mates, Dr. Erica and Ashita, thank you for your seamless coordination of lab hours so efficiently and for being an absolute pleasure to work with. I would also like to thank Lina for helping me to analyze my data. Special thanks to Brie McConnell for guiding me through the figure reuse licensing process.

I would like to thank Jean Flanagan, Central Animal Facility Manager, for her vital support, efficient procurement, and timely encouragement when research became challenging. Thanks are also due to Martin, Saedeh, and Lauren for their essential assistance within the animal facility. Additionally, a special thanks to Michelle for picking up the chicken for us

whenever Viv was unavailable.

My heartfelt thanks go to my friends for their encouragement and for always being there when I needed to talk. I am especially grateful to Megala, my first friend in Canada, as well as Himanshu, Pranav, Athira, Jyoti, Asiya, Nutan, Arya, Harmehak, Manish, Sandra, Heather, Yangchen, Sadaf, Ivy, Lauren, and Cindy for their companionship and encouragement.

Above all, I am profoundly grateful to my family, especially my mother, whose continuous love and belief in me have been the foundation of my strength throughout my life.

Finally, I would like to acknowledge my research animals, the chicks, for their essential role in this project.

Dedication

This thesis is dedicated to my beloved family, whose unconditional love, sacrifices, and belief in me crossed oceans to make this dream possible. To my mother and father, who have been the quiet pillars of my strength, and to Himanshu, this milestone belongs to you all.

Table of Contents

Examining Committee Membership ii

Author's Declaration iii

Statement of Contributions iv

Abstract v

Acknowledgements vii

Dedication ix

List of Figures xv

List of Tables xix

List of Abbreviations xx

1 Introduction **1**

2 Literature review **6**

2.1 Eye 6

2.2 Crystalline Lens 9

2.2.1 Crystallins 12

2.2.2 Microcirculatory System of the Lens 14

2.2.3 Fluid Flow Theory 25

2.3 Modulators of the Microcirculatory System 28

2.3.1 Modulators of the Sodium-Potassium ATPase Pump 28

2.3.2 Modulators of the Sodium-Potassium-Chloride Cotransporter 30

2.3.3 Modulators of the Transient Receptor Potentials Vanilloids 31

2.3.4 Modulators of the Transient Receptor Potential Melastatin 3 . . . 35

2.3.5 Modulators of the Aquaporin 0 37

2.3.6 Modulators of the Aquaporin 1 38

2.3.7 Modulators of the Aquaporin 5 39

2.3.8 Modulators of the Gap Junctions 40

2.4 Aging of the Lens 41

2.5 Avian Experimental Model 44

3 The effect of modulators of aquaporin 0 and sodium-potassium ATPase pumps on chicken lens biomechanics 50

3.1 Introduction 50

3.2 Material and Methods 53

3.2.1 Experimental model and lens dissection 53

3.2.2 Lens Treatment 54

3.2.3 Biomechanical testing 55

3.2.4 Hyperosmotic Challenge and Water Permeability Assay 58

3.2.5 Statistical analysis 59

3.3 Results 60

3.4 Discussion 71

4 TRPV1 and TRPV4 presence in the chicken crystalline lens and the effect of their modulation on biomechanics and protein expression 73

4.1 Introduction 73

4.1.1 Modulators of TRPV1 and TRPV4 76

4.2 Material and Methods 78

4.2.1 Lens Treatment 79

4.2.2 Western Blot 80

4.2.3 Potassium Assay 82

4.3 Results 83

4.3.1 The effect of the modulators of TRPV1 and TRPV4 on the lens biomechanics 84

4.3.2 The effect of the modulators of TRPV4 on its protein expressions and lens' intracellular potassium levels 91

4.4 Discussion 93

5 How modulators of the lens microcirculatory system regulate lens biomechanics at physiological temperature 97

5.1 Introduction 97

5.2 Material and Methods 98

5.2.1 Lens Treatment 100

5.3 Results 101

5.3.1 The effect of temperature on the lens biomechanics 101

5.3.2 The effect of the modulators of the AQP0 and NKA pump on the lens biomechanics at physiological temperature 102

5.4 Discussion 106

6 Discussion and conclusion 109

Letter of Copyright Permission 114

References **116**

Appendix **153**

A Supplementary Data **154**

A.1 Linear relationship between coefficients 154

A.2 Coefficients of lenses 157

A.3 Force decay slope during the 5-second hold phase 177

List of Figures

2.1 Schematic diagram of functions and location of aquaporins 0, 1, 3, 5 (AQP0, AQP1, AQP3, AQP5, respectively). 22

2.2 Schematic diagram of functions and location of connexins 43, 46, 50 (Cx43, Cx46, Cx50 respectively). 25

2.3 Microcirculatory system (MCS) of the crystalline lens 27

2.4 Schematic diagram of the signaling cascade linking TRPV1 activation to NKCC1-mediated ion and fluid regulation in the lens. 33

2.5 Schematic diagram of the proposed mechanism of TRPV4-mediated sodium-potassium ATPase (NKA) pump regulation via pannexin-dependent ATP release. 34

2.6 Schematic diagram of the proposed mechanism of TRPM3-mediated sodium-potassium ATPase (NKA) pump regulation via cyclic AMP. 36

2.7 Schematic diagram of the chicken eye. AP, annular pad; CL, cavum lenticuli; LB, lens body; CP, ciliary processes; CM, ciliary muscle; P, pecten. 45

3.1 The microtester setup and experimental testing. 56

3.2 Box plots of the biomechanical responses of lenses treated with zinc (filled boxes) or vehicle (empty boxes) at room temperature. 61

3.3 Box plots of the biomechanical responses of lenses treated with Ht31 (filled boxes) or vehicle (empty boxes) at room temperature. 62

3.4 Box plots of the biomechanical responses of lenses treated with insulin (filled boxes) or vehicle (empty boxes) at room temperature. 63

3.5 Box plots of the biomechanical responses of lenses treated with a combination of zinc and insulin (filled boxes) or vehicle (empty boxes) at room temperature. 64

3.6 Box plots of the biomechanical responses of lenses treated with ouabain (filled boxes) or vehicle (empty boxes) at room temperature. 65

3.7 Box plots of the biomechanical responses of lenses treated with a combination of zinc and ouabain (filled boxes) or ouabain (empty boxes) at room temperature. 66

3.8 Box plots of the biomechanical responses of lenses treated with a combination of zinc and ouabain (filled boxes) or zinc (empty boxes) at room temperature. 67

3.9 Paired dot plots of cross-sectional area of lenses 68

3.10 Photographs of a lens exposed to **(A)** hyperosmolar conditions and **(B)** subsequent recovery in isosmolar Tyrode's solution at room temperature. . 69

3.11 Photographs of a lens exposed to **(A)** hyperosmolar conditions and **(B)** subsequent recovery in zinc solution at room temperature. 70

3.12 Paired dot plots of subcapsular gap of lenses 70

4.1 Western blot showing the presence of TRPV4 and TRPV1 protein expression in the lens tissue of different chickens, with distinct immunoreactive bands observed at approximately 98 kDa, with a secondary upper band near 100 kDa that likely corresponds to a glycosylated form of TRPV1 [Veldhuis et al., 2012] 83

4.2 Box plots of the biomechanical responses of lenses treated with GSK1016790A (filled boxes) or vehicle (empty boxes) at room temperature. 84

4.3 Box plots of the biomechanical responses of lenses treated with RN-1734 (filled boxes) or vehicle (empty boxes) at room temperature. 85

4.4 Box plots of the biomechanical responses of lenses treated with capsaicin (filled boxes) or vehicle (empty boxes) at room temperature. 86

4.5 Box plots of the biomechanical responses of lenses treated with AMG 9810 (filled boxes) or vehicle (empty boxes) at room temperature. 87

4.6 Box plots of the biomechanical responses of lenses treated with GSK1016790A (filled boxes) or vehicle (empty boxes) at physiological temperature. 88

4.7 Box plots of the biomechanical responses of lenses treated with RN-1734 (filled boxes) or vehicle (empty boxes) at physiological temperature. 89

4.8 Box plots of the biomechanical responses of lenses treated with capsaicin (filled boxes) or vehicle (empty boxes) at physiological temperature. 90

4.9 Box plots of the biomechanical responses of lenses treated with AMG 9810 (filled boxes) or vehicle (empty boxes) at physiological temperature. 91

4.10 Western blots and paired dot plots of TRPV4 protein expressions in lenses treated with a TRPV4 agonist (GSK1016790A), antagonist (RN-1734), or vehicle control 92

4.11 Paired dot plots of potassium ion concentrations in lenses treated with a TRPV4 agonist (GSK1016790A), antagonist (RN-1734), or vehicle control 93

5.1 Box plots of the biomechanical responses of lenses in Tyrode's solution at physiological (filled boxes) or room temperature (empty boxes). 102

5.2 Box plots of the biomechanical responses of lenses treated with zinc (filled boxes) or vehicle (empty boxes) at physiological temperature. 103

5.3 Box plots of the biomechanical responses of lenses treated with Ht31 (filled boxes) or vehicle (empty boxes) at physiological temperature. 104

5.4 Box plots of the biomechanical responses of lenses treated with insulin (filled boxes) or vehicle (empty boxes) at physiological temperature. 105

5.5 Box plots of the biomechanical responses of lenses treated with ouabain (filled boxes) or vehicle (empty boxes) at physiological temperature. 106

List of Tables

1.1 List of agonists and antagonists used to modulate AQP0, NKA pump, TRPV1, and TRPV4 activity 5

6.1 Summary of the biomechanical changes in the lens as indicated by the b-coefficient and resilience under room and physiological temperatures (↑ indicates increase, ↓ indicates decrease, and = indicates no change) 113

A.1 Summary of the hold-phase relaxation slopes under room and physiological temperatures (↑ indicates increase, ↓ indicates decrease, and = indicates no change) 180

List of Abbreviations

4-PBA	4-Phenylbutyrate
AKAP	A-Kinase anchoring protein
AKAP2	A-kinase anchoring protein-2
AQP	Aquaporin
ATP	Adenosine triphosphate
BCA	Bicinchoninic acid
BSA	bovine serum albumin
cAMP	cyclic AMP
CRYA	Crystallin alpha
cryo-EM	Cryo-electron microscopy
Cx	Connexin
DI	Deionized water
DMSO	dimethyl sulfoxide
ECL	Enhanced chemiluminescence
EDTA	Ethylenediaminetetraacetic acid
ERK	extracellular signal-regulated kinase

GABA-B	Gamma-aminobutyric acid type B
GAPDH	glyceraldehyde 3-phosphate dehydrogenase
GJ	Gap junction
GRIN	Gradient refractive index
H_2O_2	Hydrogen peroxide
HCl	Hydrochloric acid
HDAC	Histone deacetylases
HP	Hydrostatic pressure
HRP	Horseradish peroxidase
LGN	Lateral geniculate nucleus
Lp82	Lens-specific Calpain
MAPK	Mitogen-activated Protein kinase
MCS	Microcirculatory system
MIP	Major intrinsic polypeptide
NKA	Sodium potassium ATPase pump
NKCC	Sodium potassium chloride cotransporter
NO	Nitric oxide
NPA	Asparagine-proline-alanine
NPY	neuropeptide Y
OD	Optical density
OSR1	Oxidative stress response 1

PARs	Protease-activated receptors
PI3K	Phosphatidylinositol 3-Kinase
PKA	Protein kinase A
PKC	Protein kinase C
PKG	Protein kinase G
PP1	Protein phosphotase 1
PregS	Pregnenolone sulphate
PVDF	Polyvinylidene difluoride
RGC	Retinal ganglion cell
RIPA	Radioimmunoprecipitation assay buffer
RPC	Retinal progenitor cell
RPE	Retinal pigmented epithelium
RT	Room temperature
SFKs	Src family tyrosine kinases
SPAK	STE20-related proline-alanine-rich kinase
TBS-T	Tris-buffered saline with Tween-20
TPA	12-O-Tetradecanoylphorbol-13-acetate
TRP	Transient receptor potentials
TRPM3	Transient receptor potential melastatin 3
TRPV	Transient receptor potential vanilloid
TS	Tyrode's solution

WNK	With-no-lysine
Zn	Zinc

Chapter 1

Introduction

The crystalline lens is a biconvex transparent structure that is suspended in the eye's posterior chamber by zonular fibres, which are in turn attached to the ciliary body [Ruan et al., 2020, von Helmholtz, 1925]. When the ciliary body contracts, the zonules that hold the lens taut relax, causing the lens to become rounder and thicker; this process, called accommodation, increases the lens's optical power, allowing near objects to be focused on the retina [von Helmholtz, 1925]. The lens is made of cuboidal epithelial cells at the anterior surface, while the rest of the lens consists of lens fibre cells. The lens capsule, the basement membrane of the epithelial cells, surrounds the entire lens. The fibre cells are arranged into shells or cortices, resembling the layers of an onion. The oldest fibres, found at the centre of the lens, comprise the nucleus. The lens grows throughout life, producing new lens fibres from the subcapsular epithelial cells at the equator. These new fibres are added to the pre-existing lens cortex [Beebe et al., 1982]. Avascularity and a tight, regular arrangement of lens fibres maintain lens transparency [Duncan and Croghan, 1969] and

enable the lens to transmit light up to 1200 nm [Artigas et al., 2012, Ruan et al., 2020]. In addition, the lens requires specialized transport channels or a microcirculatory system (MCS; [Beebe, 2008, Donaldson et al., 2001, Mathias et al., 1997]) to support transparency, maintain the required constant volume, and supply nutrients to the lens fibres. The MCS consists of the Na^+/K^+-ATPase pump (NKA; [Donaldson et al., 2010, Mathias and Rae, 2004, Mathias et al., 1997]), aquaporins (AQPs; [Varadaraj et al., 2005]), gap junctions (GJs; [Donaldson et al., 2001, Donaldson et al., 2010, Vaghefi and Donaldson, 2018]), and transient receptor potential channels of the vanilloid isoform (TRPV; [Nakazawa et al., 2019, Vaghefi and Donaldson, 2018]). Additionally, sodium-potassium-chloride cotransporter 1 (NKCC1; [Giannone et al., 2021, Shahidullah et al., 2020]), transient receptor potential melastatin 3 (TRPM3; [Bennett et al., 2014, Zhou et al., 2024]), and Piezo1, a mechanosensitive ion channel [Gao et al., 2025], also play a significant role in maintaining osmotic and hydrostatic balance in the lens by regulating ion and water transport.

With increasing age, there is a gradual loss in the ability to accommodate. This reduction in the ability causes presbyopia, and it affects approximately 1.8 billion people over the age of 40 [Holden et al., 2008, Fricke et al., 2018]. At present, there is no physiological solution to permanently restore accommodation; management of presbyopia is limited to optical and surgical aids. Uncorrected or under-corrected presbyopia can lead to productivity losses in the working population. The economic burden has been estimated to be US \$11.023 billion for every 244 million cases of uncorrected or under-corrected presbyopes < 50 years of age in North America [Frick et al., 2015]. The estimated economic burden is even higher for lower-income countries [Frick, 2012].

There are many theories about why presbyopia occurs. Most mechanisms point to a loss

of lens elasticity and/or hardening as the lens ages [Weale, 1962]. The lens changes its shape and volume during accommodation and is thought to be accompanied by fluid movement and water redistribution in the lens, facilitated by the MCS [Gerometta and Candia, 2016, Gerometta et al., 2007]. A recent study reported that the lens redistributes free water in the anterior region of the lens to aid the shape change during accommodation, and there are reduced levels of free water in the anterior part of the presbyopic lenses, suggesting a role of free water and, therefore, fluid dynamics in maintaining accommodation [Lie et al., 2024]. In addition to presbyopia, the aging lens undergoes structural and biochemical changes that lead to opacities in the lens, known as cataracts [Cheng et al., 2019, Huang et al., 2005, Kinoshita, 1974, Truscott, 2005]. Cataracts are the most common cause of blindness worldwide [Delaye and Tardieu, 1983, Harding and van Heyningen, 1987, Lin et al., 2025], accounting for more than 50% of blindness cases globally [Jiang et al., 2026].

Biochemical changes of the aging lens include protein aggregation and insolubility, crystalline oxidation, and covalent cross-linking [Budnar et al., 2022, Truscott and Friedrich, 2019, Harding, 1973, Spector, 1995]. Moreover, oxidative stressors, including depletion of antioxidants such as glutathione, accumulation of free radicals, and impaired proteostasis, contribute to the pathogenesis of cataracts [Spector, 1995, Truscott and Friedrich, 2019, Lou, 2003]. Crystalline proteins and AQPs in the lens undergo age-related modification, including post-translational modification, deamidation, truncation, and oxidation, that can compromise these structural and functional capabilities of the lens, ultimately leading to cataract development [Budnar et al., 2022, Coghlan and Augusteyn, 1977, Grey et al., 2009, Lampi et al., 1998, Schey et al., 2000, Truscott, 2005, Pierscionek, 2021, Wang et al., 2025]. There is a decrease in protein levels

of connexin46 and connexin50 and a decrease in the function of TRPV in pressure regulation with age in lens fibre cells [Gao et al., 2013, Giannone et al., 2021]. Additionally, NKA activity has been shown to reduce with age, as determined by reduced ouabain (NKA-inhibitor) binding sites in aged rodent models [Clausen, 2003, Wyckelsma and McKenna, 2016], and a similar decline in NKCC protein levels has been observed in human and rat brain tissues [Dzhala et al., 2005, Gong et al., 2021]. Furthermore, increased sodium and calcium concentrations have been reported in cortical cataracts, highlighting ionic dysregulation as a key finding in lenticular aging [Adams, 1929, Duncan et al., 1991, Truscott and Augusteyn, 1977, Tamiya and Delamere, 2006].

Considering the essential role of the MCS in maintaining lens homeostasis and transparency, the modulation of its components with the help of agonists and antagonists, as shown in Table 1.1, gives a promising avenue for therapeutic intervention. So, this study aims to investigate the following:

1. To determine whether modulators of aquaporin 0 (AQP0) and sodium-potassium ATPase (NKA) pumps affect the lens biomechanics.

2. To determine whether TRPV1 and TRPV4 are present in the chicken crystalline lens and how modulating these channels affects lens biomechanics and their protein levels.

3. Given the findings from Chapters 3 and 4, how do modulators of the lens microcirculatory system (MCS) affect the lens biomechanics at physiological temperature

Table 1.1: List of agonists and antagonists used to modulate AQP0, NKA pump, TRPV1, and TRPV4 activity

Channel/target	**Agonist**	**Antagonist**
Aquaporin 0 (AQP0)	Zinc	Ht31
Sodium–potassium ATPase pump (NKA)	Insulin	Ouabain
Transient receptor potential vanilloid 1 (TRPV1)	Capsaicin	AMG 9810
Transient receptor potential vanilloid 4 (TRPV4)	GSK1016790A	RN-1734

Chapter 2

Literature review

2.1 Eye

The eye is a specialized sensory structure that captures light and enables the formation of visual images. Structural or functional differences across species give rise to visual systems with markedly diverse perceptual capabilities [Walls, 1942]. Throughout evolutionary history, this diversity has been shaped by the emergence of multiple eye types, ranging from simple light-sensitive structures to complex image-forming organs [Darwin, 1859, Nilsson, 2009]. The basic eye is made up of light-sensitive cells that act as an eyespot and have a shadow detection and light orientation function; however, these eyes are unable to create images [Land and Nilsson, 2002, Land and Nilsson, 2012]. Planarians and jellyfish are examples of organisms with basic eyes that allow them to perceive the direction of light and respond to their environment [Garm et al., 2011, Inoue et al., 2004]. Pinhole eyes are

a form of the eye seen in some mollusks, such as nautilus [Teichert and Matsumoto, 2010]. These eyes have a tiny pinhole whose narrow aperture directs light toward the retina and minimizes the blur circle. Pinhole eyes have high depth of field but very low light sensitivity [Land and Nilsson, 2012]. Compound eyes are broadly categorized into apposition and superposition designs. In apposition compound eyes, characteristic of diurnal insects such as bees, dragonflies, and flies, each ommatidium is optically isolated by proximal receptor cells surrounded by pigment cells to ensure light reaches only its individual photoreceptor cells. This individual-optics design provides high spatial resolution in bright habitats. In contrast, superposition compound eyes, common in nocturnal insects like moths and deep-sea crustaceans like krill and lobsters, utilize convergent optics, allowing light entering through multiple lenses to bend across a clear zone and converge distally onto a single underlying distal receptor cell [Land and Nilsson, 2012]. This configuration prioritizes high sensitivity in dim environments. Despite these contrasting optical strategies, both compound eye systems share exceptional temporal resolution and the capacity for rapid motion detection across a panoramic field of view [Ball, 1977, Land and Nilsson, 2012]. Alternatively, a camera eye is an optical system consisting of a single chamber in which incoming light passes through a central aperture (pupil) and is focused by a primary refractive lens or a reflective mirror array onto the retina [Land and Fernald, 1992]. Reflective camera eyes use concave arrays of guanine crystal mirrors instead of a primary refractive lens to focus light, as seen in scallops. Refractive camera eyes rely on a single lens (and often a cornea) to focus light beams directly onto the photoreceptors of the retina, a system found in both vertebrates (such as humans, birds, and fish) and cephalopods like octopuses [Young, 1801, Helmholtz, 1855, Land and Fernald, 1992]. However, focusing strategies vary significantly across species;

while humans, birds, and ungulates like cows dynamically reshape a flexible lens, teleost fish and cephalopods translate a rigid spherical lens axially, and small rodents like mice possess a large, rigid lens with negligible accommodative capability [Helmholtz, 1855, Land and Fernald, 1992, Land and Nilsson, 2012]. Among these refractive camera systems, the human eye represents a refined model of single-lens optical design.

The intricate architecture of the human eye is established during early development, commencing around the third week of embryonic life with the appearance of the optic sulcus on the lateral side of the diencephalon. This sulcus evaginates from the neuroectoderm to form the optic vesicle [His, 1880, O'Rahilly, 1975]. Contact of the optic vesicle with the overlying surface ectoderm reciprocally induces the invagination of the surface ectoderm to form the lens placode [Lewis, 1904]. Simultaneously, the optic vesicle invaginates to form a double-layer optic cup. The outer layer of the optic cup accumulates melanin to become retinal pigment epithelium (RPE). Retinal progenitor cells (RPCs) proliferate within the inner layer of the optic cup. These RPCs first differentiate into retinal ganglion cells (RGCs), horizontal cells, and cone photoreceptor cells, followed by a second generation of amacrine and bipolar cells, and the last wave of rod photoreceptors and Müller glial cells [Ramón y Cajal, 1972]. Concurrently, the anterior rim of the optic cup gives rise to the anterior and posterior pigmented epithelia of the iris, as well as the intrinsic sphincter and dilator pupillae muscles, whereas the iris stroma of the iris arises from mesenchyme derived from the neural crest cells. Similarly, the inner layer of the optic cup gives rise to the inner non-pigmented epithelium of the ciliary body, and the outer pigmented epithelium is derived from the outer layer of the optic cup. The stroma and muscles of the ciliary body are developed from neural crest cell-derived mesenchyme [Streeter, 1912].

Concurrently, around the fourth week of development, the ectodermal cells of the induced lens placode enlarge and begin to invaginate, forming a distinct lens pit. Subsequently, the lens pit pinches off the surface ectoderm, forming an isolated lens vesicle enclosed within the optic cup. Cells from the posterior wall of the lens vesicle elongate anteriorly as primary lens fibres, completely filling the central lumen of the lens vesicle. While the anterior wall of the lens vesicle remains a quiescent epithelial monolayer, cells at the equatorial region proliferate and elongate toward both poles to form the secondary lens fibres. These secondary fibres ultimately meet at the apical and basal ends by specialized junctional complexes called lens sutures. As these secondary fibres become mature, they undergo programmed organelle degradation, losing their nuclei and mitochondria, and are filled with high concentrations of specialized crystalline proteins to establish a highly transparent gradient refractive index essential for clear vision [Lewis, 1904].

2.2 Crystalline Lens

Once fully matured, the crystalline lens functions as a biconvex macroscopic transparent structure located behind the pupil and iris and in front of the vitreous body [Helmholtz, 1855]. In the adult human eye, the ciliary body maintains the lens suspended in the optic pathway by specialized ligaments known as zonular fibres [Zinn, 1755]. Structurally, the lens is enclosed by a thick, elastic basement membrane known as the lens capsule, which is rich in type IV collagen and laminin [Timpl et al., 1979]. The lens capsule serves both as a semipermeable diffusion barrier for essential ions and metabolites while also acting as an anchoring site for the zonules of the lens. Directly beneath the anterior portion of the

lens capsule lies the lens epithelium, a single layer of cuboidal cells. The epithelium of the lens is a metabolic hub for ion transport, protein synthesis, and initiation of lens fibre cell differentiation [Bassnett and Beebe, 1992]. Mirroring the cellular patterns established during embryogenesis, the adult lens fibres are continuously generated as these epithelial cells migrate toward the equator, where they differentiate, elongate, and lose their nuclei and cell organelles, and are filled with crystallin proteins as they move from the equator to the center of the lens [Kuwabara and Imaizumi, 1974, Kuwabara, 1975, Ramaekers et al., 1981].

This precise anatomical arrangement provides the structural flexibility necessary for accommodation, a dynamic physiological process in which the lens of the eye alters its refractive power to maintain a sharp, focused image on the retina as the object distance varies [Helmholtz, 1855]. Mechanically, this process is achieved by the contraction of the ciliary sphincter muscles and relaxation of the suspensory zonular fibres; this biomechanical release allows the inherent elasticity of the capsule to shape the crystalline lens, increasing its anterior-posterior thickness and steepening its central curvature [Helmholtz, 1855, von Helmholtz, 1925]. This adjustment is governed by the parasympathetic division of the autonomic nervous system through a complex reflex arc. The afferent limb of the accommodation reflex begins with the retina, where photoreceptors transduce incident photons into electrical signals [von Helmholtz, 1925, Bridgeman and Stark, 1977]. These signals are processed through the retinal inner nuclear layer and transmitted to the retinal ganglion cells, whose bundled axons exit the globe by the optic nerve, which further continues through the optic chiasm as the optic tract and projects primarily to the lateral geniculate nucleus (LGN) of the thalamus [Ramón y Cajal, 1972]. From the lateral geniculate nucleus, the optic radiation relays visual input to the primary visual cortex,

where blur detection and disparity cues are processed [Poggio and Fischer, 1977].

Once processed, the outputs from the primary visual cortex project to the visual association cortex and ultimately to the supraoculomotor area and pretectal nuclei in the midbrain, which integrate the information and initiate the motor response [Bender and Shanzer, 1964]. The supraoculomotor area provides direct, bilateral excitatory inputs to the Edinger-Westphal nucleus of the oculomotor nerve, where preganglionic parasympathetic fibres of the efferent pathway arise. These first-order neurons travel along the oculomotor nerve to synapse within the ciliary ganglion. From the ciliary ganglion, postganglionic parasympathetic fibres emerge as the short ciliary nerves to innervate the ciliary muscle, where their activation induces muscle contraction, zonular relaxation, and immediate lens thickening for near focus [Warwick, 1954, Westheimer and Blair, 1973].

Beyond lens deformation, accommodation is integrated into a near-response triad [Donders and Moore, 1864]. This coordinated triad consists of lens accommodation, binocular convergence, and pupillary constriction. Convergence is mediated by coordinated contraction of the medial rectus muscles, ensuring that both visual axes intersect at the near target, thereby minimizing binocular disparity across the foveae (central retinas) [Bridgeman and Stark, 1977, Duane, 1897]. Simultaneously, pupillary constriction is driven by parasympathetic activation of the sphincter pupillae muscle, which narrows the pupillary aperture to reduce peripheral blur circles and increases the eye's depth of focus, thereby improving retinal image quality [Helmholtz, 1855, Westheimer, 1964]. Biophysically, the crystalline lens itself behaves like a highly specialized viscoelastic structure during these rapid deformations due to the presence of internal fibre cell architecture and crystalline-rich cytoplasm, along with external mechanisms generated by the ciliary muscles and zonules

[Fisher, 1971].

2.2.1 Crystallins

The fundamental prerequisite for both the lens's physical elasticity and optical clarity is the intracellular composition of its structural units, which maintain long-term transparency and a high refractive index due to the presence of abundant water-soluble crystalline proteins [Benedek, 1971]. Crystallins make up more than 90% of the total lens protein content within the lens matrix, being expressed predominantly within the lens and also in the corneal epithelium, retina, heart and spleen [Bloemendal, 1977, Deretic et al., 1994, Srinivasan et al., 1992]. Within the mature lens, crystallins are densely packed inside highly elongated, organelle-free fibre cells, creating a highly ordered, homogeneous optical medium that exhibits minimal light scattering [Delaye and Tardieu, 1983]. Remarkably, despite the complete absence of intracellular organelles or protein turnover within the mature, differentiated fibre cells, these crystallins remain fully soluble and non-aggregated over many decades of life [Bloemendal, 1977]. However, lifelong retention of crystalline proteins without protein turnover makes them vulnerable to irreversible post-translational modifications like deamidation, oxidation, truncation, and glycation. Over time, these modifications alter protein structure and solubility, ultimately driving the formation of light-scattering macromolecular aggregates directly linked to senile cataractogenesis [Truscott, 2005].

The human lens expresses three major classes of crystallins: α-, β-, γ- Crystallins [Wistow and Piatigorsky, 1988b]. The α- crystallins (CRYA) structurally belong to the small heat shock protein superfamily and act as ATP-independent molecular chaperones

within the vertebrate lens; they bind exposed hydrophobic regions of unfolding proteins to prevent non-specific aggregation and oxidative stress. The αA-crystallin subunit (CRYAA) is highly abundant throughout the lens epithelium and outer cortex, whereas the αB-crystallin subunit (CRYAB) is highly concentrated within the fibre cells, contributing structural stability and cellular stress resilience. Additionally, α-crystallins stabilize the lenticular cytoskeleton by interacting with intermediate filaments [Ingolia and Craig, 1982, Horwitz, 1992]. The β- crystallins represent the largest and most diverse crystallins in the lens and consist of βA1-A4 and βB1-B3 subunits. They form hetero-oligomeric complexes in the lens cortex and finely tune the gradient refractive index by their ability to assemble into dimers, tetramers, and higher-order oligomers. The β- crystallins are synthesized predominantly in the differentiating outer fibre cells and remain concentrated throughout the cortex [Lampi et al., 1998]. Lastly, the γ- crystallins exist as highly stable monomeric structural proteins found abundantly in the lens nucleus. The compact monomeric configuration of γ- crystallins allows extremely compact packing, establishing the elevated refractive index of the central nucleus while ensuring long-term structural stability with minimal light scattering [Wistow and Piatigorsky, 1988b].

The spatial distribution, specialized amino acid composition characterized by a high density of polar and sulfur-containing residues, and unique packing of these crystallins within the fibre cell layers give the lens its unique optical properties, known as gradient refractive index (GRIN). This spatial gradient is generated by the differential regional distribution of crystalline proteins, progressive fibre cell compaction, and localized variation in relative water content in the lens. Functionally, the GRIN profile allows the lens to refract and bend incident light beams smoothly and continuously throughout its

internal volume, rather than refracting light exclusively at its outer surfaces, thereby enhancing the eye's refractive power [Pierscionek and Regini, 2012]. Optically, the GRIN profile increases from the refractive index of approximately 1.36-1.38 within the outer superficial cortex to a maximum peak of approximately 1.40-1.41 within the dense central nucleus [Pierscionek and Chan, 1989, Pierscionek and Regini, 2012]. In a homogeneous lens, lacking a GRIN profile, peripheral rays would undergo stronger refraction and focus at shorter focal lengths than central rays, producing a positive spherical aberration [Campbell and Gubisch, 1966, Brown, 1974]. However, the natural GRIN profile of the crystalline lens counters this distortion because the refractive index is highest at the central nucleus and decreases smoothly toward the cortex. Consequently, central rays passing through the dense nucleus are refracted more strongly relative to peripheral rays, reducing spherical aberration and delivering a sharply focused image onto the retinal photoreceptors [Sivak and Kreuzer, 1983, Pierscionek and Chan, 1989].

2.2.2 Microcirculatory System of the Lens

Avascularity and a tight, regular arrangement of lens fibres maintain lens transparency [Duncan and Croghan, 1969] and allow the lens to transmit light up to a wavelength of 1200 nm [Artigas et al., 2012, Ruan et al., 2020]. In addition, the lens requires specialized transport channels or a microcirculatory system (MCS; [Beebe, 2008, Donaldson et al., 2001, Mathias et al., 1997]) to support transparency, maintain a constant required volume, and supply nutrients to the lens fibres. The MCS consists of the Na^+/K^+-ATPase pump (NKA; [Donaldson et al., 2010, Mathias and Rae, 2004,

Mathias et al., 1997]), aquaporins (AQPs; [Varadaraj et al., 2005]), gap junctions (GJs; [Donaldson et al., 2001, Donaldson et al., 2010, Vaghefi and Donaldson, 2018]), and transient receptor potential channels of the vanilloid isoform (TRPVs; [Nakazawa et al., 2019, Vaghefi and Donaldson, 2018]). Additionally, sodium-potassium-chloride cotransporter 1 (NKCC1; [Giannone et al., 2021, Shahidullah et al., 2020]), transient receptor potential melastatin 3 (TRPM3; [Bennett et al., 2014, Zhou et al., 2024]), and Piezo1, a mechanosensitive ion channel [Gao et al., 2025], also play a significant role in maintaining osmotic and hydrostatic balance in the lens by regulating ion and water transport.

NKA is a transmembrane enzyme that regulates the concentrations of sodium and potassium ions across the cell membrane [Fedosova et al., 2021, SKOU, 1957]. It transports sodium ions out of the cell against their electrochemical gradient. This movement of sodium ions out of the cell is coupled with the intake of potassium ions, typically in a ratio where three sodium ions are expelled for every two potassium ions brought into the cell [Glynn, 1957, Sweadner and Goldin, 1980, Wallick et al., 1979]. NKA consists of catalytic α and noncatalytic β subunits [Shull et al., 1986]. The α subunit has a molecular weight of approximately 110 kDa with 4 isoforms. The structure of NKA consists of 10 transmembrane spans, 5 extracellular loops, 4 intracellular loops, and cytoplasmic N- and C-termini [Morth et al., 2007]. The β subunit is smaller, with a variable molecular weight of 35-55 kDa and 3 isoforms. The structure of the β subunit consists of a single transmembrane segment, a longer extracellular C-terminus, and a shorter cytoplasmic N-terminus [Geering, 2001, Kaplan, 2002]. The N-terminus of the α subunit provides a site for sodium translocation [SKOU, 1957, Wang et al., 1996, Zaytseva et al., 2024]. The β subunit does not have any catalytic role but participates in the proper folding of the

α subunit and helps in the successful translocation of the α subunit to the plasma membrane [DeTomaso et al., 1994, Hilbers et al., 2016, Clausen et al., 2017]. There are species-specific and tissue-specific distributions of NKA isoforms [Delamere and Tamiya, 2004, Fambrough et al., 1994, Geering, 2001]. NKA is distributed both in fibre cells and the epithelium of the lens; however, its activity is substantially higher in the epithelium compared to the fibre cells, with maximal activity at the equatorial epithelium compared to the anterior pole [Delamere and Dean, 1993, Garner and Kong, 1999, Unakar and Tsui, 1980]. NKA maintains the sodium and potassium ion concentrations and cellular osmolarity in the lens; dysfunction of the NKA can lead to lens opacification [Delamere and Tamiya, 2009]. NKA is also associated with cell differentiation from equatorial epithelial cells to fibre cells by providing potassium ions for the elongation of the cells [Beebe et al., 1982, Parmelee and Beebe, 1988]. Sodium concentrations increase in aged lenses and can lead to cataractogenesis due to a decrease in the activity of NKA to hydrolyze ATP and transport ions [Delamere and Tamiya, 2004, Duncan and Bushell, 1975, Takemoto et al., 1982].

The cation-chloride cotransporters represent an important family of membrane transport proteins [Gamba et al., 1994, Hartmann et al., 2014] that play an essential role in various physiological processes, such as regulating cell volume, transepithelial transport, and modulation of neuronal excitability [Hebert et al., 2004]. These channels mediate the electroneutral movement of chloride ions alongside sodium and potassium ions across the plasma membrane of both epithelial and neuronal cells [Crewther et al., 2008, Russell, 2000]. Members of this family include the sodium-potassium-chloride cotransporter (NKCC; [Delamere and Shahidullah, 2021, Russell, 2000]). NKCC is expressed in two isoforms in the body: NKCC1 and NKCC2. NKCC2 is exclusively present in the kidney and

not found in the lens [Nielsen et al., 1998, Chee et al., 2010], while NKCC1 is widely distributed in the body as well as in the epithelium of the human, rabbit, and rat lenses [Lauf et al., 2008, Alvarez et al., 2001, Chee et al., 2010]. NKCC1 has a role in maintaining lens ionic homeostasis and transparency [Chee et al., 2010, Mandal et al., 2018]. The structure of NKCC1 consists of 12 transmembrane helices with 1205 amino acids and cytoplasmic N- and C-domains. The N-terminus contains key threonine residues that serve as regulatory phosphorylation sites. Phosphorylation of these sites activates the cotransporter and is governed by a well-established kinase cascade involving with-no-lysine (WNK), serine/threonine protein kinase STE20-related proline-alanine-rich kinase (SPAK), and oxidative stress response 1 (OSR1) [Dowd and Forbush, 2003, Piechotta et al., 2002, Vitari et al., 2006]. Once the cellular ion levels are maintained, NKCC1 is dephosphorylated by protein phosphatase 1 (PP1; [Darman et al., 2001]). NKCC1 also plays a key role in regulating cell volumes by increasing sodium ion inflow in the lens; it counteracts the shrinkage effect of the ouabain-sensitive NKA pump [Geck et al., 1980].

Transient receptor potential (TRP) channels are members of the specialized receptors that respond to a wide range of physical and chemical stimuli [Montell and Rubin, 1989]. TRP channels have a tetrameric structure with six transmembrane helices and cytoplasmic C- and N-ends [Clapham, 2003, Delamere et al., 2020, Liao et al., 2013, Liedtke and Heller, 2007, Zhang et al., 2023]. Around 7 subfamilies of TRP channels have been identified [Clapham, 2003, Zhang et al., 2023]. However, in various species, including humans, the lens only expresses two members of the TRP subfamily: transient receptor potential vanilloid (TRPV1 and TRPV4; [Mandal et al., 2018, Shahidullah et al., 2012b]) and transient receptor potential melastatin (TRPM3; [Bennett et al., 2014, Clapham, 2003]).

TRPV1 is a non-selective cation channel composed of 839 amino acids and plays a role in thermoregulation in skin [Caterina et al., 1997, Tominaga et al., 1998]. It has been shown that in porcine and human lenses, TRPV1 is only expressed in the epithelial cells; TRPV1 is activated in response to a hyperosmotic challenge and leads to a transient increase in the activity of NKCC1 [Shahidullah et al., 2018, Shahidullah et al., 2020, Mandal et al., 2018]. TRPV4 regulates cell volume in response to various stimuli like temperature, chemicals, and osmotic and mechanical changes [Clapham, 2003, Liedtke et al., 2000, White et al., 2016]. The TRPV4 structure is composed of 871 amino acids [Garcia-Elias et al., 2014]. In human skin keratinocyte cell lines exposed to hypo-osmotic stress, TRPV4 regulates cell volume by enabling the influx of calcium ions, therefore reducing cell swelling [Becker et al., 2005]. It has also been demonstrated that TRPV4 activates when there is a hypo-osmotic challenge, which further triggers a transient increase in Na-K-ATPase activity [Shahidullah et al., 2012a]. It is reported that failure in homeostasis by TRPVs in the lens may lead to cataract formation [Shahidullah et al., 2012a, Shahidullah et al., 2012b]. TRPM3 is a heat-sensitive, non-selective cation channel [Grimm et al., 2003, Vriens et al., 2011], and full-length TRPM3 consists of 1744 amino acids [Shiels, 2020]. TRPM3 is expressed in lens epithelial cells and indirectly regulates the NKA by affecting ion homeostasis in the lens by regulating calcium influx. The mutation of TRPM3 has been shown to disrupt calcium influx in the lens and lead to cataract formation [Bennett et al., 2014, Zhou et al., 2024]. In addition to TRP, the mechanosensitive channel Piezo1 is expressed in the lens epithelium, where its activation triggers calcium influx and subsequently stimulates NKA pump activity. Piezo1 functions as a more sensitive mechanosensor than TRPV4 [Shahidullah et al., 2022, Gao et al., 2025].

Aquaporins (AQPs) are membrane-bound water channels that facilitate the rapid and efficient movement of water [Heymann and Engel, 1999, Preston et al., 1992] and small molecules such as glycerol, urea, and hydrogen peroxide (H_2O_2) [Li and Wang, 2014, Tsukaguchi et al., 1998] across the cell membrane. Thus far, 13 isoforms of the AQPs have been identified in mammalian cells. AQPs are quite diverse and have been identified in various tissues of the body [Agre et al., 1993, Schey et al., 2022]. All AQPs have a similar molecular structure with a single chain of ∼260 amino acids, six transmembrane loops, intracellular N- and C-termini, and two asparagine-proline-alanine (NPA) motifs [Preston et al., 1993]. Two NPA motifs come together within the channel to form a pore that is crucial for the movement of water through AQP channels [Murata et al., 2000]. AQPs are present as a tetramer in the cell membrane [Preston et al., 1993, Verbavatz et al., 1993]. Six isoforms of AQPs are found in the lens: AQP0, AQP1, AQP3, AQP5, AQP7, and AQP8 (Fig. 2.1) [Gao et al., 2015, Schey et al., 2022, Schey et al., 2017, Petrova et al., 2024].

AQP0, or major intrinsic polypeptide (MIP), is predominantly expressed in the lens fibre cells and comprises a major proportion (∼50%) of the plasma membrane [Bloemendal et al., 1972, Fitzgerald et al., 1983, Bok et al., 1982]. In cortical fibre cells, AQP0 also has a subcellular distribution; however, during nuclear and organelle degradation in the differentiating fibre cells, AQP0 aggregates as a large plaque-like structure in the cell membrane [Lo et al., 2014, Petrova et al., 2015]. Although AQP0 is a poor water channel [Saboe et al., 2017, Jensen et al., 2008], it is the most prevalent aquaporin in the lens and is responsible for 80% of the lens' water permeability [Grey et al., 2009, Varadaraj et al., 2005]. AQP0 maintains water homeostasis and lens transparency, and mutations in AQP0 channels lead to cataracts [Berry et al., 2000,

Ruiz-Ederra and Verkman, 2006, Tang et al., 2021]. Towards the lens cortex, AQP0 acts as a water channel; however, in the lens nucleus, AQP0 shows cell adhesion properties, which are essential to maintain the minimum gap between the lens fibres that contributes to lens transparency [Kumari and Varadaraj, 2009, Li et al., 2022]. Besides acting as water channels and cell adhesion molecules, AQP0 also plays a role in suture formation and provides structural support to the lens fibres by interacting with intermediate filaments [Al-Ghoul et al., 2003, Lindsey Rose et al., 2006]. Phosphorylation of AQP0 plays a key role in regulating its water-channel permeability [Németh-Cahalan and Hall, 2000]. Protein kinase A (PKA), with the help of the A-kinase anchoring protein-2 (AKAP2), binds to and phosphorylates AQP0 [Gold et al., 2012]. Phosphorylation of AQP0 prevents the interaction between AQP0 and calmodulin. Calmodulin binds to the AQP0 C-terminal and reduces the water permeability of the AQP0 [Gold et al., 2012, Kreida et al., 2024, Reichow and Gonen, 2008, Reichow et al., 2013]. Detachment of the PKA from the AKAP2-AQP0 complex is associated with loss of lens transparency [Gold et al., 2012]. Additionally, protein kinase C (PKC)-induced phosphorylation of AQP0 at serine 235 facilitates its translocation from the cytoplasm to the plasma membrane of the lens epithelial cells [Golestaneh et al., 2008]

In the lens, AQP1 is expressed only in lens epithelial cells and plays a role in maintaining lens transparency [Ruiz-Ederra and Verkman, 2006]. There is a change in the distribution of AQP1 as the lens ages; it is present in the central epithelium of younger lenses and in the equatorial and central epithelia of older lenses [Lo et al., 2020]. The importance of AQP1 in maintaining lens transparency and regulating water content is demonstrated by studies showing that in cataractous lenses, AQP1 protein expression is increased, leading to

recovery of transparency of the lens [Barandika et al., 2016]. In contrast, AQP1-knockout mice show lens opacification and loss of epithelial water permeability [Hua et al., 2019, Ruiz-Ederra and Verkman, 2006].

AQP5 is a membrane protein and contributes to only a small percentage (∼0.36%) of the lens proteins [Schey et al., 2022]. It is primarily detected in the cytoplasm of epithelial and young cortical-maturing cells; however, in the lens nucleus, its expression is limited to the cell membrane [Petrova et al., 2015]. In the young cortical fibre cells, autophagy and mitochondrial markers colocalize with AQP5, suggesting AQP5 insertion into the cell membrane is associated with the autolysosomal pathway [Gletten et al., 2022, Grey et al., 2013]. A recent study reported that AQP5 changes its location according to the mechanical changes within the lens; specifically, when zonular tension decreases in the lens, AQP5 internalizes from the membrane to the cytoplasm, resulting in reduced water permeability of the AQP5 [Petrova et al., 2023]. Phosphorylation is essential in the internalization of AQP5, as AQP5 contains two consensus protein kinase A/protein kinase G-activated (PKA/PKG) phosphorylation motifs [Kumari et al., 2012]. AQP5 is highly permeable to water, with 20 times more water permeability than AQP0 and 18.5% water permeability of lens fibres [Kumari et al., 2012, Petrova et al., 2018, Sindhu Kumari and Varadaraj, 2013, Tang et al., 2021]. AQP5 functions include regulating osmotic balance and maintaining lens transparency [Sindhu Kumari and Varadaraj, 2013, Tang et al., 2021]. In addition to its role in water transport, AQP5 has been found to facilitate transmembrane transport of hydrogen peroxide (H_2O_2) and maintain the redox balance of the lens. Knockout of AQP5 has been shown to cause a cataractous lens in mice, possibly exacerbated by significant H_2O_2 accumulation in the lens [Sindhu Kumari and Varadaraj, 2013, Varadaraj and Kumari, 2020].

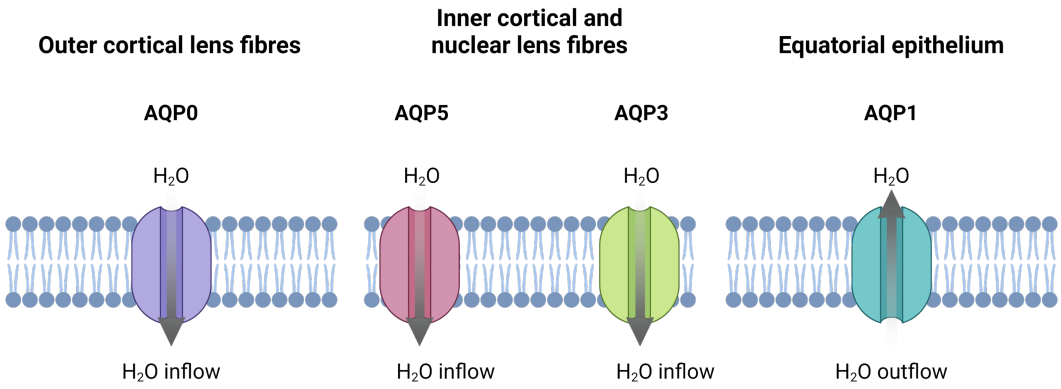


Figure 2.1: Schematic diagram of functions and location of aquaporins 0, 1, 3, 5 (AQP0, AQP1, AQP3, AQP5, respectively).

Three addional AQPs are present in the lens: AQP3 [Petrova et al., 2024], AQP7 [Tran et al., 2013] and AQP8 [Hayashi et al., 2017]. AQP3 exhibits a dual localization profile: within the cytoplasm of the epithelial cells and outer cortical fibre cells, while embedded in the membrane of inner cortical and nuclear fibre cells. Functionally, AQP3 facilitates the transmembrane transport of water, glycerol, and H_2O_2, with a cellular location and water permeability profile comparable to AQP5 [Petrova et al., 2024]. Both AQP7 and AQP8 are expressed in the lens epithelial cells [Tran et al., 2013, Hayashi et al., 2017]. Although the precise role of AQP7 in the lens is not well-known, it can transport glycerol, water, and urea in male and female reproductive organs, kidneys, brain, skeletal muscles, heart, and intestines [Ishibashi et al., 1997a, Sohara et al., 2009]. AQP8 is also expressed in several body systems, such as the urinary, digestive, respiratory, and male reproductive systems [Ishibashi et al., 1997b, Takata et al., 2004]. AQP8 acts as a peroxiporin, which

allows the transport of H_2O_2 and urea across the cell membrane [Bienert et al., 2007, Ma et al., 1997]. AQP8 has been shown to prevent H_2O_2 toxicity and maintain lens transparency [Krüger et al., 2021, Varadaraj and Kumari, 2020].

Gap junctions (GJs) are specialized intercellular connections that facilitate the direct communication between the cytoplasm of neighboring cells [Revel and Karnovsky, 1967]. In vertebrates, GJs consist of integral proteins called connexins, and each connexin has four transmembrane domains, two extracellular loops, and cytoplasmic N and C termini [Evans and Martin, 2002]. A single connexin unit located on one plasma membrane of a cell is termed a connexin; multiple connexins oligomerize to form a connexon or hemichannel. Adjacent connexons from neighboring cells align to form a complete GJ [Jagielnicki et al., 2024, Revel and Karnovsky, 1967]. GJs have been shown to play an essential role in the MCS, maintaining intercellular fluid flow in the lens and providing metabolic and ionic balance between the lenticular cells [Gao et al., 2011, Goodenough, 1979]. GJs play an essential role in maintaining the hydrostatic pressure and the transparency of the lens [Gao et al., 2011, Mathias et al., 2007]. In the mammalian lens, three connexin (Cx) proteins are present (Fig. 2.2): connexin 43 (Cx43), connexin 46 (Cx46), and connexin 50 (Cx50). Cx43 is present in the epithelial cells and in newly differentiating fibre cells, where it maintains epithelial cell-cell communication. Cx46 connects cortical differentiating cells, and Cx50 is present in both lens epithelial and fibre cells [Berthoud and Ngezahayo, 2017, Gao et al., 2011, Mathias et al., 2007, Paul et al., 1991]. Cx50 plays an essential role in lens development, including lens fibre differentiation and elongation [DeRosa et al., 2005, Xia et al., 2006]. Knockout of Cx50 molecules results in impaired lens development [Goodenough and Paul, 2003, White et al., 1998]. Additionally,

Cx50 has cell adhesion properties, and it is the only connexin in the lens that interacts with AQP0. The adhesion properties of Cx50 are crucial for epithelial-to-fibre cell differentiation; mutation of the second extracellular loop on the Cx50 molecule disrupts the differentiation process [Hu et al., 2017]. Studies have shown that mutation of Cx46 and Cx50 is associated with congenital cataract formation [DeRosa et al., 2005, Thomas et al., 2008]. Cx46 is essential for maintaining calcium balance in the lens. Disruption of these junctions leads to calcium accumulation, activating lens-specific calpain (Lp82), a calcium-activated protease, and triggering α crystallin cleavage and aggregation, ultimately resulting in cataract formation [Baruch et al., 2001, Gong et al., 1997]. Berthoud and Ngezahayo (2017) reported that Cx43 downregulation does not significantly impact lens function and clarity because of the lens's compensatory mechanism by other connexins to maintain lens gap junction communication [Berthoud and Ngezahayo, 2017].

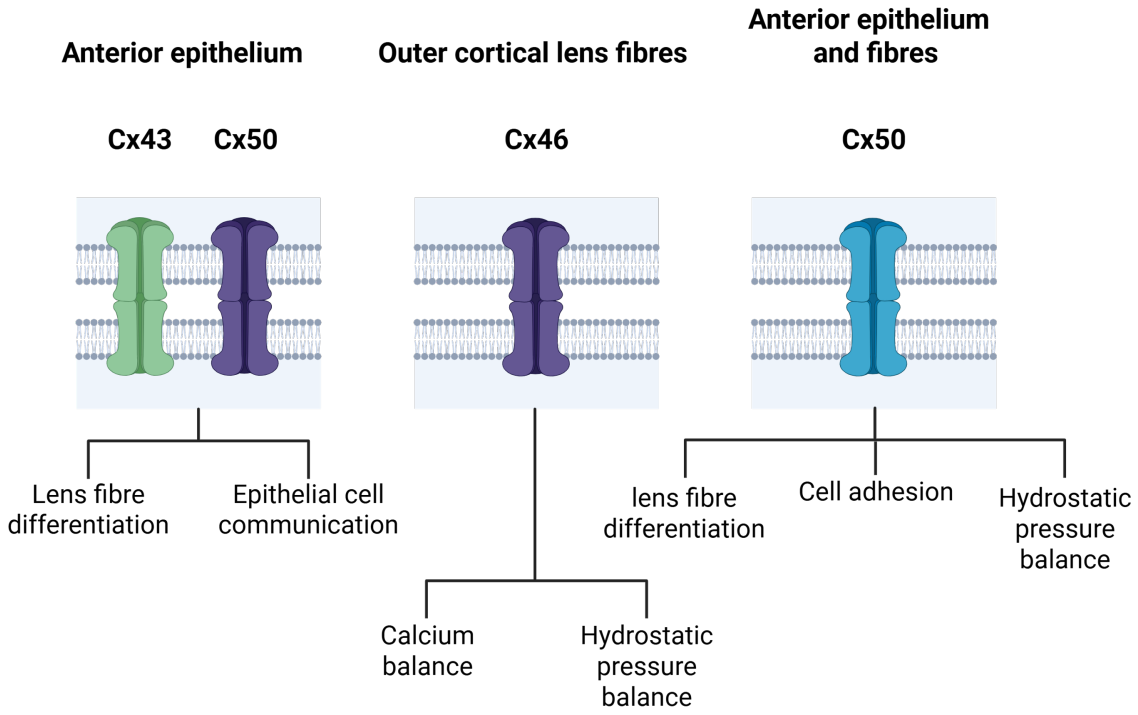


Figure 2.2: Schematic diagram of functions and location of connexins 43, 46, 50 (Cx43, Cx46, Cx50 respectively).

2.2.3 Fluid Flow Theory

The ionic current radiator model (Fig. 2.3) for bringing ions to the center of the lens involves sodium ions entering the lens at the anterior and posterior sutures. These ions are taken up by the lens fibre cells in the cortex through simple diffusion [Donaldson et al., 2001, Mathias et al., 1997, Donaldson et al., 2017]. Once inside, they are further circulated within the lens fibres by Cx46 and Cx50 gap junction channels towards the lens equator, where they are actively transported out of the lens by the

NKA pumps concentrated at the equator [Donaldson et al., 2010, Donaldson et al., 2001]. The active pumping of sodium ions at the equator creates an osmotic gradient and facilitates an isotonic flow of water and other nutrients through the lens, aided by AQPs [Donaldson et al., 2001, Gao et al., 2015].

AQP0 mediates the influx of water in the lens fibre cells [Schey et al., 2017], AQP1, which is located on the lens epithelium, regulates the outflow of the water from the lens [Ruiz-Ederra and Verkman, 2006], and AQP5, a regulated water channel that is present in both the lens epithelium and fibre cells, regulates both the influx and efflux of the water in the lens [Petrova et al., 2023]. There is a large hydrostatic pressure (HP) gradient in the lens; in the surface cells, the HP is 0 mmHg; however, in the central lens fibre cells, it is approximately 340 mmHg [Gao et al., 2011, Gao et al., 2015]. To maintain this HP gradient homeostasis, surface-localized TRPV1 and TRPV4 channels act as key sensors monitoring local pressure and osmolarity changes, providing a feedback mechanism to regulate ion transport and fluid movement. When there is an increase in the surface HP ($> 0\,\text{mmHg}$), TRPV4 on the lens surface senses this change and activates a cascade of transporters, which in turn stimulates NKA. The result is a transient increase in the pumping of sodium at the equator. Due to sodium pumping from the lens, intracellular osmolarity decreases, which further increases water outflow and restores the surface HP to 0 mmHg. In contrast, if the surface HP decreases ($< 0\,\text{mmHg}$), TRPV1 is activated, which further activates NKCC1. The activation of NKCC1 increases the influx of sodium, potassium, and chloride ions, which further increases intracellular osmolarity and decreases water outflow, bringing the surface HP back to normal to 0 mmHg [Delamere et al., 2020, Gao et al., 2015, Shahidullah et al., 2020].

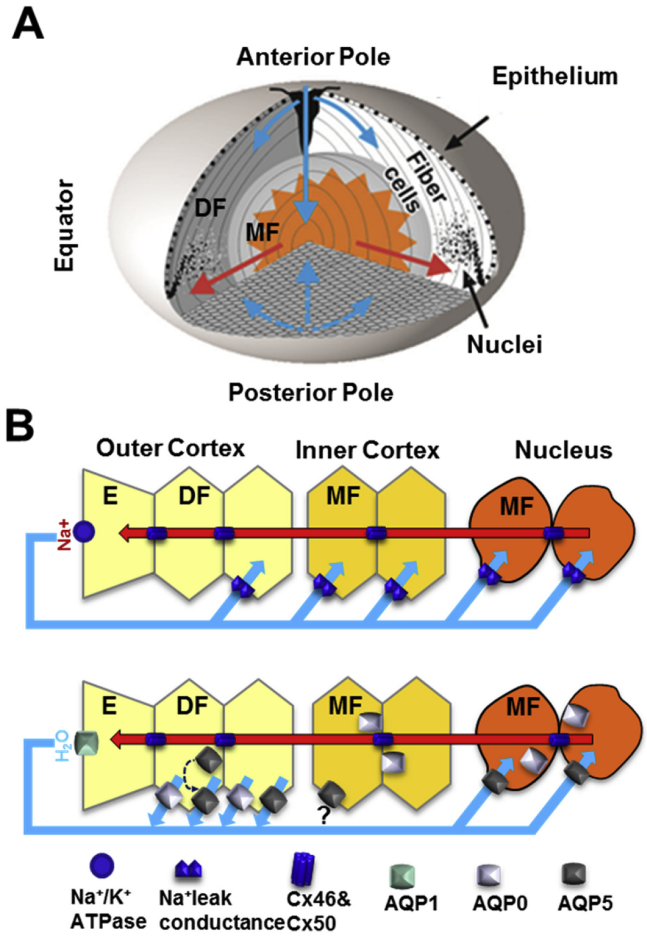


Figure 2.3: **(A)** Microcirculatory system (MCS) of the crystalline lens showing how ions and other nutrients enter the lens at the anterior and posterior poles (blue arrows), and exit the lens at the equator (red arrows). **(B)** A cross-sectional view at the equator showing the different components of the MCS regulating the fluid flow in the lens. The upper diagram shows the transport of sodium ions out of the lens via the sodium-potassium ATPase pumps at the equator. The bottom diagram shows how water and other nutrients exit the lens through aquaporins (AQPs) and gap junctions (Cx46 and Cx50) driven by the sodium ion outflow. DF = differentiating fibres, MF = mature fibres, E = equator. Adapted from Donaldson et al. (2017) with permission [Donaldson et al., 2017].

.

2.3 Modulators of the Microcirculatory System

Although the microcirculatory system (MCS) plays an essential role in regulating lens hydration and transparency, modulators of MCS have not been systematically explored as therapeutic targets. Given this gap, exploring modulators of MCS components may offer a new class of lens-softening interventions.

2.3.1 Modulators of the Sodium-Potassium ATPase Pump

Insulin is a well-known peptide hormone essential for glucose and ion homeostasis across the plasma membrane and has various other physiological roles in cellular growth and metabolism [Pirkmajer and Chibalin, 2016, Saltiel and Kahn, 2001]. Insulin facilitates the movement of sodium ions out of the cells and draws potassium ions into them across various body tissues [Moore, 1983]. In the corneal endothelium, insulin is also reported to promote DNA synthesis and cell proliferation [Feldman et al., 1993]. Insulin has been shown to enhance the activity of Na^+/K^+-ATPase pump (NKA) in uterine endometrial epithelial cells [Deachapunya et al., 1999] and corneal endothelial cells [Hatou et al., 2010]. Insulin increases the activity of the NKA by enhancing the phosphorylation of the α_1-subunit of NKA [Sweeney et al., 2001] with the help of protein kinases C and A [Hatou et al., 2010]. This phosphorylation further elevates the pump's efficiency to pump ions across the membrane [Hatou, 2011, Hatou et al., 2010]. Additionally, insulin stabilizes the sodium-potassium pump on the plasma membrane by preventing its degradation by ubiquitin and autophagy-lysosomal pathways [Wen and Wan, 2021] and also increases the presence of the α_1-subunit on the cell surface of corneal endothelial cells [Hatou et al., 2010]. Catecholamines, such as

epinephrine, norepinephrine, and dopamine, can also increase the activity of NKA by activating β-adrenergic receptors, increasing cyclic adenosine monophosphate (cAMP) and protein kinase A (PKA) activity. PKA further phosphorylates α_1-subunit of NKA, which increases NKA turnover and transport function [McKenna et al., 2024, Therien and Blostein, 2000]. Some studies suggested that nitric oxide (NO) can enhance NKA activity in skeletal muscle through pathways involving protein kinase G and protein kinase A, which phosphorylate NKA and increase NKA enzymatic activity and membrane localization [Pirkmajer and Chibalin, 2016].

Ouabain is a cardiac glycoside used to treat various heart conditions, such as congestive heart failure and tachycardia. It inhibits the sodium-potassium pumps' ATPase activity and disturbs the concentration of sodium ions in the lens, leading to cataract formation [Albal et al., 1987, Bonting et al., 1963, Murphy and Crewther, 2013, Møller et al., 1990, Prassas and Diamandis, 2008]. Ouabain binds to the extracellular domain of the α subunit with a high affinity [Bonting et al., 1963, Cornelius and Mahmmoud, 2009]. The binding results in conformational changes in the NKA structure and increases the activity of src kinase, a non-receptor tyrosine kinase, which further activates mitogen-activated protein kinase (MAPK; [Cornelius and Mahmmoud, 2009, Feldmann et al., 2007]). The activation of the MAPK leads to internalization of the NKA and thereby reduces its expression to the plasma membrane [Hodeify et al., 2024]. Ouabain can induce cellular changes such as cell detachment, swelling, and vacuole formation in the lens fibres [Pellegrino de Iraldi et al., 2003, Takemoto et al., 1982]. Ouabain has also been shown to translocate β-catenin, a cell-adhering molecule, to the cell's nucleus, disrupting cellular adhesion [Contreras et al., 1999]. Furthermore, ouabain increases the aqueous humor outflow

by inhibiting the sodium-potassium pump activity and changing the cytoskeleton of the trabecular meshwork [Dismuke et al., 2009]. Thrombin is a serine protease involved in the process of blood clotting and maintaining homeostasis [Andrews et al., 1997]. Thrombin has been shown to increase intracellular sodium ion concentration, possibly by inhibiting the activity of NKA in human platelet cells [Borin and Siffert, 1991]. In porcine lens epithelial cells, thrombin has been shown to reduce the activity of the NKA by binding to protease-activated receptors (PARs) on the lens epithelial cells. This binding further activates non-receptor tyrosine kinases and phosphorylates NKA, resulting in a decrease in NKA pump enzymatic activity [Okafor et al., 1999].

2.3.2 Modulators of the Sodium-Potassium-Chloride Cotransporter

Forskolin is a natural compound derived from a medicinal plant [Chen and Wu, 2023], and it activates adenylyl cyclase, which in turn catalyzes the conversion of adenosine triphosphate cyclic adenosine monophosphate (cAMP) and leads to increases in cAMP levels intracellularly. The elevated cAMP levels, in turn, activate protein kinase A (PKA). PKA further phosphorylates two threonine residues on the N-terminus of the NKCC1 and leads to NKCC1 activation and reabsorption of chloride ions [Flemmer et al., 2010, Lytle and Forbush, 1992, Lytle and Forbush, 1996]. Additionally, forskolin has also been shown to increase the protein expression of NKCC1 in intestinal epithelial cells via the cAMP pathway [D'Andrea et al., 1996]. Isoproterenol, a β-adrenergic receptor agonist, has been shown to increase potassium uptake by activating

the NKCC1 in the skeletal muscles of rats. It binds to β-adrenergic receptors on muscle cells, which activate the mitogen-activated protein kinase/extracellular signal-regulated kinase (MAPK/ERK) phosphorylation pathway, which is essential for NKCC activation [Gosmanov and Thomason, 2002].

Bumetanide and furosemide, commonly used as diuretics, are known inhibitors of NKCC [Crewther et al., 2008, Geck et al., 1980]. They bind to the chloride-binding site on NKCC by competitive inhibition, and this binding disrupts the reabsorption of the sodium, chloride, and potassium ions and overall ionic homeostasis [O'Grady et al., 1987]. The inhibition of NKCC1 by bumetanide prevents the accumulation of chloride ions intracellularly and reduces neuron excitability [Dzhala et al., 2008]. Furosemide, which has been reported to be beneficial in hypertension and edema, is also a competitive inhibitor; it acts by decreasing the NKCC-mediated potassium influx and thereby reducing the intracellular potassium accumulation [Geck et al., 1980].

2.3.3 Modulators of the Transient Receptor Potentials Vanilloids

Capsaicin is a plant-derived compound that gives chilli peppers their characteristic feeling of heat and has long been known to act on the TRPV1 receptor [Braga Ferreira et al., 2020, Caterina et al., 1997]. Application of capsaicin activates TRPV1 by binding to a hydrophobic pocket, stabilizes the open state of the TRPV1 channel, and allows for the influx of calcium ions. This elevation of intracellular calcium activates calcium-dependent kinases such as PKC, ERK1/2 and WNK, which subsequently phosphorylate and activate NKCC1, increasing the hydrostatic pressure within the lens (Fig. 2.4)

[Shahidullah et al., 2020, Yang and Zheng, 2017]. Magnesium ions and low pH have been shown to potentiate the activation of the TRPV1 channel by lowering the temperature threshold needed for channel opening [Tominaga et al., 1998, Yang et al., 2014]. A889425 is a synthetic small-molecule drug and competitive antagonist of TRPV1, which binds to the vanilloid-binding pocket of TRPV1, preventing the conformational changes required for TRPV1 channel opening and therefore also preventing the calcium influx and the downstream signaling pathway [McArthur et al., 2019, Zhai et al., 2020]. A889425's strong antagonist effect has been demonstrated by its ability to eliminate capsaicin-induced hydrostatic pressure changes in the bovine lens [Chen et al., 2022], as well as to reduce capsaicin-mediated pain effects from various tissues in animal models [Mandal et al., 2018, McGaraughty et al., 2008, Shahidullah et al., 2020].

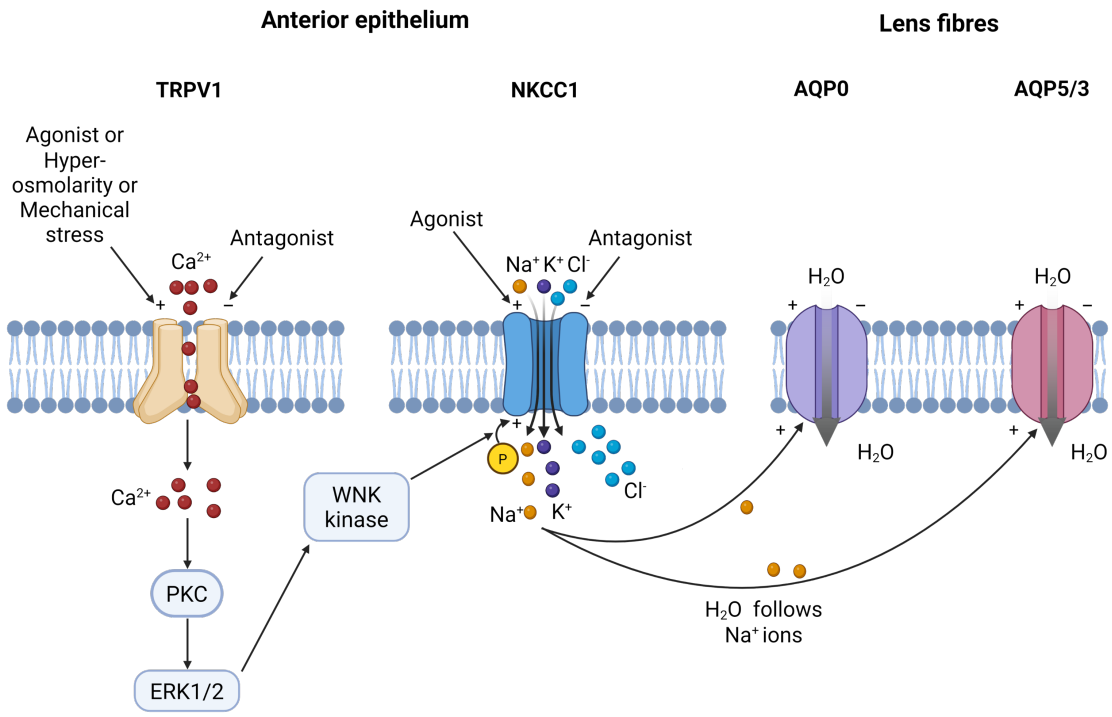


Figure 2.4: Schematic diagram of the signaling cascade linking TRPV1 activation to NKCC1-mediated ion and fluid regulation in the lens.

GSK1016790A is a synthetic compound by GlaxoSmithKline and a potent and selective agonist of TRPV4, which causes an influx of calcium into the cell. This calcium influx activates calcium/calmodulin-dependent protein kinase II (CaMKII). Active CaMKII triggers the opening of pannexin hemichannels by phosphorylation, leading to ATP release [Mihara et al., 2011]. This released ATP then activates NKA(Fig. 2.5) [Shahidullah et al., 2012a]. Hypo-osmotic conditions that typically lead to fluid build-up in the lens can activate mechanosensitive TRPV4 channels, also leading to the re-

lease of ATP from the lens, in the same manner as with GSK1016790A, i.e., through increased hemichannel opening. This mechanism is elucidated by a study, using the hemichannel inhibitors 18 α- glycyrrhetinic acid and probenecid, resulting in suppression of ATP release [Shahidullah et al., 2012a]. RN-1734 and HC 067047 are selective and synthetic antagonists of TRPV4 channels that prevent the release of ATP from hemichannels, even in the presence of stimuli like hypo-osmotic stress or agonists like GSK1016790A [Shahidullah et al., 2012a]. In porcine lens epithelial cells, both RN-1734 and HC 067047 have been shown to prevent TRPV4-mediated ATP release, resulting in reduced NKA activity [Shahidullah et al., 2012b].

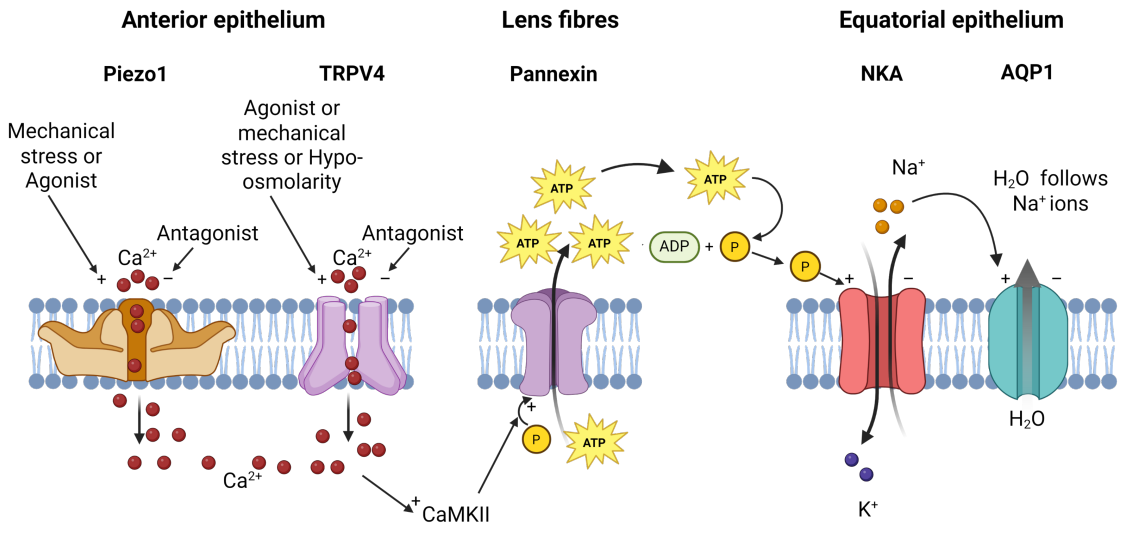


Figure 2.5: Schematic diagram of the proposed mechanism of TRPV4-mediated sodium-potassium ATPase (NKA) pump regulation via pannexin-dependent ATP release.

2.3.4 Modulators of the Transient Receptor Potential Melastatin 3

Pregnenolone sulfate (PregS) is a steroid that directly binds to the extracellular side of the transient receptor potential melastatin 3 (TRPM3) and induces conformational changes; TRPM3 channels open, resulting in an increased inflow of calcium ions [Harteneck, 2013, Wagner et al., 2008]. Activation of TRPM3 and subsequent calcium entry are associated with the transcriptional upregulation of ion-transport ATPase genes and regulation of ion and water homeostasis [Zhou et al., 2024]. In skeletal muscle, the TRPM3 upregulation is associated with stimulation of the NKA [Löhn and Wirth, 2024]; however, the only report about TRPM3 in the lens comes from an ARVO abstract, which reported that high temperature activates TRPM3, promoting an influx of calcium that drives up intracellular cAMP. This TRPM3-mediated cAMP rise decreases active NKA pump (Fig. 2.6) [Shahidullah et al., 2017]. Another well-known agonist of TRPM3 is nifedipine, a calcium channel blocker, which synergistically enhances PregS-induced TRPM3 activation [Drews et al., 2014]. Additionally, CIM0216, a synthetic agonist of TRPM3 of high potency [Held et al., 2015], binds to the extracellular domain of TRPM3, resulting in conformational changes in the intracellular domain of the TRPM3, resulting in activation of the TRPM3 channel [Kumar et al., 2026].

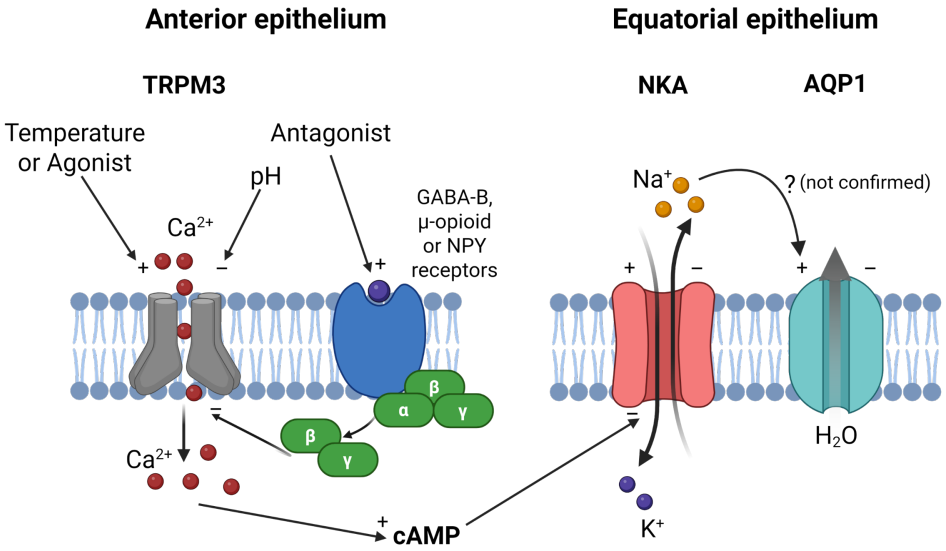


Figure 2.6: Schematic diagram of the proposed mechanism of TRPM3-mediated sodium-potassium ATPase (NKA) pump regulation via cyclic AMP.

The activation of gamma-aminobutyric acid type B (GABA-B), μ-opioid, and neuropeptide Y (NPY) receptors, which are G-protein-coupled receptors, triggers the release of G-protein $\beta\gamma$ subunits (Fig. 2.6). These subunits bind to the TRPM3 channel, alter its structure, and suppress its activity [Badheka et al., 2017, Quallo et al., 2017]. The pore vestibule of the TRPM3 is pH-sensitive and acidic pH inhibits the TRPM3 channels both intracellularly and extracellularly by interacting with amino acid residues located in the pore vestibule. The binding of protons induces a structural shift in the TRPM3 channel, reducing conductance and inflow of calcium ions [Hossain Saad et al., 2021].

2.3.5 Modulators of the Aquaporin 0

Zinc is an essential mineral for human health [Aggett and Comerford, 1995], and its deficiency is associated with various ocular diseases, cataracts in the lens of commercial rainbow trout [Ketola, 1979], oxidative damage in the retinal pigment epithelium and photoreceptors [Tate et al., 1999], age-related macular degeneration [Chiu and Taylor, 2007, Group, 2001], and diabetic retinopathy [Faure et al., 1995]. Zinc is the most abundant trace element in the crystalline lens and is predominantly localized in the anterior epithelial cell layer [González-Iglesias et al., 2017]. Zinc serves as an essential cofactor for carbonic anhydrase, an enzyme widely distributed throughout the lens that plays a key role in pH and fluid regulation [Galin et al., 1962]. Zinc may aid in the lens's transparency by protecting the lens proteins' structural integrity [Grahn et al., 2001]. Lenses with senile cataracts contain a lower concentration of zinc than younger, clear lenses [Swanson and Truesdale, 1971]. In oocytes, zinc and low pH can modulate the AQP0 and increase the water permeability. Zinc and protons bind to the histidine residues (His40) of the extracellular domain of AQP0, bringing conformational changes in the tetrameric structure of AQP0, which leads to an increase in the pore size and water permeability [Németh-Cahalan and Hall, 2000, Németh-Cahalan et al., 2007]. The water permeability of AQP0 has also been reported to increase with decreasing calcium ion concentration. This effect is mediated by the detachment of calmodulin from the C-terminus of AQP0 [Németh-Cahalan and Hall, 2000]. Calmidazolium is a calmodulin inhibitor that prevents calmodulin from binding to the C-terminus of the AQP0 channel, resulting in an increase in water permeability [Kalman et al., 2008].

Ht31 is a synthetic peptide that blocks the interaction between A-kinase anchoring proteins (AKAPs) and protein kinase A (PKA; [Carr et al., 1991]). Ht31 binds to the regulatory unit of the PKA and mimics the binding generally made by AKAP [Carr et al., 1992]. This binding disrupts the localized signalling pathway [Kreida et al., 2024, Kreida et al., 2018] and further prevents the phosphorylation of the AQP0 by promoting the binding of calmodulin, thereby inhibiting the water permeability of the AQP0 [Kreida et al., 2024].

2.3.6 Modulators of the Aquaporin 1

AqF026 is derived from a medication called furosemide, which is commonly used to treat conditions where the body retains excess fluid, such as high blood pressure, edema, and liver cirrhosis [Ponto and Schoenwald, 1990, Yool et al., 2013]. AqF026 has been reported to increase the water permeability of the AQP1 in the Xenopus oocyte by binding to a specific region, called the loop D domain, on the AQP1 protein [Yool et al., 2013]. The loop D domain is an intracellular domain related to channel gating, and AqF026 binding to the domain stabilizes the open conformation of the AQP1 channel and increases the water permeability in treated oocytes by 20% compared to the untreated oocytes [Kourghi et al., 2018, Yool et al., 2013, Tsai, 2020].

The bumetanide derivative, AqB013, is a synthetically designed compound to inhibit AQP1, which can cross the cell membrane and occlude the AQP1 pore from the cytoplasmic side, thereby reducing the water flux [Dorward et al., 2016, Migliati et al., 2009]. Mercuric chloride, a highly reactive mercury salt, inhibits AQP1 water permeability by binding to thiol groups (-SH) on the cysteine 189 residue. This binding induces a conformational change

that obstructs the gating mechanism of the water pore or channel [Zhang et al., 1993, Hirano et al., 2010]. Additionally, tetraethylammonium is widely used as a potassium channel blocker in electrophysiological studies and acts as a potential inhibitor for human AQP1 by binding to a tyrosine residue (Y186) on AQP1 to physically obstruct the water pore and interfere with the flow of water molecules through the channel [Brooks et al., 2000, Müller et al., 2008, Yool et al., 2002].

2.3.7 Modulators of the Aquaporin 5

Isoproterenol, a non-selective β-adrenergic receptor agonist, functionally regulates both NKCC1 and AQP5. However, this compound activates AQP5 via a different downstream pathway than NKCC1, i.e., for AQP5, it activates adenyl cyclase, an enzyme that catalyzes the production of cyclic adenosine monophosphate (cAMP), instead of engaging the MAPK/ERK pathway. The cAMP and its derivatives increase the expression of both AQP5 mRNA and protein [Susa et al., 2013, Chen et al., 2014]. In salivary glands, the increased cAMP levels also lead to phosphorylation of AQP5, which induces the translocation of AQP5 to the apical plasma membrane, where it acts as a water channel to enhance water permeability [Susa et al., 2013, Chen et al., 2014, Hosoi et al., 2020]. Niclosamide, a drug used for treating parasite infections, has been shown to increase the protein expression of AQP5 in human lung epithelial cells. Niclosamide reduces the ubiquitination of AQP5, resulting in reduced degradation and increased cellular abundance of AQP5 [Villandre et al., 2022].

H89, a synthetic compound, is a potent and selective inhibitor of PKA and competes with ATP for binding to the catalytic subunit of PKA [Chijiwa et al., 1990,

Lochner and Moolman, 2006]. Since PKA is a key modulator of the cAMP signaling pathway, the inhibition by H-89 prevents PKA-regulated phosphorylation of downstream targets, effectively blocking the signal transduction [Paine et al., 2009, Yang et al., 2003]. It has been shown that inhibiting PKA with H-89 reduces the membrane localization of AQP5 in the corneal epithelial cells [Kumari et al., 2012]. Methazolamide is a sulfonamide-based carbonic anhydrase inhibitor used for the treatment of glaucoma [Wistrand, 1984] and has been shown to reduce the AQP5 mRNA levels by downregulating its transcription [Rump et al., 2024].

2.3.8 Modulators of the Gap Junctions

Leupeptin, a bacterial protease inhibitor [Aoyagi et al., 1969], inhibits the activity of proteases like cathepsin B, H, and L, which are involved in connexin degradation [Leithe and Rivedal, 2004, Salminen, 1984], suggesting that inhibiting these cathepsins can stabilize connexin levels and increase gap junction communication. 4-phenylbutyrate (4-PBA) is a chemical chaperone and a special type of histone deacetylase (HDAC) inhibitor that can improve protein folding and has been found to successfully increase the levels of both Cx46 and Cx50 in the lenses of mice [Jara et al., 2018, Kaufman et al., 2013]. HDACs are enzymes that regulate gene expression by modifying histone proteins and suppressing the expression of Cx43 in cardiac and prostate cancer cells, leading to reduced gap junction communication [Hernandez et al., 2006, Xu et al., 2013]. It has been shown that by inhibiting HDACs, the protein expression of Cx43 and gap junction communication can be restored in the neural progenitor cells [Khan et al., 2007]. Forskolin, a known activator of

cAMP, elevates cAMP levels, which further activate PKA, promoting phosphorylation of Cx50, resulting in increased gap junction communication [Liu et al., 2011].

High intracellular calcium levels lead to the closure of the GJs by activating calcium-dependent proteases, Lp82 and m-calpain, both of which are present in the lens cells. When these proteases are activated, they can cleave connexins and degrade crystallins, decreasing the permeability of GJs and causing crystallins to aggregate, ultimately leading to cataract formation [Baruch et al., 2001, Nakamura et al., 2000]. 12-O-tetradecanoylphorbol-13-acetate (TPA), a potent semi-synthetic activator of PKC, can significantly decrease dye transfer between lenticular cells, indicating reduced gap junction intercellular communication. This effect was correlated with the activation of PKC-β, leading to phosphorylation of Cx43 and then a conformational change, which reduces GJ communication and permeability [Johnson, 1997, Pun et al., 2023, Berthoud et al., 2000, Husøy et al., 2001, Lampe et al., 2000]. Triarylmethanes are synthetic compounds and selective inhibitors of Cx50 and have been shown to reduce the conductance of Cx50 in lens epithelial cells of the mouse [Bodendiek et al., 2012]. N-benzylquinium, a derivative of quinine, is also a selective inhibitor of Cx50 that binds to the channel pore; the open probability of the channel is reduced, which stabilizes the closed state of the Cx50 channel [Rubinos et al., 2012].

2.4 Aging of the Lens

The crystalline lens is a unique ocular structure characterized by lifelong growth and the retention of cells without shedding. Epithelial cells at the equator differentiate into fibre cells that are continuously deposited onto the existing lens core. To preserve op-

tical clarity along the visual axis, differentiating fibre cells undergo programmed loss of organelles, creating an inner organelle-free zone. Consequently, the deep nuclear fibre cells lack mitochondria, nuclei, and metabolic machinery, relying primarily on anaerobic glycolysis for energy generation [Fernald and Wright, 1983, Bassnett and Mataic, 1997]. While this structural architecture minimizes light scattering, it leaves the central lens nuclear proteins reliant on passive transport and the microcirculatory system for metabolic support [Mathias et al., 1997]. Because central lens proteins do not undergo cellular turnover, long-lived crystallins accumulate post-translational modifications, including deamidation, truncation, glycation, oxidation, and covalent cross-linking [Budnar et al., 2022, Truscott and Friedrich, 2019, Harding, 1973]. Over time, these modifications compromise both structural crystallins and transmembrane proteins, such as aquaporins (AQPs), triggering protein aggregation, insolubility, and light-scattering chromophore formation in the lens [Harding, 1973, Spector, 1995, Budnar et al., 2022, Truscott and Friedrich, 2019]. Moreover, oxidative stressors, including depletion of antioxidants such as glutathione, accumulation of free radicals, and impaired proteostasis, contribute to the pathogenesis of cataracts [Spector, 1995, Truscott and Friedrich, 2019, Lou, 2003]. Additionally, there is a decrease in protein levels of connexin46 and connexin50 and a decrease in the function of transient receptor potential vanilloids (TRPVs) in pressure regulation with age in lens fibre cells [Gao et al., 2013, Giannone et al., 2021]. Sodium-potassium ATPase (NKA) pump activity has been shown to reduce with age in skeletal muscles, as determined by reduced ouabain binding sites in aged rodent models [Clausen, 2003, Wyckelsma and McKenna, 2016], and a similar decline in sodium-potassium chloride co-transporter 1 (NKCC1) protein levels has been observed in human and rat brain tissues [Dzhala et al., 2005, Gong et al., 2021].

Furthermore, increased sodium and calcium concentrations have been reported in cortical cataracts, highlighting ionic dysregulation as a key finding in lenticular aging [Adams, 1929, Tamiya and Delamere, 2006].

Continuous compaction and addition of lens fibre cells progressively alter both the optical density and mechanical compliance of the lens. Helmholtz proposed that presbyopia is caused by progressive loss of elasticity and hardening of the lens with age, rather than a failure of the ciliary muscle [Helmholtz, 1855]. Later, Fisher quantified lens stiffness and the exponential increase of the stiffness with age [Fisher, 1971]. Presbyopia affects approximately 1.8 billion people worldwide as of 2015 [Fricke et al., 2018]. Age-related cataractogenesis is a pathophysiological transition characterized by opacities in the lens [Cheng et al., 2019, Huang et al., 2005, Kinoshita, 1974, Truscott, 2005]. Cataracts are the most common cause of blindness worldwide [Delaye and Tardieu, 1983, Harding and van Heyningen, 1987, Lin et al., 2025], accounting for more than 50% of blindness cases globally [Jiang et al., 2026]. The progression of cataracts is accelerated by a diverse range of environmental, lifestyle, and systemic risk factors, including but not limited to chronic exposure to ultraviolet (UV) radiation [Harding, 1970, Borges-Rodríguez et al., 2023], diabetes mellitus [Ang and Afshari, 2021], chronic tobacco smoking, and prolonged corticosteroid therapy [Urban and Cotlier, 1986, Ang and Afshari, 2021]. These extrinsic factors feed directly into distinct clinical cataract phenotypes. Nuclear cataracts are predominantly driven by chronic oxidative stress, environmental exposures, and nuclear glutathione depletion [Harding, 1970, Truscott and Augusteyn, 1977]. Accumulation of insoluble crystalline aggregates and fluorescence chromophores induces progressive homogeneous browning of the

nuclear core [Spector, 1995]. However, cortical cataract is primarily driven by ionic dysregulation, membrane permeability alterations, and localized shear stress generated during accommodative effort [Fisher, 1973, Duncan and Bushell, 1975, Bron and Michael, 2011]. Elevated intracellular calcium and sodium concentrations disrupt osmotic equilibrium, forming localized wedge-shaped opacities [Adams, 1929, Duncan and Bushell, 1975].

2.5 Avian Experimental Model

Aside from non-human primates, the domestic chicken serves as a primary experimental model for studying lenticular accommodation. Primates rely primarily on lenticular curvature changes driven by a smooth ciliary muscle acting through the zonular fibres. In contrast, the avian crystalline lens employs a dual mechanism involving both corneal and lenticular accommodation, supported by a specialized ciliary apparatus and a uniquely deformable lens [Sivak, 2004]. Comparative work across vertebrates established that birds possess some of the largest accommodative amplitudes known, driven by extreme lens softness and rapid ciliary muscle action [Sivak et al., 1986]. The avian lens is an exceptionally soft, highly deformable, and strongly refractive optical component, particularly in species with large accommodative ranges. Diving birds such as the hooded merganser, which can accommodate up to approximately 70-80 diopters, reflect the need to compensate for refractive changes between air and water [Sivak et al., 1985]. Diurnal raptors such as red-tailed hawks exhibit amplitudes up to 17-28 diopters of accommodation, with additional corneal contributions of 3-6 diopters [Glasser et al., 1997]. Chickens also have notably soft lenses and are widely used as a model for studying lenticular biomechanics [Choh et al., 2002].

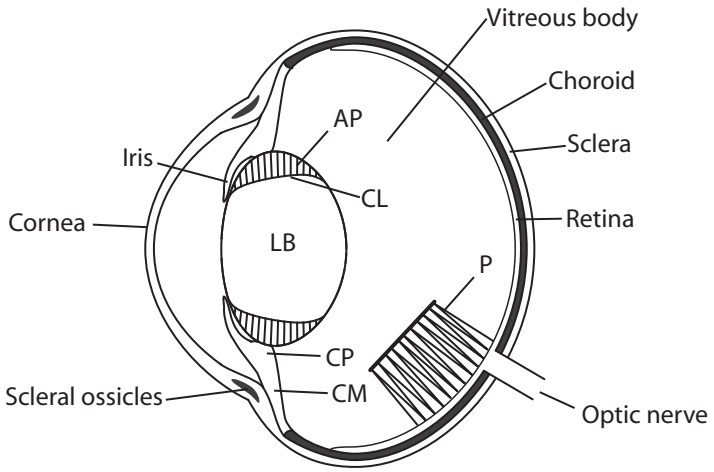


Figure 2.7: Schematic diagram of the chicken eye. AP, annular pad; CL, cavum lenticuli; LB, lens body; CP, ciliary processes; CM, ciliary muscle; P, pecten.

A defining anatomical specialization of the avian lens is the presence of an annular pad, a thick circumferential pad of modified secondary lens fibres, which occupies nearly half of the coronal cross-section of the lens (Fig. 2.7) [Walls, 1942]. This structure is unique to birds and is absent in primates and most mammals. The annular pad is composed of highly compacted, radially oriented, and mechanically specialized fibres that differ from those of the central lens nucleus: they are shorter, more densely packed, radially oriented, and exhibit a distinct curvature profile, giving the annular pad a stiffer equatorial band capable of transmitting force efficiently from the ciliary apparatus [Walls, 1942]. It is also reported that this specialized equatorial architecture plays a central role in enabling the large, rapid lens-shape change characteristics of avian accommodation [Sivak et al., 1986].

Unlike primates, where the ciliary muscle acts indirectly through the zonular fibres, birds possess a direct mechanical interface between the ciliary body and the annular

pad [Sivak et al., 1986]. Large, radially projecting ciliary processes insert directly onto the surface of the annular pad, forming a physical contact zone that increases the surface area for force transfer and enables efficient equatorial compression of the lens [Sivak et al., 1986]. This arrangement is powered by the avian striated ciliary muscle, which is capable of rapid, high-force contractions far exceeding the speed of smooth muscle in mammals [Pardue and Sivak, 1997, Tedesco et al., 2005]. The ciliary apparatus is further reinforced by a ring of scleral ossicles, which form a rigid interlocking bony support around the corneoscleral junction and stabilize the ciliary ring during contraction [Walls, 1942]. Together, the combination of direct ciliary lens articulation, large ciliary processes, striated muscle, and ossicular stabilization creates a highly specialized biomechanical system that enables the fast, high-amplitude accommodation characteristics of visually demanding avian species such as raptors, diving birds, and chickens [Glasser et al., 1997, Sivak et al., 1985, Choh et al., 2002].

Between the annular pad and the central lens body lies a narrow, lubricated cleft (cavum lenticuli); the inner ends of annular pad fibres secrete a viscous mucopolysaccharide-rich substance into this space, creating a low-friction surface interface [Walls, 1942]. This lubricated cleft is hypothesized to permit shearing and sliding between the annular pad and central lens mass during ciliary muscle contraction [Walls, 1942]. Such sliding enables equatorial compression coupled with axial steepening required for the high accommodative amplitudes observed in birds [Sivak et al., 1986]. As in humans, the avian ciliary muscle receives postganglionic parasympathetic innervation from the short ciliary nerves, whose preganglionic fibres arise from the oculomotor nerve and relay in the ciliary ganglion before entering the eye [Walls, 1942, Glasser et al., 1997, Choh et al., 2002].

The chicken offers a uniquely advantageous model for studying ocular accommodation and lens biomechanics due to the combination of anatomical, physiological, and experimental features. Anatomically, the chicken lens is exceptionally soft, making it ideal for studying deformation and age-related changes in stiffness [Glasser et al., 1995]. They also exhibit robust lenticular accommodation early in life, and there is an age-related decline in accommodative amplitude [Choh et al., 2002]. This decline mirrors the progressive loss of lens elasticity in humans, making the chicken an effective model for studying the mechanism behind the age-related lens stiffening. Although chickens utilize both corneal and lenticular mechanisms during accommodation [Schaeffel and Howland, 1987], the intrinsic biomechanical properties of the lens itself can still be effectively isolated ex vivo, providing a valuable model to investigate lens-specific responses. Neural stimulation of the ciliary nerve in chickens [Choh et al., 2002] also parallels the parasympathetic control of accommodation in humans, enabling controlled activation of the accommodative apparatus.

At the molecular level, the chicken lens expresses the same three ancestral crystallin families: α-, β-, and γ, but the amounts and relative contributions of each family differ markedly from those in humans [Wilmarth et al., 2004, Chen et al., 2017]. α-crystallins (αA, αB) serve as ATP-independent chaperones in both species, though chickens rely more heavily on αA, whereas humans show stronger αB expression associated with stress response proteostasis [Cvekl et al., 2015]. β-crystallins form the major structural scaffold in both human and avian lenses [Wistow and Piatigorsky, 1988a]. The biggest difference between chickens and humans is in the γ-crystallin family. Humans possess a full set of γ-crystallin genes (γA-γF in the lens nucleus, and γS predominantly in the lens cortex. Birds, however, lost most γ-crystallin genes (γA-γF) during evolution, compensating for this loss through

high expression of δ-crystallin [Piatigorsky, 1984]. Consequently, chickens produce only trace amounts of γS and γN, whereas humans express high levels of γS while rendering γN a non-functional pseudogene [Chen et al., 2017].

Complementing these protein-level differences, the gap-junction architecture of the chicken lens closely parallels that of humans. In both species, lens communication is mediated by connexin43 (Cx43) in the anterior lens epithelium and fibre-cell connexins encoded by GJA3 and GJA8. In chickens, fibre connexins are historically named Cx45.6 and Cx56 based on their predicted molecular masses, and they represent the avian orthologs of mammalian Cx46 and Cx50, respectively [Rup et al., 1993, Jiang et al., 1994]. Avian studies show that Cx43 is expressed in the chicken lens epithelium, whereas Cx45.6 and Cx56 are expressed in differentiating and mature fibre cells, forming high-conductance gap junctions essential for rapid post-hatch lens growth [Wang et al., 2012]. Connexin expression in chick embryos is tightly linked to fibre-cell elongation and organelle loss, mirroring mammalian lens development [Jiang et al., 1994].

Additionally, the chicken lens also expresses AQP1 in the anterior lens epithelium and supports osmotic balance and fluid transport [Isokpehi et al., 2009]. In fibre cells, AQP0 is the dominant membrane protein and serves dual roles as a water channel and adhesion molecule, interacting with avian fibre connexins Cx45.6 and Cx56 [Yu and Jiang, 2004]. The ion-transport machinery that drives the lens microcirculation system is also conserved in chickens. Sodium-potassium ATPase (NKA) is highly enriched in the equatorial epithelium of the lens [Kinsey and Reddy, 1965].

Thus, despite anatomical differences, such as the presence of an annular pad and direct

ciliary body lens articulation in birds, the chicken lens remains a powerful translational model because it not only demonstrates robust accommodation and an age-related decline in accommodative amplitude but also preserves fundamental molecular systems: crystallins, connexin-mediated intercellular communication, the water channels, and epithelial ion transport machinery. These together provide insight into lenticular biomechanics and age-related changes relevant to human accommodation and the mechanism of presbyopia.

I hypothesize that the pharmacological modulation of the lens microcirculatory system via targeting the fluid transport pathway will change lens biomechanics such as lens stiffness and resilience in chicken lenses.

Chapter 3

The effect of modulators of aquaporin 0 and sodium-potassium ATPase pumps on chicken lens biomechanics

3.1 Introduction

The microcirculatory system (MCS) plays an essential role in maintaining ion homeostasis and volume in the lens [Donaldson et al., 2001, Mathias et al., 1997]. Two main components of MCS are aquaporin 0 (AQP0) and the sodium-potassium ATPase pumps (NKA). The AQP0 water channel, also called a major intrinsic polypeptide (MIP; [Gorin et al., 1984]), contributes to 50% of the total membrane proteins of the lens fibre cells [Fitzgerald et al., 1983]. AQP0 is exclusively present in the lens fibre cells and maintains water homeostasis across the membrane [Ball et al., 2003]. It has been reported that 80% of the water permeability of the lens fibre cells is contributed by AQP0 [Grey et al., 2009, Varadaraj et al., 2005]. Additionally, AQP0 has cell adhesion properties, which maintain the minimum gap between the lens fibre cells and contribute to the lens

transparency [Kumari and Varadaraj, 2009, Michea et al., 1994]. It has been suggested that there is a change of 2-8% of water volume in the lens during accommodation, and these changes are thought to be aided by AQPs [Gerometta et al., 2007]. Phosphorylation has been reported to play an essential role in maintaining AQP0 function as a water channel [Kalman et al., 2008], calmodulin binds to the C-terminal of AQP0 and closes the cytoplasmic water pore of AQP0 [Reichow and Gonen, 2008]. Protein kinase A (PKA), along with A-kinase anchoring protein-2 (AKAP2), makes a PKA-AKAP2-AQP0 complex and phosphorylates AQP0, which further protects the binding of calmodulin from the C-terminal of the AQP0. Detachments of the PKA from the AKAP2-AQP0 complex are associated with loss of lens transparency [Gold et al., 2012]. Mutation of the AQP0 channels has been shown to be associated with loss of the transparency of the lens and cataract formation [Berry et al., 2000].

NKA is a transmembrane enzyme, and its maximum activity is located at the equatorial epithelium of the lens [Delamere and Dean, 1993, Unakar and Tsui, 1980]. NKA actively transports sodium ions out of the cell and potassium ions into the cell against their electrochemical gradients [Kaplan, 2002, Wallick et al., 1979]. NKA plays an essential role in maintaining cellular osmolarity by regulating intracellular sodium and potassium ion concentrations in the lens. NKA also creates an osmotic gradient within the lens by actively transporting sodium ions at the equator, which further facilitates the movement of water and other nutrients through the lens [Donaldson et al., 2010, Gao et al., 2011, Gao et al., 2015]. Dysfunction of the NKA can lead to lens opacification [Beebe et al., 1982, Duncan and Bushell, 1975, Parmelee and Beebe, 1988]. Thus, modulating AQP0 and sodium-potassium pumps with modulators makes them a potential target

for developing treatments for age-related conditions in humans, such as cataracts and presbyopia.

Zinc (Zn) has been shown to significantly increase the water permeability of human and Xenopus AQP0 as well as human AQP5 by modulating the channels through cooperative tetrameric allosteric mechanisms [Németh-Cahalan et al., 2007, Mom et al., 2024] and AQP5 [Mom et al., 2024]. Rather than altering the physical dimensions of pores [Mom et al., 2024], the binding of Zn^{2+} to a single monomer induces a conformational shift that is cooperatively transmitted across the tetramer, stabilizing the entire complex in a highly conductive state [Németh-Cahalan et al., 2007]. On the other hand, Ht31 is a known inhibitor of A-kinase anchoring proteins (AKAP) associated with AQP0; it acts by uncoupling protein kinase A (PKA) from the AKAP2-AQP0 complex, thereby disrupting the normal phosphorylation of AQP0 and disturbing water permeability in the lens [Gold et al., 2012, Ma et al., 2011].

In endometrial epithelial cells, insulin has been shown to increase the activity of the NKA pump by activating the PI3K pathway and protein phosphatases, which enhances the pump's binding affinity for intracellular sodium ions and increases its maximum velocity [Deachapunya et al., 1999]. Additionally, insulin is known to stimulate the translocation of NKA pump subunits to the plasma membrane in the lung epithelial cell [Comellas et al., 2010]. Ouabain is an inhibitor of NKA pumps, which blocks the enzyme's ATPase activity, subsequently disrupting the intracellular sodium and potassium ion concentrations in both the lens [Bonting et al., 1963] and the retina [Murphy and Crewther, 2013]. This study is undertaken to examine whether modulators of AQP0 and NKA lead to changes in lenticular biomechanics. I hypothesized that the pharmacological modulation of the lens

AQP0 and NKA significantly alters chicken lens biomechanics such as lens stiffness and resilience.

3.2 Material and Methods

3.2.1 Experimental model and lens dissection

White Leghorn chickens (Gallus gallus domesticus) were used as an experimental model, as the optical properties of the chicken lens are similar to those of humans, and they can change the shape of their lenses to accommodate. Additionally, like humans, chickens show robust accommodation into adulthood before also developing presbyopia as they age [Choh et al., 2002]. Chicken hatchlings were purchased from the Maple Leaf hatchery in New Hamburg, Ontario. Chickens were reared in brooders with proper heating and humidity sources kept on a 14h:10h light-dark cycle and provided with food and water ad libitum. The standards of the Canadian Council on Animal Care and the ARVO Statement for the Use of Animals in Ophthalmic and Vision Research were followed in the rearing of chickens (AUPP-43774). Sample size was determined a priori using G*Power with an alpha error of 0.05, a beta error of 0.80, an effect size of 0.14, and a moderate correlation of 0.43. This calculation indicated a requirement of at least 13 birds per experimental group.

14-day-old healthy young chickens were euthanized by decapitation using a guillotine. Immediately after decapitation, chicken eyes were enucleated and immersed in oxygenated Tyrode's solution (TS), composition: 134 mM NaCl, 3 mM KCl, 20.5 mM $NaHCO_3$, 1 mM $MgCl_2$, and 3 mM $CaCl_2$, to preserve tissue viability. Under a dissecting microscope,

the posterior globe of the eye was removed to expose the vitreous humor by making a circumferential incision around the corneal-scleral junction. Then the lenses were carefully separated from the ciliary body and vitreous humor without damaging the lens capsule. All dissections were performed in Tyrode's solution to maintain physiological conditions.

3.2.2 Lens Treatment

For the AQP0 activation, lenses (n=18) were treated with AQP0 agonist zinc (80 µg/ml; 208086, Millipore Sigma, Oakville, Ontario, Canada) for 15 minutes. A 100 times concentrated zinc stock solution was prepared by dissolving 834 mg of zinc chloride in 1 mL of 6N hydrochloric acid (HCl) to ensure complete dissolution and prevent the precipitation of zinc hydroxide. This mixture was brought to a final volume of 50 mL using deionized water. The final working solution of 80 µg/ml of zinc was prepared fresh before each experiment by diluting the stock solution 1:100 in oxygenated Tyrode's solution (TS) by adding 500 µL of stock to 50 mL of TS. Note that the buffering capacity of TS neutralized the trace acid from the stock, maintaining a physiological pH of 7.4 and an osmolarity around 300 mOsm/L (iso-osmotic condition). Paired control lenses were exposed to a vehicle control matching the trace acid and osmolarity environment of the treatment solution without zinc chloride for the same duration.

For the AQP0 inhibition, lenses (n=14) were exposed to the AQP0 antagonist st-Ht31 (10 µM; 6286, Bio-Techne Canada, Toronto, Ontario, Canada) for 15 minutes. The 10 µM working solution was prepared by adding 1 mg of st-Ht31 in 35.74 µL of TS. The contralateral control lenses were incubated in TS alone, without traces of st-Ht31.

For the NKA activation, lenses (n=15) were treated with the NKA agonist insulin (150 nM; I6634, Millipore Sigma, Oakville, Ontario, Canada) alone for 15 minutes. Due to its low solubility at neutral pH, a concentrated insulin stock solution was first prepared by dissolving 2 mg insulin powder in 1 mL of hydrochloric acid, which was then brought to a total volume of 23.26 mL using oxygenated TS. The final 150 nM working solution was prepared fresh before each experiment by diluting this stock solution 1:100 in TS. The contralateral control lenses were incubated in a vehicle control solution matching the trace acidity of the treatment group in the absence of insulin.

For the NKA inhibition, lenses (n=14) were incubated in the NKA antagonist ouabain (1 mM; O3125, Millipore Sigma, Oakville, Ontario, Canada) in TS for 15 minutes. The 1 mM working solution was prepared by dissolving 36.44 mg of ouabain octohydrate directly in TS. Due to its toxicity, ouabain was handled strictly according to standard UW safety protocols. Fellow control lenses were treated with a corresponding vehicle (TS).

Following their respective treatments and immediately before biomechanical compression under the microtester, all lenses were rinsed in fresh TS for 1 minute. No cloudiness of the lens was detected with any agonist or antagonist treatment under the testing conditions.

3.2.3 Biomechanical testing

Lenses were compressed using a CellScale Micro Tester G2 (Ontario, Canada) to check their mechanical properties. The microtester consists of a microbeam (tungsten shaft, size) that is fixed with a vertical actuator and a square stainless-steel platen (compression plate), which is attached to the end of the microbeam (Fig. 3.1).

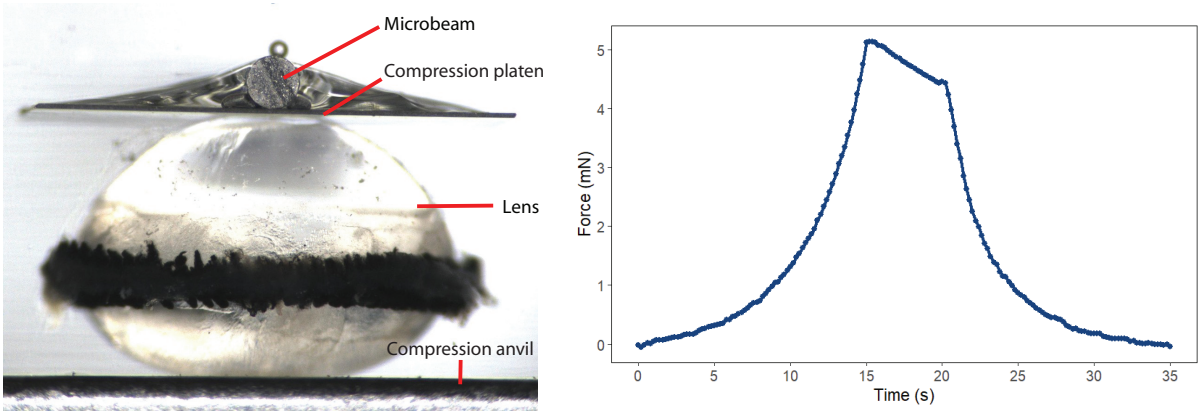


Figure 3.1: The microtester setup and experimental testing. **(A)** The chicken lens positioned under the microtester platen. **(B)** Force-time curve during the 15-second compression, 5-second hold, and 15-second recovery phase.

Each lens was placed posterior pole side up on a compression anvil located in the fluid bath (test chamber) filled with Tyrode's solution. Compression was applied by a microbeam-connected platen. The experimental testing profile consisted of three distinct sequential phases over a total duration of 35 seconds: first, a 15-second compression phase where lenses were then progressively compressed up to a displacement of 750 µm at a constant speed of 50 µm/s [Won et al., 2015]; second, a 5 second hold phase where the platen was held stationary at the maximum displacement; and third, a 15-second recovery phase where the platen was retracted at a constant velocity of 50 µm/s back to its position to monitor the elastic recoil of the tissue.

To isolate the true resistance and mechanical forces of the lens tissue from the experimental artifacts, a baseline fluid control test was executed individually for every single lens. Immediately following the completion of a lens's compression run, the lens was removed from the chamber, and the platen was run through the exact same 35-second displacement

profile in the fluid bath containing only TS. The resulting buoyancy force exerted by the fluid alone was recorded. Force compression data were collected from the MicroTester G2 software (ver. 1.0.0.1, Waterloo, Ontario, Canada) for subsequent mathematical modeling.

First, individual baseline fluid-force values (buoyancy) were subtracted from the raw experimental force data. To quantify the mechanical behaviour of the lenses, the baseline-corrected force-displacement data from the 15-second compression phase were fit to a non-linear exponential curve using the equation $y = y_0 + ae^{bx}$, where y represents the baseline-corrected force exerted by the lens (mN), x represents the platen displacement or compression depth (µm) and y_0 represents the baseline force at zero displacement. The a-coefficient represents the initial force amplitude of the exponential curve, indicating the early-stage resistance of the lens tissue. The b-coefficient represents the exponential rate constant and signifies the change in force with compression. A higher b-coefficient indicates a steeper exponential increase in lens stiffness with increasing displacement, thereby serving as a direct indicator of a stiffer lens matrix.

The viscoelastic energy dissipation or structural recovery was evaluated by calculating the lens's structural resilience. Resilience was mathematically determined using the areas under the force-displacement curves by the following equation:

$$Resilience = \frac{\text{Area under the recovery curve}}{\text{Area under the compression curve}}$$

The areas under both the compression and recovery curves represent the mechanical work input and work returned, respectively. A higher resilience value indicates highly efficient energy conservation and shape recovery (greater tissue elasticity), and lower hysteresis

(minimal energy lost during deformation).

3.2.4 Hyperosmotic Challenge and Water Permeability Assay

Freshly enucleated eyes were carefully dissected to isolate intact crystalline lenses. Immediately following removal, paired lenses from the same chicken were transferred to individual containers filled with a hyperosmolar Tyrode's solution (>60 mOsm/L above the baseline 300 mOsm/L; 1 hour) formulated to induce controlled osmotic stress by causing water efflux and measurable shrinkage. At the end of this hyperosmolar incubation, each lens was briefly rinsed in isomolar Tyrode's solution, gently positioned on a calibrated imaging stage in a microtester fluid bath container filled with Tyrode's solution, and a high-resolution photograph was captured to document morphological and volume changes resulting from the hyperosmotic stress.

After imaging, the lenses were rinsed in isomolar (300 mOsm/L) Tyrode's solution for 1 minute to remove residual hyperosmolar solution, then one lens from each pair was treated with Tyrode's solution supplemented with zinc for 15 minutes, while the contralateral control lens was incubated with Tyrode's solution alone for the same duration. Following incubation, lenses were briefly rinsed in isomolar Tyrode's solution and re-imaged using the same optical setup and magnification parameters to ensure consistency across time points. Morphometric image analysis was performed using ImageJ (version 1.54g; National Institutes of Health, Bethesda, MD, USA) [Schneider et al., 2012]. The relative changes in total lens cross-sectional area were calculated to evaluate volume recovery. Additionally, during hyperosmotic incubation, an unexpected subcapsular gap formed between the lens

capsule and the underlying cortex, probably due to fluid loss; therefore, the diameter of this subcapsular gap was also quantified in ImageJ. The degree of osmotic recovery in zinc-treated lenses relative to their paired controls was used as an indicator of zinc-mediated enhancement in water permeability.

3.2.5 Statistical analysis

Statistical analyses were performed using R (version 4.5.3; [R Core Team, 2026] within the RStudio integrated development environment (version 2026.01.1+403; [Posit Team, 2026]. To evaluate the exponential relationship between baseline-corrected force (y) and platen displacement (x) during the 15-second compression, a model was fitted using the core stats package [R Core Team, 2026]. For each lens, the force compression data were fit to the exponential model equation $y = y_0 + ae^{bx}$ to extract the initial force amplitude (a-coefficient) and exponential rate constant (b-coefficient). Because the microtester system is extremely sensitive to ambient environment vibrations, minor background disturbances and the opening or closing of lab doors during the run can introduce high-frequency noise and produce jittery force curves. To ensure basic curve consistency and eliminate environmentally compromised runs, only curves demonstrating a high quality of fit with a coefficient of determination (R^2) greater than or equal to 0.97 were considered acceptable for final parameter estimation.

Data cleaning, manipulation, and structural transformations were conducted using the "tidyverse" collection of packages [Wickham et al., 2019], primarily utilizing "readr" for data import, "dplyr" and "tidyr" for data restructuring, "stringr" for string manipulation,

"forcats" for date-time parsing, and "purrr" for functional programming pipelines. High-resolution figures and data visualization were generated using "ggplot2." Normality of the extracted parameters (a-coefficient, b-coefficient, and resilience) across the experimental and control groups was assessed using the Shapiro-Wilk normality test, and homogeneity of variances was verified using Levene's test by the "rstatix" package [Kassambara, 2026]. The differences between the experimental treatment lenses (zinc, Ht31, insulin, or ouabain) and their respective contralateral vehicle control lenses were evaluated using a t-test for normally distributed data or a Wilcoxon signed-rank test for non-normally distributed data. All statistical tests were two-tailed, and the differences were considered statistically significant at a threshold of $p < 0.05$.

3.3 Results

We found that the treatment with 80 µg/ml of zinc (Fig. 3.2), an agonist of AQP0, showed a statistically significant increase in the b-coefficient (p-value = 0.001), with the treated group exhibiting a mean value of 4.508 ± 0.594 compared to the control lenses' mean of 4.031 ± 0.337. This elevation indicates that the lens's stiffness increases exponentially with compression, indicating stiffer lenses. In contrast, there was no significant change in structural resilience (p-value = 0.124) between zinc-treated lenses (73.118 ± 7.139) and control lenses (77.009 ± 12.000).

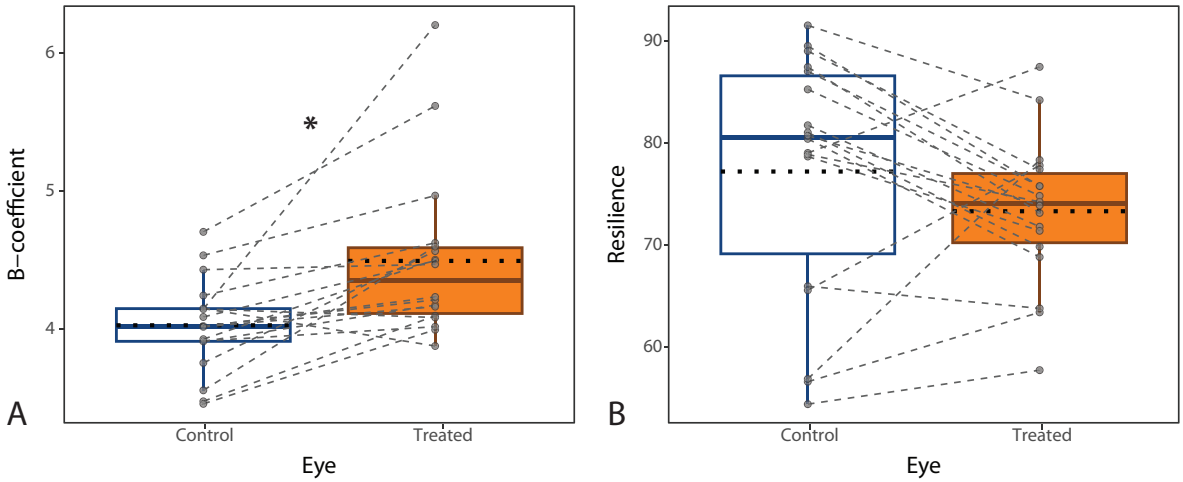


Figure 3.2: Box plots of the biomechanical responses of lenses treated with zinc (filled boxes) or vehicle (empty boxes) at room temperature. **(A)** Exponential stiffness (b-coefficient) of lenses treated with zinc was significantly higher compared to vehicle solution ($p = 0.001$). **(B)** Resilience values showed no significant difference between zinc and vehicle treatments ($p = 0.124$). Data are presented as mean ± sd ($n = 18$; paired t-test). Each pair of eyes is linked by dashed grey lines. Dotted black line = mean; dotted solid lines = median

Conversely, treatment of lenses with Ht31 (Fig. 3.3), an inhibitor of AQP0-signalling chain, resulted in a significant reduction in the b-coefficient (p = 0.037); Control lenses exhibited a mean b-coefficient of 4.350 ± 0.541, whereas Ht31-treated lenses dropped to a mean of 4.123 ± 0.620. This decrease in the b-coefficient reflects an exponential reduction in lens stiffness under compression, consistent with a softer mechanical response. Despite this change in stiffness, structural resilience was not significantly altered (p-value = 0.518), with treated lenses showing a mean resilience of 79.970 ± 8.743 and controls 77.997 ± 5.215.

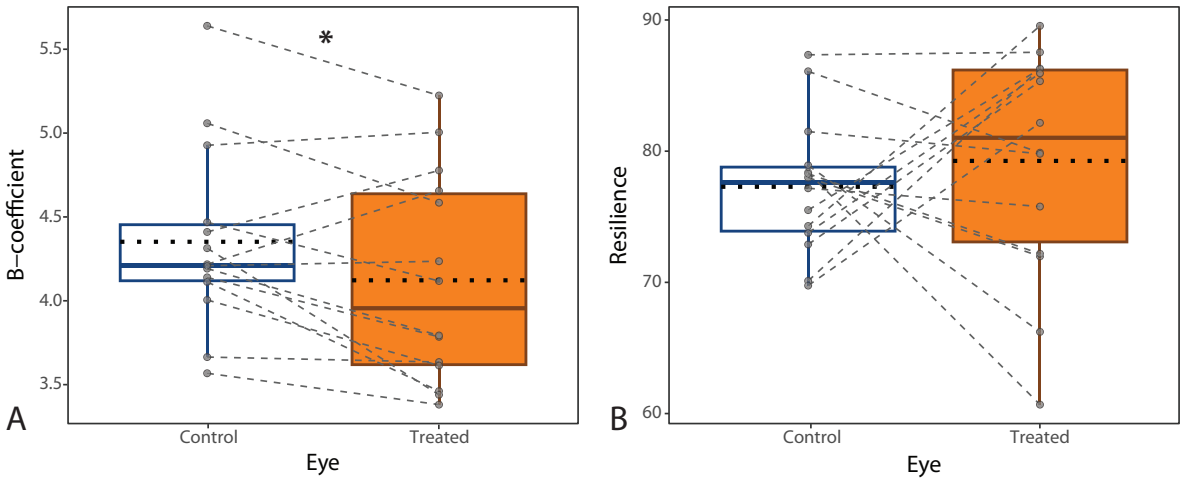


Figure 3.3: Box plots of the biomechanical responses of lenses treated with Ht31 (filled boxes) or vehicle (empty boxes) at room temperature. **(A)** Exponential stiffness (b-coefficient) of lenses treated with Ht31 was significantly lower compared to vehicle solution ($p = 0.037$). **(B)** Resilience values showing no significant difference between Ht31 and vehicle treatments ($p = 0.518$). Data are presented as mean ± sd ($n = 14$; paired t-test). Each pair of eyes is linked by dashed grey lines. Dotted black line = mean; dotted solid lines = median.

Next, we target the NKA pump with insulin (Fig. 3.4), which is the agonist of the NKA pump. We found no significant change in whole lens biomechanics. No significant shifts were detected in the b-coefficient (p = 0.214; treated: 4.142 ± 0.484, control: 3.973 ± 0.360) or structural resilience (p = 0.480; treated: 81.778 ± 6.992, control: 83.638 ± 6.306) across the paired cohorts.

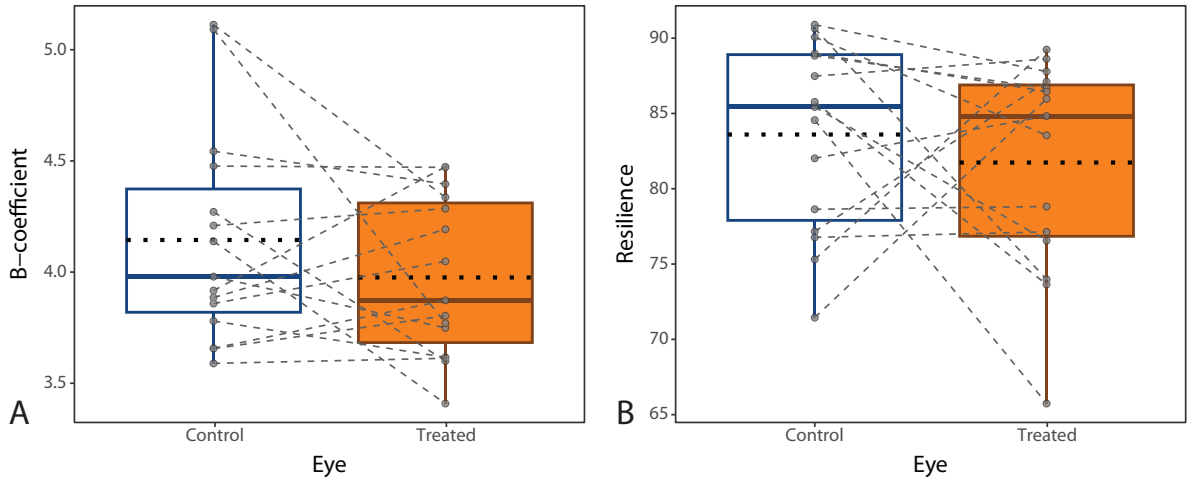


Figure 3.4: Box plots of the biomechanical responses of lenses treated with insulin (filled boxes) or vehicle (empty boxes) at room temperature. **(A)** Exponential stiffness (b-coefficient) of lenses treated with insulin remained comparable to vehicle solution ($p = 0.214$). **(B)** Resilience values showed no significant difference between insulin and vehicle treatments ($p = 0.480$). Data are presented as mean ± sd ($n = 15$; paired t-test). Each pair of eyes is linked by dashed grey lines. Dotted black line = mean; dotted solid lines = median.

To assess potential synergistic interaction between zinc and insulin, lenses were treated with a combination of zinc and insulin (Fig. 3.5). We found that there is no significant deviation in the b-coefficient (p = 0.937) in treated lenses (4.095 ± 0.446) compared to the contralateral controls (4.109 ± 0.520). Notably, the previously observed zinc-induced increase in stiffness (b-coefficient) was no longer present under this combined treatment. Structural resilience similarly showed no significant change (p = 0.062), with treated lenses at 71.165 ± 8.050 and controls at 77.180 ± 7.136.

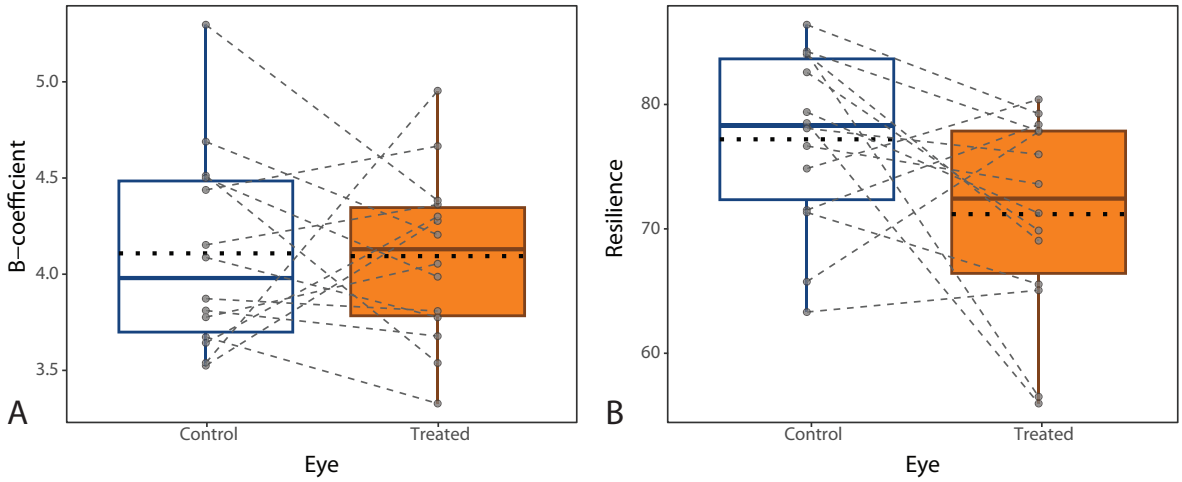


Figure 3.5: Box plots of the biomechanical responses of lenses treated with a combination of zinc and insulin (filled boxes) or vehicle (empty boxes) at room temperature. **(A)** Exponential stiffness (b-coefficient) of lenses treated with zinc + insulin with remained comparable to vehicle solution ($p = 0.937$). **(B)** Resilience values showed no significant difference between insulin and vehicle treatments ($p = 0.062$). Data are presented as mean ± sd ($n = 14$; paired t-test). Each pair of eyes is linked by dashed grey lines. Dotted black line = mean; dotted solid lines = median.

The treatment with ouabain, an inhibitor of the NKA pump, likewise did not significantly affect lens biomechanics (Fig. 3.6). There was no change in the b-coefficient (p = 0.274; treated: 4.132 ± 0.598, control: 4.243 ± 0.560). Furthermore, resilience showed no significant difference (p = 0.123) following NKA inhibition (treated: 79.662 ± 8.921, control: 82.997 ± 3.319).

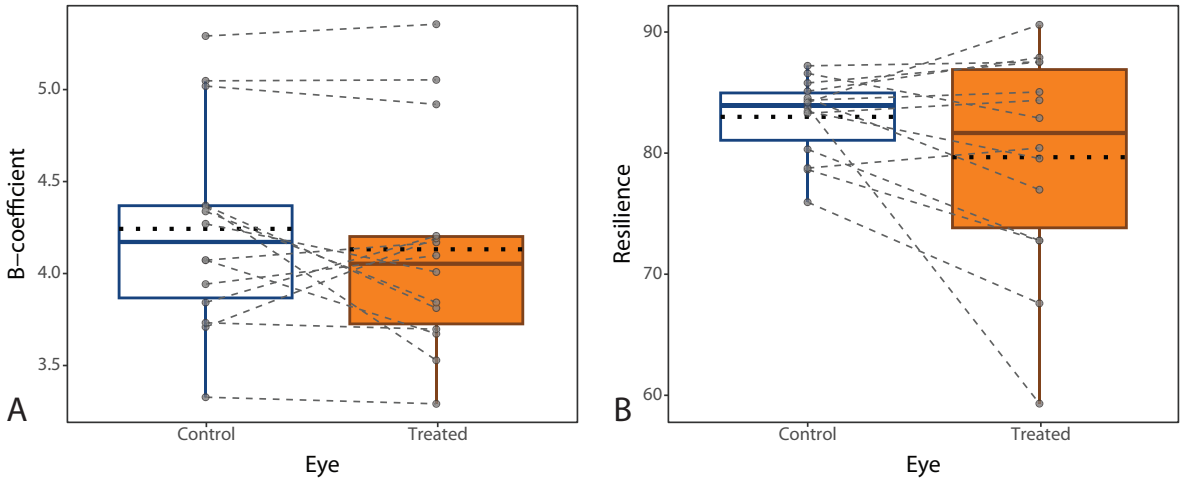


Figure 3.6: Box plots of the biomechanical responses of lenses treated with ouabain (filled boxes) or vehicle (empty boxes) at room temperature. **(A)** Exponential stiffness (b-coefficient) of lenses treated with ouabain remained comparable to vehicle solution ($p = 0.274$). **(B)** Resilience values showed no significant difference between ouabain and vehicle treatments ($p = 0.123$). Data are presented as mean ± sd ($n = 14$; paired t-test). Each pair of eyes is linked by dashed grey lines. Dotted black line = mean; dotted solid lines = median.

To determine whether zinc and ouabain exert synergistic effects on lens biomechanics, lenses were treated with both agents and compared to ouabain-alone controls (Fig. 3.7) and to zinc alone (Fig. 3.8). When the zinc + ouabain treatment group was compared to ouabain-alone controls, a significant increase in the b-coefficient was observed (treated: 4.343 ± 0.422; control: 4.131 ± 0.454; p = 0.001). This increase mirrors the stiffening effect previously observed with zinc alone, indicating that the zinc-dependent elevation in the b-coefficient is still detectable when ouabain is present. In contrast, ouabain alone did not alter the b-coefficient, as confirmed both in the ouabain-only experiments and in the combined zinc + ouabain comparison against ouabain controls.

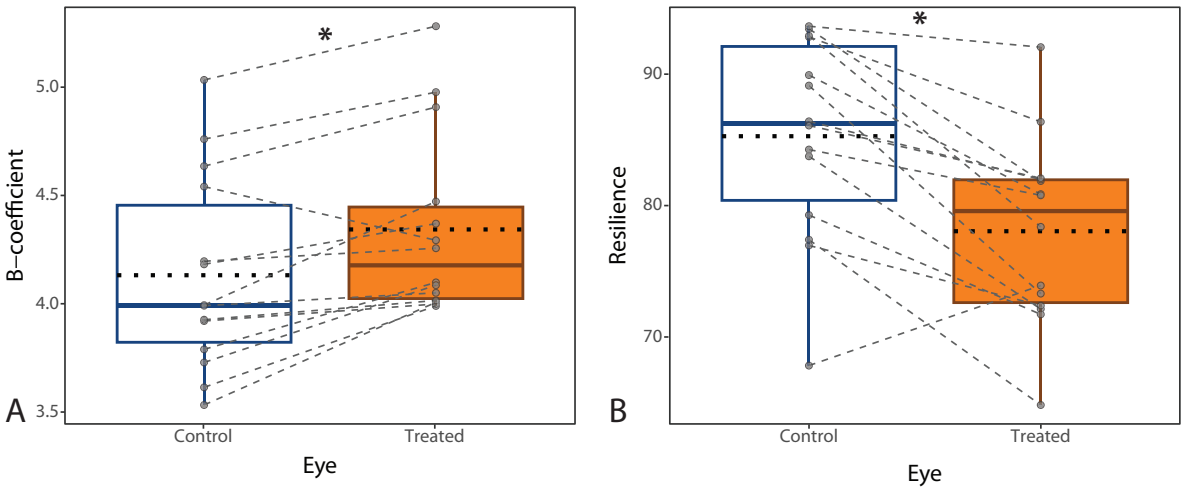


Figure 3.7: Box plots of the biomechanical responses of lenses treated with a combination of zinc and ouabain (filled boxes) or ouabain (empty boxes) at room temperature. **(A)** Exponential stiffness (b-coefficient) of lenses treated with zinc + ouabain remained comparable to ouabain solution ($p = 0.001$). **(B)** Resilience values showed a significant decrease between zinc + ouabain and ouabain treatments ($p = 0.001$). Data are presented as mean $\pm$ sd ($n = 14$; paired t-test). Each pair of eyes is linked by dashed grey lines. Dotted black line = mean; dotted solid lines = median.

However, when the zinc + ouabain group was compared to zinc-alone controls, the b-coefficient remained statistically unchanged (p = 0.177; treated: 4.109 $\pm$ 0.291, control: 4.246 $\pm$ 0.421). This indicates that combined treatment does not further enhance or suppress the change in zinc-related stiffness; rather, the effect on the b-coefficient remains consistent with the zinc-alone response.

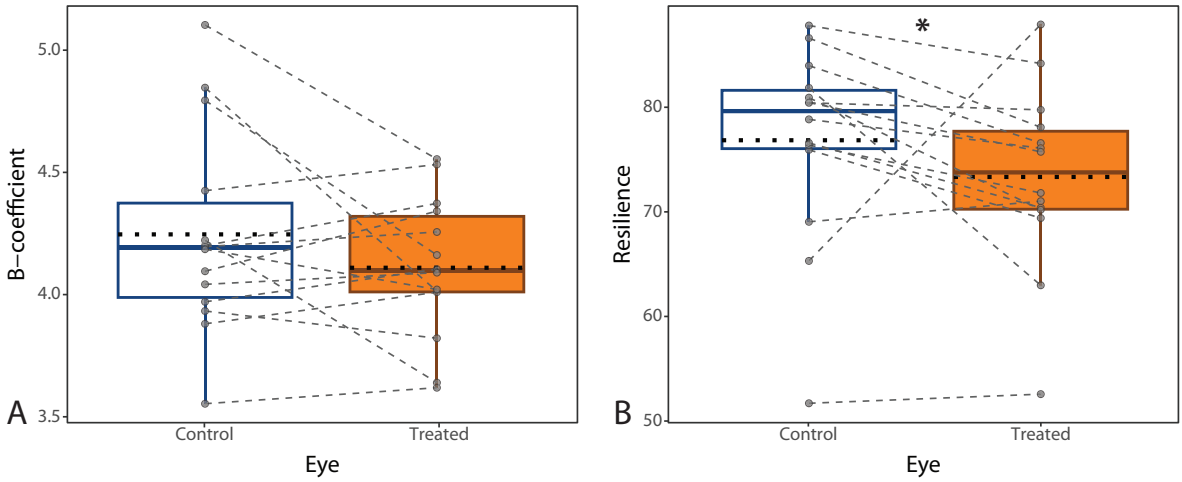


Figure 3.8: Box plots of the biomechanical responses of lenses treated with a combination of zinc and ouabain (filled boxes) or zinc (empty boxes) at room temperature. **(A)** Exponential stiffness (b-coefficient) of lenses treated with zinc + ouabain with remained comparable to zinc solution ($p = 0.177$). **(B)** Resilience values showed a significant decrease between zinc + ouabain and zinc treatments ($p = 0.035$). Data are presented as mean ± sd ($n = 14$; paired t-test). Each pair of eyes is linked by dashed grey lines. Dotted black line = mean; dotted solid lines = median.

In contrast, a different pattern emerged for resilience. Ouabain alone did not significantly affect resilience, but the combination of zinc and ouabain produced a significant reduction in resilience relative to both zinc-alone controls (treated: 73.338 ± 8.761; control: 76.847 ± 9.468; p = 0.035) and ouabain-alone controls (treated: 77.468 ± 7.065; control: 84.697 ± 7.676; p = 0.001). Thus, although ouabain does not independently alter resilience, its presence in combination with zinc unmasks a measurable decrease in the lens's ability to recover after compression. Together, these findings show that zinc and ouabain do not synergize to modify zinc-dependent changes in stiffness (b-coefficient), but they do interact to significantly reduce resilience, revealing a combined effect on the recovery phase of lens biomechanics.

Next, to check the effect of zinc on the lens water content, lenses were treated with hyperosmolar Tyrode's solution. This treatment produced a distinct subcapsular gap between the anterior capsule and underlying lens substance in both treated and control groups, as both were subjected to the same hyperosmolar stress. The same lenses were returned to iso-osmolar conditions: control lenses were incubated in iso-osmolar Tyrode's solution, whereas treated lenses were incubated in Tyrode's solution containing 80 µg/ml zinc.

We found that both control and zinc-treated lenses exhibited a significant increase in total cross-sectional area (Fig. 3.9) relative to their hyperosmolar state (control: $p < 0.001$; zinc-treated: $p = 0.012$).

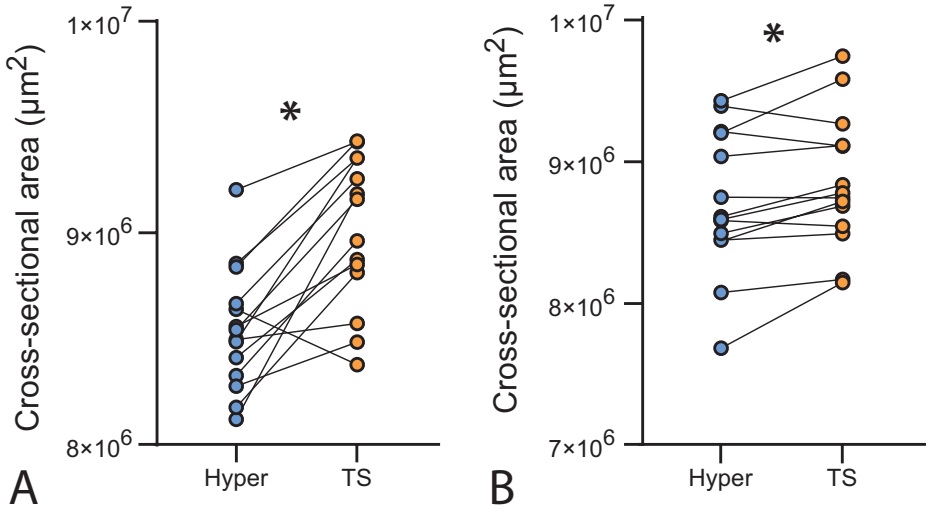


Figure 3.9: Paired dot plots of cross-sectional area of lenses **(A)** treated with hyperosmolar solution and followed by recovery in isosmolar Tyrode's solution ($p < 0.001$). **(B)** Shows the cross-sectional area of lenses treated with hyperosmolar solution and subsequent recovery in zinc solution ($p = 0.012$).

In control lenses, incubation in iso-osmolar Tyrode's solution did not alter the subcapsular

gap (Fig. 3.10 and Fig. 3.12) compared with the hyperosmolar condition ($p = 0.669$), indicating that simple osmotic recovery was insufficient to restore capsule-cortex apposition.

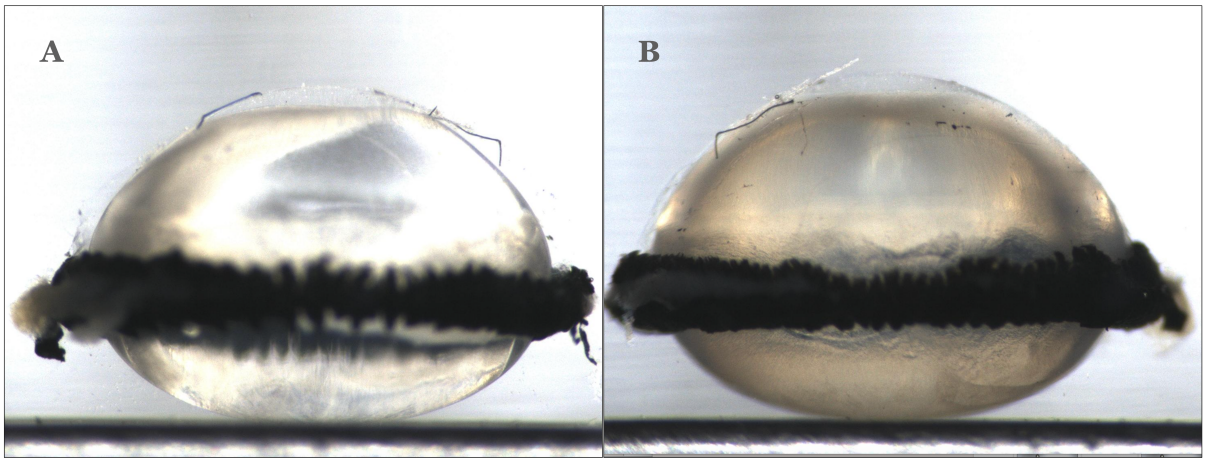


Figure 3.10: Photographs of a lens exposed to **(A)** hyperosmolar conditions and **(B)** subsequent recovery in isosmolar Tyrode's solution at room temperature.

In contrast, lenses treated with zinc following hyperosmolar stress showed a significant reduction in the subcapsular gap ($p > 0.001$), demonstrating that zinc uniquely promotes re-apposition of the capsule to the underlying lens tissue (Fig. 3.11 and Fig. 3.12).

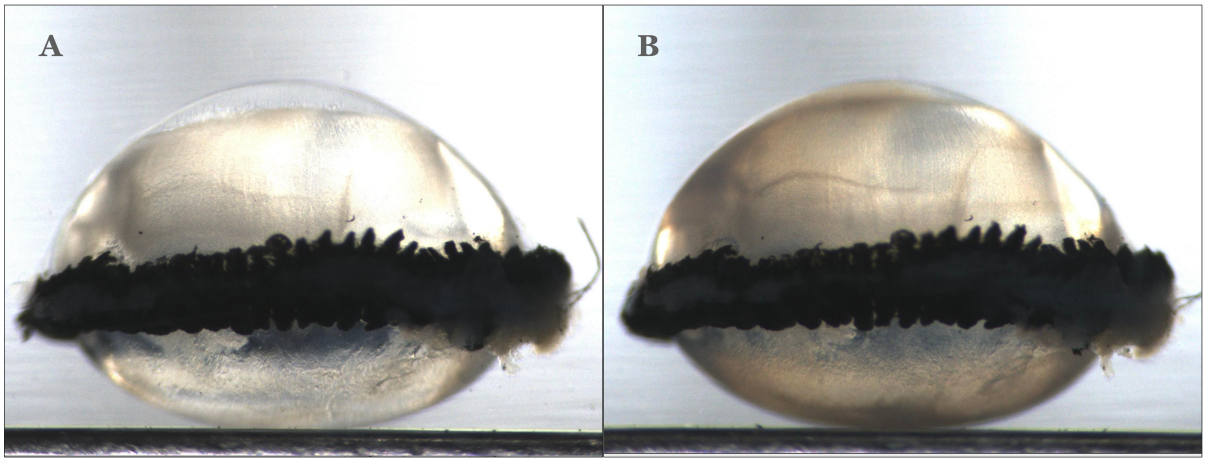


Figure 3.11: Photographs of a lens exposed to **(A)** hyperosmolar conditions and **(B)** subsequent recovery in zinc solution at room temperature.

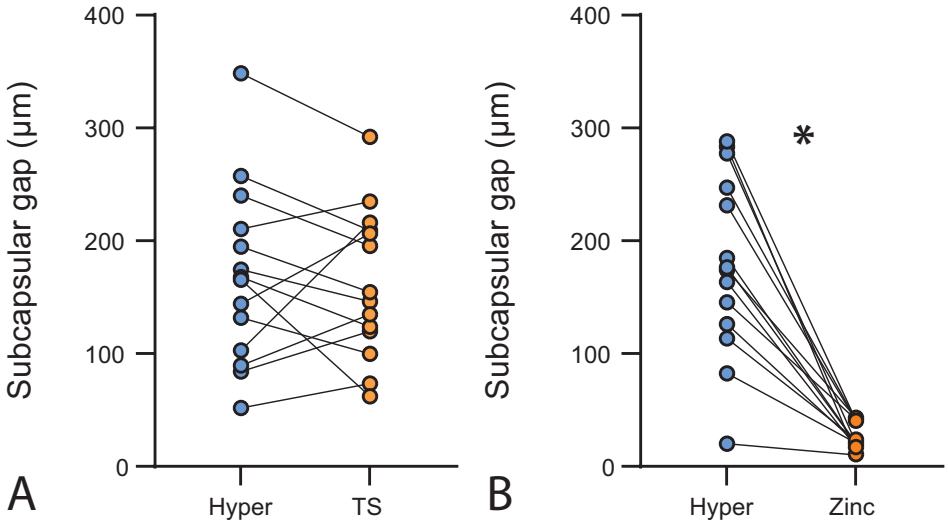


Figure 3.12: Paired dot plots of the subcapsular gap of lenses **(A)** treated with hyperosmolar solution and followed by recovery in isosmolar Tyrode's solution. **(B)** Shows the subcapsular gap of lenses treated with hyperosmolar solution and subsequent recovery in zinc solution ($p > 0.001$).

3.4 Discussion

The precise mechanism underlying the increase in the stiffness of the lenses with the application of zinc (Fig. 3.2) remains unclear. However, findings from the permeability study (Fig. 3.12) suggest that this increased stiffness might be due to an increase in the water content within lens fibres, driven by zinc-AQP0-mediated water inflow. This concept aligns with a previous study showing that zinc increases the water permeability of AQP0 in *Xenopus* oocytes [Németh-Cahalan et al., 2007]. In contrast, the reduction in stiffness observed with Ht31 treatment (Fig. 3.3) further supports the water permeability hypothesis. Specifically, Ht31 uncouples PKA from the AQP0-AKAP signalling complex, decreasing PKA-mediated phosphorylation of AQP0 and allowing calmodulin to bind and suppress AQP0 water permeability. [Reichow and Gonen, 2008, Reichow et al., 2013, Kalman et al., 2008]. This antagonist-driven channel closure is expected to decrease water content in the lenses, thereby yielding softer lenses. Additionally, reduction in the subcapsular gap size with zinc treatment demonstrates that zinc accelerates water re-entry into the lens, supporting the idea that AQP0 acts as an inherently slow water channel under baseline conditions [Jensen et al., 2008]. Both control and zinc-treated lenses can overcome the shrinkage/compaction induced by hyperosmolarity. This suggests that the lens may possess an intrinsic volume-regulatory mechanism that restores water balance following osmotic stress.

Although zinc and Ht31 altered lens stiffness, resilience remained unchanged in both conditions (Fig. 3.2 and 3.3). This suggests that stiffness and resilience may be controlled by different mechanisms: stiffness appears to depend primarily on lens water content, whereas resilience may rely on the structural integrity of the cytoskeleton or cell matrix.

Co-treatment with zinc and insulin removed the zinc-induced increase in stiffness (Fig. 3.5). This finding implies that insulin-stimulated NKA activity counteracts zinc-driven water influx, consistent with the role of NKA in extruding ions to promote water efflux [Mathias et al., 2007] and oppose AQP0-mediated water influx. The lack of effect on resilience further supports the idea that insulin restores osmotic balance without disturbing structural recovery pathways.

Compared to ouabain-alone, the combined treatment of zinc and ouabain preserved the zinc-dependent increase in stiffness, indicating that ouabain does not prevent the zinc-induced stiffening (Fig. 3.7). This suggests that AQP0-mediated water influx can still increase lens hydration even when NKA is inhibited. However, resilience was significantly reduced relative to both zinc-alone (Fig. 3.8) and ouabain-alone controls (Fig. 3.7). This impairment of structural recovery (resilience) suggests that while zinc increases water influx, NKA inhibition by ouabain likely prevents efficient ion redistribution and volume regulation following mechanical compression, consistent with an established role of NKA in volume regulation [Shahidullah et al., 2012b].

The absence of significant changes in stiffness or resilience following treatment with either insulin (Fig. 3.4) or ouabain (Fig. 3.6) indicates that the lens relies on compensatory mechanisms to buffer NKA activity. While individual treatments fail to alter stiffness or resilience, these findings suggest that modulating NKA activity only affects lens biomechanics under homeostatic stress, such as during zinc-induced osmotic disturbance.

Chapter 4

TRPV1 and TRPV4 presence in the chicken crystalline lens and the effect of their modulation on biomechanics and protein expression

4.1 Introduction

Transient receptor potential (TRP) channels form a wide superfamily of ion channels [Cosens and Manning, 1969, Minke et al., 1975, Chen et al., 2020] and play an essential role as cellular sensors of temperature, pain [Caterina et al., 1997], pressure, and osmotic changes [Sackin, 1995]. TRPs are broadly categorized into subfamilies [Clapham, 2003, Zhang et al., 2023], with the vanilloid receptor subfamily being notable for its roles in sensing various stimuli [Caterina et al., 1997]. Among these, the transient receptor potential vanilloid 1 (TRPV1) and transient receptor potential vanilloid 4 (TRPV4) channels exhibit unique structural features and functional properties

[Caterina et al., 1997, Liedtke et al., 2000, Gladkikh et al., 2021]. TRPV1 is composed of 838-839 amino acids and forms a tetramer with intracellular N- and C-termini [Caterina et al., 1997, Moiseenkova-Bell et al., 2008]. Each unit of TRPV1 consists of six transmembrane helices, which are topographically similar to voltage-gated potassium channels [Liao et al., 2013, Aguado-Llera et al., 2012]. TRPV1 plays a crucial role in thermoregulation and osmoregulation in various tissues [Tominaga et al., 1998, Nishihara et al., 2011]. TRPV4 consists of 871 amino acids with a similar structure to that of TRPV1 [Liedtke et al., 2000]. TRPV4 is also implicated in a wide range of physiological functions, including mechanotransduction, osmoregulation, and inflammatory responses [Michalick and Kuebler, 2020]. TRPV4 also has a significant role in maintaining cellular and systemic homeostasis [Kumar et al., 2018, Goswami et al., 2010].

TRPV1 and TRPV4 are found in retinal ganglion cells and control the apoptosis of the cells [Sappington et al., 2009, Ryskamp et al., 2011]. TRPV1 is located in sensory neurons of the cornea, where it helps to detect various stimuli [Alamri et al., 2015]. TRPV1 is also located in both the corneal epithelium and stroma, and during corneal injury, TRPV1-expressing nerve cells are in close relationship to the corneal immune cells and associated with neuropathic pain [Jiao et al., 2021]. TRPV1 and TRPV4 are co-expressed in the non-pigmented ciliary epithelium and respond to mechanical and osmotic stress and are hypothesized to regulate intraocular pressure in the eye [Shahidullah and Delamere, 2023, Delamere and Shahidullah, 2022]. TRPV1 responds to cell shrinkage, leading to an influx of calcium ions and activation of the PI3K-ERK-Akt-WNK cascade, which further upregulates the activity of sodium-potassium-chloride cotransporter 1 (NKCC1) and restores ion and water balance. However, TRPV4 activates

in response to cell swelling or mechanical stretch, which opens the connexon hemichannels and allows calcium influx. This leads to the release of ATP and the activation of purinergic receptors, which further stimulates the sodium-potassium ATPase pump (NKA) and maintains epithelial homeostasis [Gao et al., 2015, Shahidullah et al., 2020]. TRPV1 and TRPV4 are important parts of the lens microcirculatory system (MCS), which is essential to maintain the lens's constant volume, transparency, and nutrient supply [Gao et al., 2015, Nakazawa et al., 2019, Vaghefi and Donaldson, 2018].

TRPV1 is present in the dorsal root ganglion and regulates nociceptive behavior in chickens. It is also reported that the activity of chicken TRPV1 is regulated by extracellular sodium ions [Uzura et al., 2020]. It has been shown that chickens express the TRPV4 channel. Its regulatory N-terminus is highly conserved across species, with the chicken N-terminus sharing around 67% similarity with human TRPV4 [Goretzki et al., 2022]. TRPV4 is expressed in chicken skin and has a role in peripheral thermal regulation [Cristina-Silva et al., 2022]. Despite extensive work on TRP channels in avian physiology, no studies have demonstrated the presence of TRPV1 and TRPV4 in chicken lenses. Because chickens rely on active lenticular accommodation and develop age-related presbyopia similar to humans [Choh et al., 2002], identifying the homeostatic mechanisms governing the avian lens provides critical insight into broader vertebrate lens biomechanics. The present study was therefore designed to determine whether TRPV1 and TRPV4 are expressed in the chicken lens and to examine how selective activation or inhibition of these channels affects the lens biomechanics. I hypothesized that TRPV1 and TRPV4 are present in the chicken lenses and can be modulated to change lens stiffness and resilience.

4.1.1 Modulators of TRPV1 and TRPV4

Capsaicin is a naturally occurring homovanillic acid derived from the capsicum that imparts the characteristic pungency and thermal sensation to chili peppers. Functionally, it acts as a highly lipophilic agonist of the TRPV1 ion channel [Bevan and Szolcsányi, 1990, Caterina et al., 1997, Yang and Zheng, 2017]. Structural studies using cryo-electron microscopy (cryo-EM) have demonstrated that capsaicin partitions into the lipid bilayer plasma membrane to access the allosteric, hydrophobic binding pocket located within the transmembrane domain of TRPV1. This molecular docking initiated a downstream structural shift, widened the lower activation gate, and stabilized the open conformation of the central non-selective cation pore [Cao et al., 2013, Liao et al., 2013]. It has been shown that capsaicin-mediated activation of TRPV1 in the mouse lens epithelial cells initiates a signaling cascade that rapidly phosphorylates the sodium-potassium-chloride cotransporter 1 (NKCC1). Once phosphorylated, NKCC1 drives a large influx of sodium, potassium, and chloride ions into the cells, followed by an increase in the intracellular hydrostatic pressure [Shahidullah et al., 2020]. However, Nakazawa et al. (2021) have discovered that applying capsaicin to activate TRPV1 in the lens actually causes TRPV4 to insert into the membrane and initiate a biphasic increase in surface hydrostatic pressure. The ultimate physiological result is an anti-swelling compensatory response mediated by shifting TRPV4 to the membrane [Nakazawa et al., 2021]

On the other hand, this activation cascade of TRPV1 can be selectively inhibited by AMG9810, a synthetic N-aryl cinnamide and potent antagonist [Gavva et al., 2005]. Structural and cryo-electron microscopy analyses indicate that AMG9810 competitively occupies

the orthosteric vanilloid pocket located within the transmembrane domain of the TRPV1 channel [Cao et al., 2013]. By physically occluding this binding pocket, AMG9810 effectively prevents the docking of both exogenous and endogenous vanilloid ligands [Gavva et al., 2005]. This molecular interaction stabilizes the lower activation gate of TRPV1 in a rigid, non-conducting apo-closed conformation [Cao et al., 2013]. Therefore, the binding of AMG9810 functionally uncouples multiple upstream chemical and noxious stimuli from channel pore opening and downstream ion conduction [Gavva et al., 2005].

The synthetic GlaxoSmithKline compound GSK1016790A functions as a highly potent and selective agonist of the TRPV4 ion channel [Thorneloe et al., 2008, Shahidullah et al., 2012b]. Upon binding, GSK1016790A promotes a conformational change that stabilizes the TRPV4's open state, facilitating a robust influx of extracellular calcium down its electrochemical gradient into the cell [Shahidullah et al., 2012b, Mihara et al., 2016]. This immediate, localized elevation in cytoplasmic calcium concentrations acts as a secondary messenger, triggering the functional opening of connexin and pannexin hemichannels. The open probability of these hemichannels allows the outward passage of intracellular purinergic molecules, facilitating the localized release of adenosine triphosphate (ATP) in the extracellular clefts. This extracellular ATP acts through an autocrine or paracrine feedback loop by binding to local purinergic receptors, which activate downstream Src family tyrosine kinases (SFKs). This signaling cascade upregulates sodium-potassium ATPase (NKA) catalytic pump activity to drive regulatory volume changes and preserve homeostatic ionic concentrations [Shahidullah et al., 2012b, Shahidullah et al., 2017].

Conversely, RN-1734 is a highly selective, synthetic small-molecule TRPV4 antagonist that effectively uncouples multiple upstream stimuli from pore opening [Vincent et al., 2009,

Shahidullah et al., 2012b]. It locks the channel in an apo-closed, non-conducting state, preventing hemichannel-mediated ATP release and downstream cascades even when cells are challenged by mechanical stretch, hypo-osmotic swelling, or direct chemical agonist stimulation by RN-1747 [Shahidullah et al., 2012b, Thorneloe et al., 2008]. Specifically, in porcine lens epithelial cells, RN-1734-mediated blockade of TRPV4 suppresses the initial cytoplasmic calcium transient, completely blocking downstream hemichannel-mediated ATP release and NKA activity [Shahidullah et al., 2012b]

4.2 Material and Methods

Western blotting was used to confirm the presence of TRPV1 and TRPV4 in the chicken lens; the procedure for which is detailed below in Section 4.2.2 (Western Blot). The experimental model and lens dissection protocol were similar to those in Section 3.2.3 (Biomechanical testing) of Chapter 3. The sole modification in the experimental design is the use of physiological temperature ($36 - 37°C$) in addition to room temperature (RT).

Unlike section 3.2.3 (Biomechanical testing) of Chapter 3, which only used the room temperature (RT) environment, the microtester fluid bath chamber was also equipped with continuous thermal regulation to maintain the testing fluid bath container with Tyrode's solution at a physiological temperature ($36 - 37°C$) throughout the duration of the biomechanical testing.

All statistical analyses were conducted as in Section 3.2.5 of Chapter 3; the impact of the treatments (GSK1016790A, RN-1734, capsaicin, and AMG 9810) on lens biomechanics

(stiffness and resilience), TRPV4 protein expression, and intracellular potassium levels was assessed using a paired t-test, comparing treated lenses with their respective vehicle-treated controls. A p-value of less than 0.05 was considered significant for all tests.

4.2.1 Lens Treatment

One lens from each bird was exposed to an experimental treatment, while the contralateral lens served as a vehicle control. To evaluate the TRPV4 activation, GSK1016790A (M2028, Millipore Sigma, Oakville, Ontario, Canada; 100 nM) was prepared using a multistep serial dilution protocol to ensure precise molarity. A master stock solution was initially prepared by dissolving 1 mg of solid GSK1016790A in 100 µL of anhydrous dimethyl sulfoxide (DMSO). The intermediate stock solution was subsequently prepared by diluting 1 µL of this master stock into 999 µL of Tyrode's solution (TS). Finally, the experimental 100 nM working solution was prepared in a total volume of 50 mL by adding 328 µL of the intermediate dilution into 49.672 mL of TS. Contralateral control lenses were subjected to an identical protocol using a control solution, which was prepared by adding an equivalent volume of pure DMSO vehicle to TS in the absolute absence of the GSK1016790A compound.

For TRPV4 inhibition, the lenses were treated with a selective antagonist, RN-1734 (616520, Millipore Sigma, Oakville, Ontario, Canada; 10 µM). A master stock solution was prepared by dissolving 3.533 mg of RN-1734 in 1 mL of 100% DMSO to achieve a stable concentrate. Final 10 µM working solution was subsequently prepared by adding 50 µL of the master stock into 50 mL volumes of TS.

For TRPV1 activation, the lenses were treated with capsaicin (M2028, Millipore Sigma,

Oakville, Ontario, Canada; 5 µM). A master stock was prepared by dissolving 3.054 mg of solid capsaicin in 1 mL of pure DMSO. The final working concentration of 5 µM was achieved by introducing 25 µL of this master stock into 50 mL of TS.

For TRPV1 inhibition, AMG 9810 (A2731, Millipore Sigma, Oakville, Ontario, Canada; 10 µL) was used, and a master stock was prepared by dissolving 3.374 mg of the compound in 1 mL of 100 % DMSO, and a final working concentration of 10 µM was achieved by quantitatively transferring 50 µL of the master stock into 50 mL volumes of TS. Contralateral control lenses were subjected to an identical incubation protocol using a vehicle control buffer prepared by adding an equivalent volume of pure DMSO to TS in the absolute absence of agonists or antagonists. The final concentration of the DMSO vehicle across all treated and control lenses was strictly maintained at a negligible, non-toxic baseline ($\ll 0.1\%$ v/v), and preliminary measurements confirmed that the addition of agonist/antagonist induced no significant changes in solution osmolarity. All lenses were incubated either at room temperature ($\sim 22^{\circ}$C) or physiological temperature of $36 - 37^{\circ}$C for 2 hours prior to subsequent biomechanical testing, western blotting, or potassium assays.

4.2.2 Western Blot

After treatment with modulators and compression under the microtester, the same lenses were used for western blotting to evaluate changes in the protein expression of TRPV4 following the application of modulators. The lenses were homogenized with a small pestle in radioimmunoprecipitation assay buffer (RIPA; 20-188, Millipore Sigma, Oakville, Ontario, Canada) with ethylenediaminetetraacetic acid (EDTA)-free protease inhibitor

cocktail (1183617001, Millipore Sigma, Oakville, Ontario, Canada) and phosphatase inhibitors (4906845001, Millipore Sigma, Oakville, Ontario, Canada). Then, the lysates were centrifuged at 14000 RCF for 15 minutes at 4°C, and the supernatants were collected. The quantification of the total protein concentration in each lens was performed using the Bicinchoninic acid (BCA) assay protein kit (71285-3, Millipore Sigma, Oakville, Ontario, Canada). Then the protein lysates were mixed with Laemmli sample buffer and a reducing agent, ß-mercaptoethanol, and heated at 95°C for 5 minutes. Equal amounts of total protein (40 µg per well) were loaded alongside a molecular weight marker (ladder) in precast 4-15% TGX Stain-free gels (4568084, Bio-Rad Laboratories Ltd, Mississauga, Ontario, Canada) and separated according to molecular weight.

The gels were transferred to polyvinylidene difluoride (PVDF; 1704274, Bio-Rad Laboratories (Canada) Ltd, Mississauga, Ontario, Canada) membranes. Then the membranes were incubated in 5% bovine serum albumin (BSA) for 1 hour at room temperature (RT), followed by primary antibodies TRPV1 (1:1000, OST00105W, Osenses, Keswick, Australia) and TRPV4 (1:1000, OST00146W, Osenses, Keswick, Australia), incubated overnight at 4°C. The membranes were washed in Tris-buffered saline with Tween-20 (TBS-T) and incubated in horseradish peroxidase (HRP)- conjugated secondary antibody for 1 hour at RT. The membranes were washed again with TBS-T and visualized using an enhanced chemiluminescence (ECL) substrate on a ChemiDoc MP Imaging system (Bio-Rad Laboratories Ltd, Mississauga, Ontario, Canada). Both anti-GAPDH antibody (LS-C285516, Vector Labs, USA) and anti-beta-actin antibody (ab8224, Abcam Inc., Toronto, Ontario, Canada) were used as reference proteins to ensure equal loading across samples. The amount of protein expression was analyzed using ImageJ analysis software.

4.2.3 Potassium Assay

To evaluate how TRPV4 channel activation by GSK1016790A modulates NKA pump function, intracellular potassium ion concentration was quantified within chicken lenses. A paired contralateral experimental design was utilized for each animal (n=6), wherein one lens was isolated and exposed to the TRPV4 agonist GSK1016790A (100 nM), while the fellow control lens was treated with the respective vehicle control solution for 2 hours of incubation at $36 - 37$°C. Following the treatment, the lenses were stored at -80°C. On the day of the potassium assay, lenses were removed from -80°C storage and thawed on ice. Excess surface liquid was gently blotted using a filter paper (pre-rinsed with deionized water) before the lenses were weighed. Deionized water (DI) was used as the homogenization medium, as recommended by the colorimetric potassium (K) assay kit [NBP3-25780; Novus Biologicals, Centennial, CO, USA]. The homogenization medium was added at a ratio of 9:1 (e.g., 0.18 mL of DI water per 0.02 g of lens tissue; v:w). The lenses were homogenized on ice using a small pestle for 6-8 min. Subsequently, homogenates were centrifuged at $1,500 \times g$ for 10 min at 4°C. The resulting supernatants (tissue extracts) were transferred to clean tubes, and aliquots were stored at -80°C for subsequent analysis.

The protein precipitant was prepared by mixing Reagent 1 and Reagent 2 at an 8:1 (v/v) ratio. The lens homogenate supernatant (tissue extract) was then mixed with the protein precipitant at a 1:9 ratio (20 µL supernatant to 180 µL of protein precipitant). This mixture was centrifuged at $1,100 \times g$ for 10 min at 4°C, and the clarified supernatants (samples) were collected for each lens. Then 50 µL of both samples and standards (50 µL) were loaded into individual wells of a 96-well plate, followed by the addition of 200 µL of

chromogenic agent to each well. The plate was covered with a lid and incubated for 5 min at room temperature. Immediately after incubation, the optical density (OD) was measured at 450 nm using a microplate reader. Standard curves were generated by plotting OD (y) against standard concentration (x). Total protein concentration was measured concurrently in the same supernatant using a (BCA) assay to normalize potassium levels per gram of protein.

4.3 Results

Western blot analysis was performed to verify the presence of TRPV1 and TRPV4 channels in the control lens tissue. The analysis revealed distinct bands for both TRPV1 and TRPV4 at approximately 98 kDa (Fig. 4.1), confirming the presence of both channel types within chicken lenses.

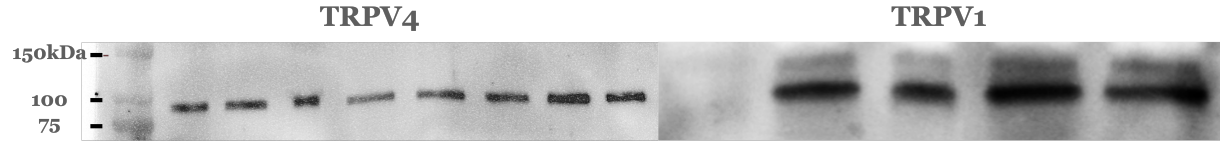


Figure 4.1: Western blot showing the presence of TRPV4 and TRPV1 protein expression in the lens tissue of different chickens, with distinct immunoreactive bands observed at approximately 98 kDa, with a secondary upper band near 100 kDa that likely corresponds to a glycosylated form of TRPV1 [Veldhuis et al., 2012]

.

4.3.1 The effect of the modulators of TRPV1 and TRPV4 on the lens biomechanics

We found that activation or inhibition of TRPV4 channels did not significantly alter lens stiffness or resilience at room temperature. The b-coefficient for lenses treated with TRPV4 agonist -GSK1016790A was 4.623 ± 0.582 (mean ± sd), which did not significantly differ (p = 0.275) from vehicle-treated controls (4.854 ± 0.546) (Fig. 4.2).

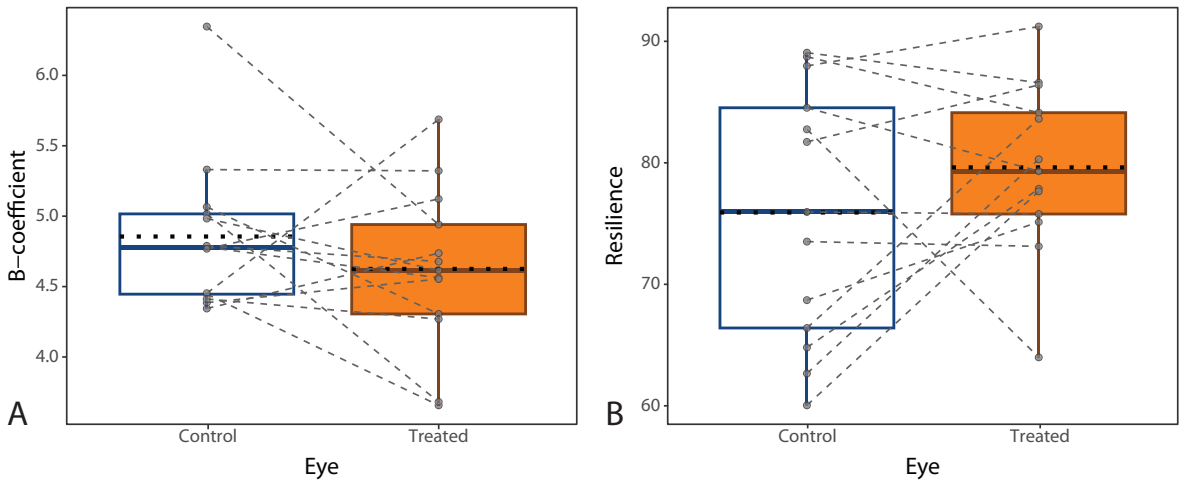


Figure 4.2: Box plots of the biomechanical responses of lenses treated with the TRPV4 agonist (GSK1016790A; filled boxes) or vehicle (empty boxes) at room temperature. **(A)** Exponential stiffness (b-coefficient) of lenses treated with GSK1016790A remained comparable to vehicle solution ($p = 0.275$). **(B)** Resilience values showed no significant difference between GSK1016790A and vehicle treatments ($p = 0.237$). Data are presented as mean ± sd ($n = 13$; paired t-test). Each pair of eyes is linked by dashed grey lines. Dotted black line = mean; dotted solid lines = median.

Targeted inhibition of TRPV4 using the antagonist RN-1734 yielded comparable results, showing no significant shifts in the b-coefficient (4.841 ± 0.407 vs. control: 4.740 ± 0.550; p = 0.635) (Fig. 4.3). Lens resilience at room temperature was likewise unaffected by

TRPV4 modulation, remaining statistically indistinguishable from controls during both GSK1016790A treatment (79.643 ± 7.039 vs. control: 75.930 ± 10.555; p = 0.237) and RN-1734 treated (80.325 ± 7.278 vs. control: 76.814 ± 10.112; p = 0.315).

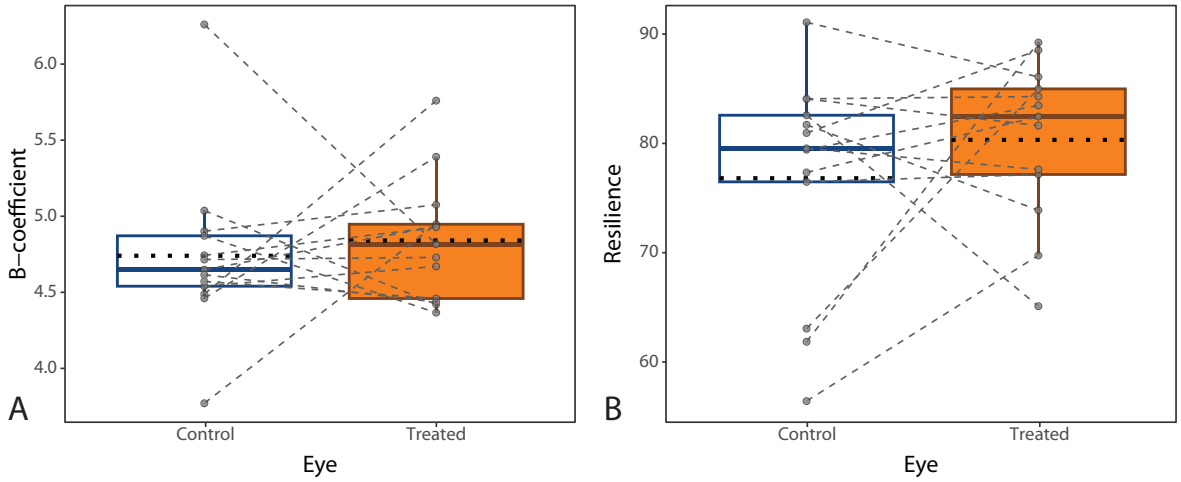


Figure 4.3: Box plots of the biomechanical responses of lenses treated with the TRPV4 antagonist (RN-1734; filled boxes) or vehicle (empty boxes) at room temperature. **(A)** Exponential stiffness (b-coefficient) of lenses treated with RN-1734 remained comparable to vehicle solution ($p = 0.635$). **(B)** Resilience values showed no significant difference between RN-1734 and vehicle treatments ($p = 0.315$). Data are presented as mean ± sd ($n = 13$; paired t-test). Each pair of eyes is linked by dashed grey lines. Dotted black line = mean; dotted solid lines = median.

Parallel experiments targeting TRPV1 channels at room temperature reveal a similar lack of mechanical responsiveness. The TRPV1 agonist capsaicin induced no significant changes in the b-coefficient (4.797 ± 0.365 vs. control: 4.828 ± 0.324; p = 0.822) or resilience (79.060 ± 6.914 vs. 80.848 ± 2.606; p = 0.243) (Fig. 4.4).

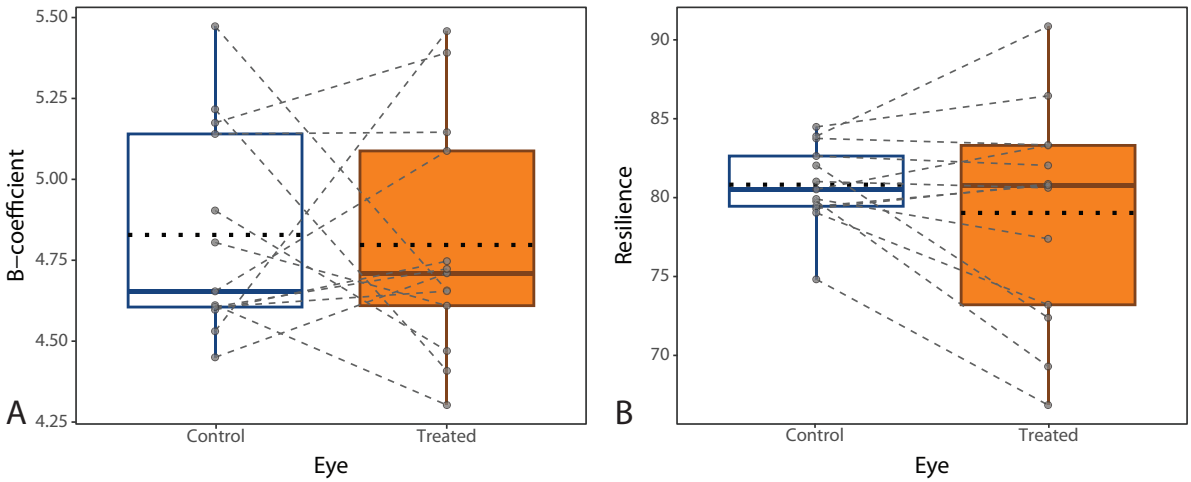


Figure 4.4: Box plots of the biomechanical responses of lenses treated with TRPV1 agonist (capsaicin; filled boxes) or vehicle (empty boxes) at room temperature. **(A)** Exponential stiffness (b-coefficient) of lenses treated with capsaicin remained comparable to vehicle solution ($p = 0.822$). **(B)** Resilience values showed no significant difference between capsaicin and vehicle treatments ($p = 0.243$). Data are presented as mean ± sd ($n = 13$; paired t-test). Each pair of eyes is linked by dashed grey lines. Dotted black line = mean; dotted solid lines = median.

Furthermore, treating lenses with TRPV1 antagonist, AMG 9810 failed to elicit any significant deviations in the b-coefficient (4.890 ± 0.398 vs. control: 4.917 ± 0.374; p = 0.847) or resilience (76.896 ± 5.281 vs. control: 74.254 ± 8.497; p = 0.308) (Fig. 4.5).

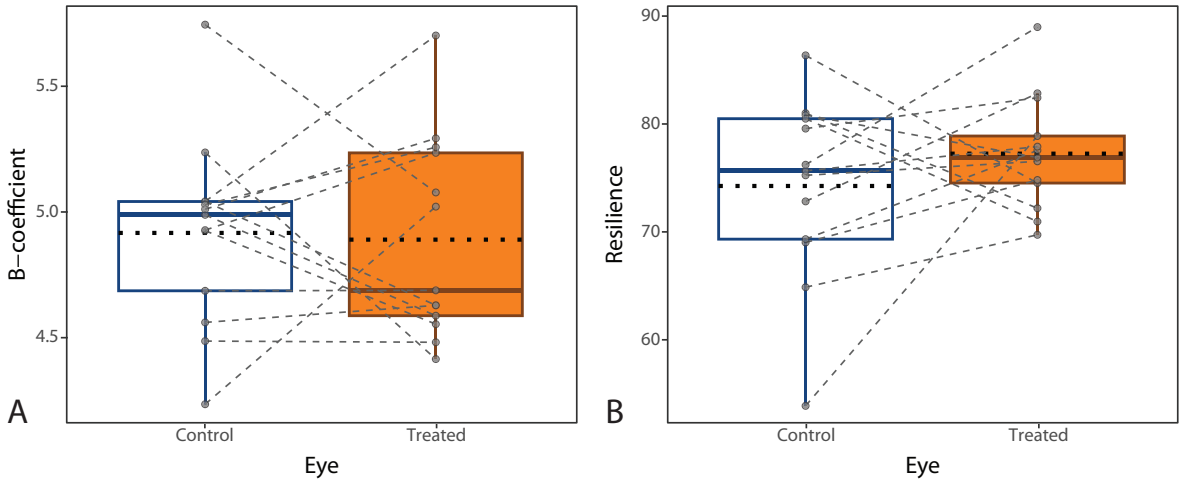


Figure 4.5: Box plots of the biomechanical responses of lenses treated with TRPV1 antagonist (AMG 9810; filled boxes) or vehicle (empty boxes) at room temperature. **(A)** Exponential stiffness (b-coefficient) of lenses treated with AMG 9810 remained comparable to vehicle solution ($p = 0.847$). **(B)** Resilience values showed no significant difference between AMG 9810 and vehicle treatments ($p = 0.308$). Data are presented as mean ± sd ($n = 13$; paired t-test). Each pair of eyes is linked by dashed grey lines. Dotted black line = mean; dotted solid lines = median.

In contrast to the results obtained at room temperature, shifting the experimental conditions to physiological temperature unmasked significant opposing biomechanical responses specifically linked to TRPV4 activities. When incubated at physiological temperature, TRPV4 activation via GSK1016790A significantly reduced the b-coefficient (Fig. 4.6) to 4.765 ± 0.310 compared to 5.022 ± 0.337 in the vehicle group (p = 0.033).

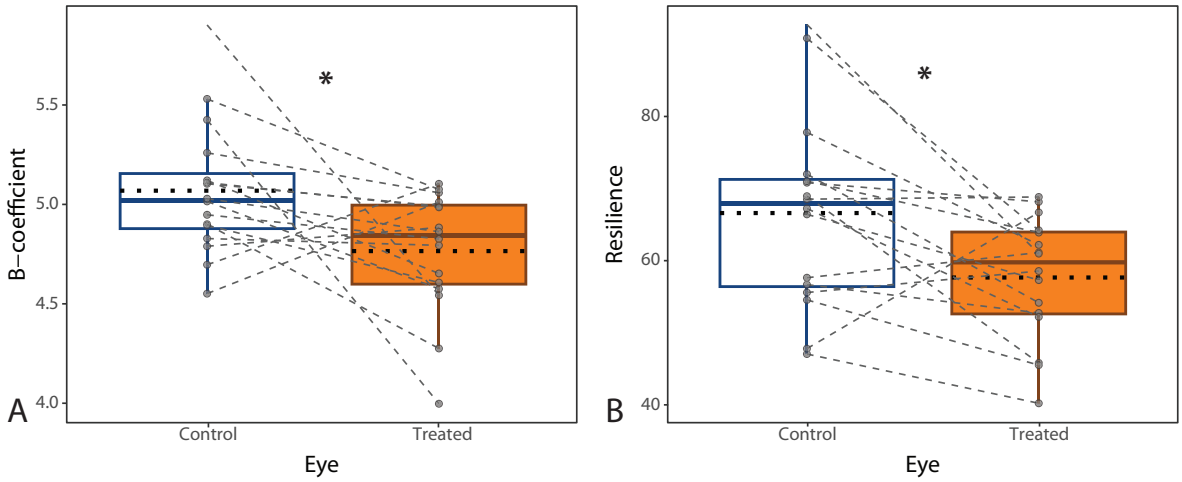


Figure 4.6: Box plots of the biomechanical responses of lenses treated with TRPV4 agonist (GSK1016790A; filled boxes) or vehicle (empty boxes) at physiological temperature. **(A)** Exponential stiffness (b-coefficient) of lenses treated with GSK1016790A showed a significant difference compared to the vehicle solution ($p = 0.033$). **(B)** Resilience values showed a significant difference between GSK1016790A and vehicle treatments ($p = 0.013$). Data are presented as mean ± sd ($n = 16$; paired t-test). Each pair of eyes is linked by dashed grey lines. Dotted black line = mean; dotted solid lines = median.

Conversely, TRPV4 inhibition via the antagonist RN-1734 significantly elevated the b-coefficient (Fig. 4.7)to 5.326 ± 0.476, relative to its respective vehicle-control of 4.952 ± 0.485 (p = 0.020). This pattern of TRPV4-mediated regulation was also reflected in the lens's resilience. GSK1016790A treatment significantly depressed lens resilience (57.662 ± 8.568 vs. control: 66.604 ± 13.304; p = 0.013). In contrast, targeted TRPV4 blockade with RN-1734 resulted in a resilience of 66.635 ± 11.724, which did not significantly differ (p = 0.526) from its corresponding vehicle control (62.833 ± 17.372).

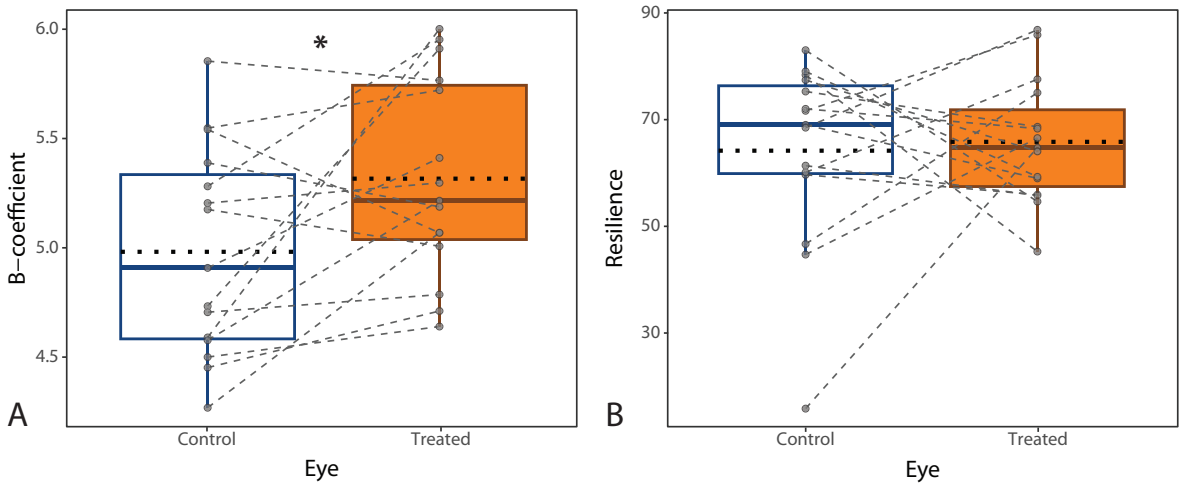


Figure 4.7: Box plots of the biomechanical responses of lenses treated with TRPV4 antagonist (RN-1734; filled boxes) or vehicle (empty boxes) at physiological temperature. **(A)** Exponential stiffness (b-coefficient) of lenses treated with RN-1734 (10 μM) significantly reduced compared to the vehicle solution ($p = 0.020$). **(B)** Resilience values showed no significant difference between RN-1734 and vehicle treatments ($p = 0.526$). Data are presented as mean ± sd ($n = 15$; paired t-test). Each pair of eyes is linked by dashed grey lines. Dotted black line = mean; dotted solid lines = median.

Unlike the changes observed within the TRPV4 channel, the TRPV1 channel remained unresponsive at physiological temperature. Exposure to the TRPV1 agonist capsaicin induced no significant changes (Fig. 4.8) in the b-coefficient (4.887 ± 0.347 vs. control: 4.953 ± 0.332; p = 0.576) or resilience (71.283 ± 11.209 vs. control: 71.306 ± 11.480; p = 0.996).

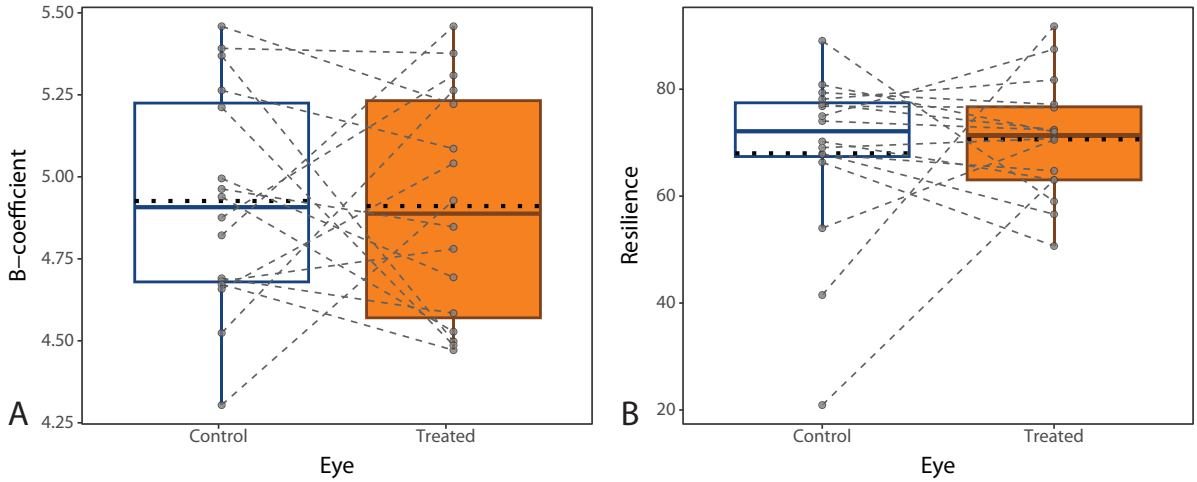


Figure 4.8: Box plots of the biomechanical responses of lenses treated with TRPV1 agonist (capsaicin; filled boxes) or vehicle (empty boxes) at physiological temperature. **(A)** Exponential stiffness (b-coefficient) of lenses treated with capsaicin remained comparable to the vehicle solution ($p = 0.576$). **(B)** Resilience values showed no significant difference between capsaicin and vehicle treatments ($p = 0.996$). Data are presented as mean ± sd ($n = 14$; paired t-test). Each pair of eyes is linked by dashed grey lines. Dotted black line = mean; dotted solid lines = median.

Similarly, the treatment with the TRPV1 antagonist AMG 9810 failed to elicit any statistically significant changes (Fig. 4.9) in the b-coefficient (4.829 ± 0.516 vs. control: 4.738 ± 0.327; p = 0.597) or resilience (66.391 ± 9.444 vs. control: 69.686 ± 10.262; p = 0.438).

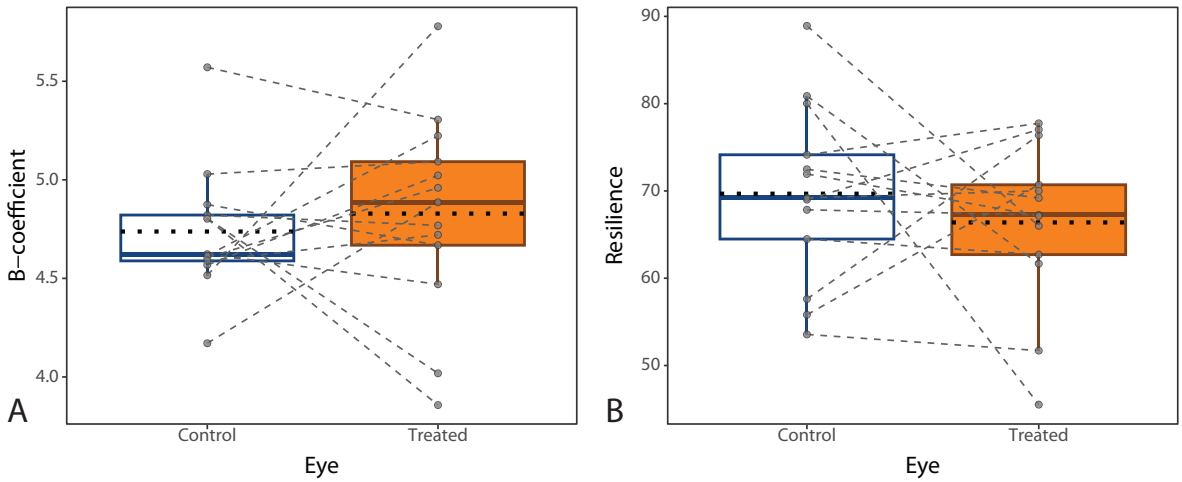


Figure 4.9: Box plots of the biomechanical responses of lenses treated with TRPV1 antagonist (AMG 9810; filled boxes) or vehicle (empty boxes) at physiological temperature. **(A)** Exponential stiffness (b-coefficient) of lenses treated with AMG 9810 (10 μM) remained comparable to the vehicle solution ($p = 0.597$). **(B)** Resilience values showed no significant difference between AMG 9810 and vehicle treatments ($p = 0.438$). Data are presented as mean ± sd ($n = 13$; paired t-test). Each pair of eyes is linked by dashed grey lines. Dotted black line = mean; dotted solid lines = median.

4.3.2 The effect of the modulators of TRPV4 on its protein expressions and lens' intracellular potassium levels

To determine whether TRPV4 agonist (GSK1016790A) and TRPV4 antagonist (RN-1734) also affect the protein expression of TRPV4 in the lens, western blotting was performed. The protein expression level in agonist-treated lenses was 4.387 ± 6.454 (mean ± sd), which did not significantly differ (p = 0.723) from vehicle-treated controls (1.796 ± 0.938). Similarly, the protein expression in antagonist-treated lenses (0.814 ± 0.427) remained unchanged (p = 0.691) relative to its respective controls (0.762 ± 0.247) (Fig. 4.10).

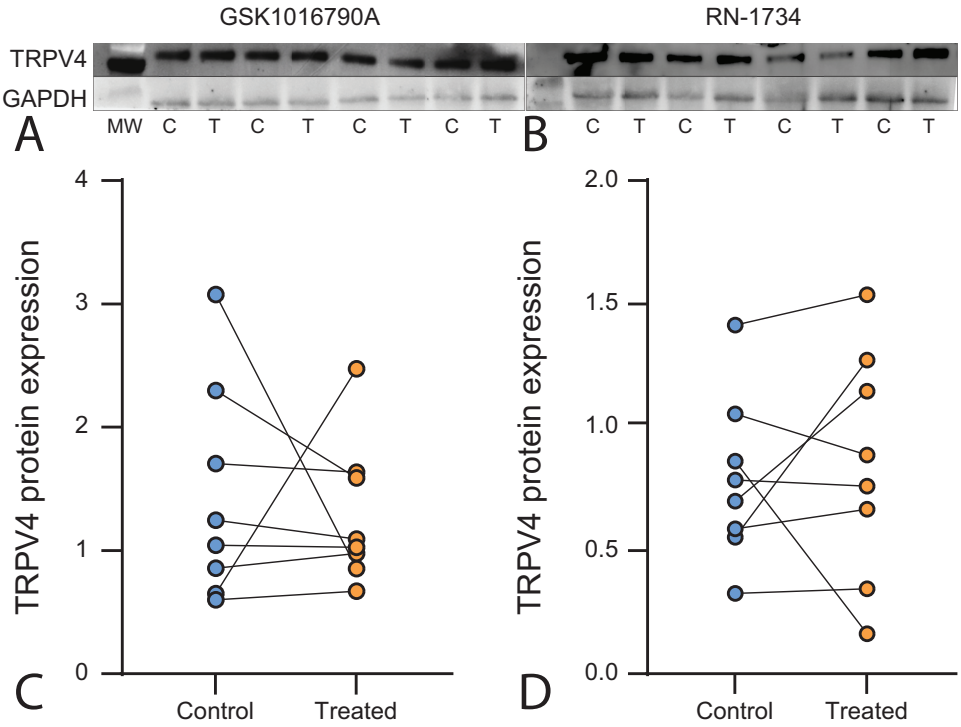


Figure 4.10: Western blots and paired dot plots of TRPV4 protein expressions in lenses treated with a TRPV4 agonist (GSK1016790A), antagonist (RN-1734), or vehicle control. **(A, C)** TRPV4 protein expressions in GSK1016790A treated lenses remained comparable to their vehicle control ($p = 0.723$). **(B, D)** Similarly, RN-1734 treatment showed no significant difference compared to its respective control ($p = 0.691$). TRPV4 signals were normalized to GAPDH and beta-actin (not shown). Data are presented as mean ± sd ($n = 8$, paired t-test). MW = molecular weight marker; C = control lenses; T = treated lenses.

In parallel, intracellular potassium levels were evaluated to determine the downstream activity of the sodium-potassium ATPase (NKA) pump following the application of the agonist (GSK1016790A) and antagonist (RN-1734) of TRPV4. The potassium level of GSK1016790A-treated lenses was 440.455 ± 53.272 (mean ± SD), which did not differ significantly (p = 0.856) from vehicle-treated controls (409.635 ± 116.797). Likewise,

intracellular potassium levels following antagonist treatment (371.137 ± 156.385) remained statistically unchanged (p = 0.492) from corresponding control values (426.121 ± 61.626) (Fig. 4.11).

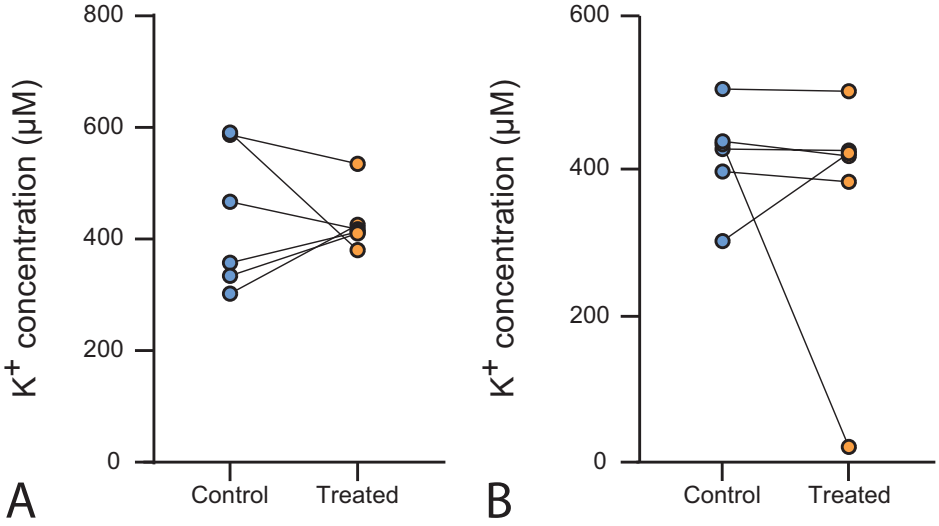


Figure 4.11: Paired dot plots of potassium ion concentrations in lenses treated with a TRPV4 agonist (GSK1016790A), antagonist (RN-1734), or vehicle control. **(A)** Potassium concentration in lenses treated with GSK1016790A remained comparable to their vehicle control ($p = 0.856$). **(B)** Similarly, potassium concentration in lenses treated with RN-1734 ($p = 0.492$) did not change compared to their respective vehicle controls. Data are presented as mean ± sd ($n = 6$; paired t-test).

4.4 Discussion

The confirmed protein expression of both TRPV1 and TRPV4 (Fig. 4.1) in chicken lens tissue, similar to findings in mammalian models such as mice, rats, and bovines [Delamere and Shahidullah, 2021, Shahidullah et al., 2020], suggests that the avian system may serve as a relevant model for studying microcirculation and biomechanics of the lens.

The absence of significant biomechanical changes with TRPV1 modulation with capsaicin or AMG9810 at room temperature (Fig. 4.4, 4.5) suggests that TRPV1 remains inactive at room temperature. This finding aligns with the understanding that TRPV1 typically responds to heat ($> 43°C$) [Caterina et al., 1997], protons, and vanilloids, with an activation threshold substantially higher than ambient experimental temperature. Similarly, the lack of biomechanical response at physiological temperature (Fig. 4.8, 4.9) could imply that TRPV1 activation primarily functions to stimulate NKCC1 cotransporter activity to mediate regulatory volume increase during hyper-osmotic stress or tissue shrinkage [Delamere et al., 2020, Gao et al., 2015]. Because these experiments were conducted under normo-osmotic conditions, the TRPV1 pathway may have remained functionally dormant, potentially explaining the lack of any changes in stiffness and resilience.

Likewise, the lack of change in stiffness and resilience following treatment with agonists or antagonists (Fig. 4.2, 4.3) at room temperature ($\sim 22°C$) suggests that TRPV4 may be insufficiently gated at room temperature. This is consistent with prior studies showing that TRPV4 is a polymodal, temperature-sensitive ion channel with an activation threshold near physiological body temperature ($\sim 27°C$ to $34°C$), displaying significant baseline activity under normal physiological conditions [Vriens et al., 2004, Güler et al., 2002].

At physiological temperature, the decrease in stiffness of lenses (Fig. 4.6) observed with the TRPV4 agonist (GSK1016790A) is likely driven by a dual-action mechanism involving both structural and osmotic remodeling. Specifically, TRPV4 activation might induce a localized influx of calcium, which can trigger calcium-dependent proteases (such as calpains). These proteases are known to target and degrade major cytoskeletal and structural proteins within the lens [Ryskamp et al., 2016]. This targeted remodeling of the cytoskeletal network

can directly reduce lens stiffness. Concurrently, elevated intracellular calcium may also promote pannexin hemichannel opening, ATP release, and downstream stimulation of sodium-potassium ATPase activity [Vincent et al., 2009, Shahidullah et al., 2012b]. These events could collectively promote structural remodeling and water efflux from the lens, explaining the observed lens softening upon application of a TRPV4-agonist. Conversely, the increased stiffness seen with inhibition of TRPV4 by RN-1734 suggests that blocking TRPV4 may reduce calcium influx and limit water efflux. This interpretation aligns with mammalian studies showing that TRPV4 blockade can elevate hydrostatic pressure by inhibiting NKA- mediated fluid flux [Gao et al., 2015, Delamere et al., 2020].

Reduction in the resilience of the lenses with TRPV4 activation could be linked to two potential mechanisms. First, agonist-induced TRPV4 activation might stimulate Na^+/K^+-ATPase activity and hemichannel opening, leading to water efflux and a loss of intracellular hydrostatic pressure [Gao et al., 2015]. This reduced fluid turgor could diminish the lens tissue's restorative force, preventing rapid shape recovery following microbeam compression. Alternatively, TRPV4-mediated calcium influx might trigger remodeling of the cytoskeleton and actin reorganization [Ryskamp et al., 2016], which could reduce tissue stiffness and accelerate stress relaxation during compression. In contrast, the absence of significant change in resilience with TRPV4 inhibition suggests that blocking the channel alters fluid flux without compromising the structural cytoarchitecture, thereby preserving the lens's baseline elastic recoil.

Finally, the lack of change in TRPV4 protein expression following GSK1016790A or RN-1734 treatments suggests that TRPV4 modulation likely involves channel gating rather than transcriptional or translational regulation, consistent with TRPV4's role as an

immediate mechanosensor that shows rapid activation kinetics independent of transcriptional regulation [Vriens et al., 2004]. Similarly, intracellular potassium levels remained unchanged following TRPV4 modulation, which aligns with prior studies suggesting that TRPV4 may influence NKA pump activity indirectly through purinergic signaling rather than through immediate changes in overall ion content or pump turnover [Shahidullah et al., 2012a, Shahidullah et al., 2012b].

Chapter 5

How modulators of the lens microcirculatory system regulate lens biomechanics at physiological temperature

5.1 Introduction

In Chapter 3, I found that modulating aquaporin 0 (AQP0) alone and co-modulating AQP0 and the Na^+/K^+-ATPase (NKA) pump alters lens biomechanics at room temperature. However, Chapter 4 revealed that TRPV4 channel modulation affects lens biomechanics only at physiological temperature. Given the temperature-dependent gating of TRPV4 channel, these observations highlight the need to evaluate whether the AQP0 and NKA-dependent mechanisms observed at room temperature are preserved under physiological thermal conditions.

Temperature plays a significant role in lens physiology. It has been shown that cooling

at 4°C induces reversible cataract formation, driven by γ- crystallin aggregation within the lens nucleus [Zigman and Lerman, 1964, Siezen et al., 1985]. Temperature shifts cause bovine α- crystallin oligomers to reorganize, expanding from approximately 550 kDa into larger, more polydisperse assemblies at both low (4°C) and high (50°C) temperatures [Vanhoudt et al., 1998]. Additionally, it has been shown that incubating corneas at 37°C leads to a minor decline in ATP levels [Greiner et al., 1983]. In mammalian lenses, it has been shown that there is a significant decline in the calcium efflux at 4°C compared to 37°C [Hightower et al., 1980]. An increase in the calcium level in the lens can lead to the activation of calcium-dependent proteases like calpains, which can digest membrane and cytoskeletal proteins like vimentin, filensin, and spectrin [Wang et al., 2001, Sanderson et al., 1996].

While temperature clearly alters crystalline interactions, ionic transport, and optical and structural properties, its direct effect on how room- and physiological-temperature conditions influence lens biomechanics has not been investigated. Therefore, the present study was designed to investigate these temperature-dependent biomechanical effects. I hypothesized that temperature significantly impacts lens biomechanics and that modulating AQP0 and NKA pump at physiological temperature yields distinct effects on lens stiffness and resilience compared to room temperature.

5.2 Material and Methods

To assess biomechanical changes under physiological temperature in response to modulators of AQP0 and NKA, the lens isolation protocol and compression testing were adapted from the methodology detailed in Section 3.2.3 (Biomechanical testing) of Chapter 3.

The experimental design is modified exclusively by the introduction of a physiological temperature ($36 - 37°C$).

For the initial comparative baseline experiments, the system was adjusted to evaluate lenses under both room temperature and physiological conditions. For all subsequent experiments involving AQP0 and NKA modulators, the microtester fluid bath chamber was maintained exclusively within a strict physiological range ($36 - 37°C$) for the entire duration of the mechanical compression.

All statistical analyses were performed using the protocols and software configurations detailed in section 3.2.5 of Chapter 3. As previously described, the threshold for statistical significance was established a priori at $p < 0.05$. To evaluate the independent effect of temperature on lens stiffness and resilience, differences between the room-temperature and physiological-temperature groups were analyzed using a two-tailed paired t-test to account for the contralateral, inter-ocular experimental design. For the subsequent modulation conducted exclusively at physiological temperature, treatment groups (zinc, Ht31, insulin, or ouabain) were compared directly against their respective contralateral vehicle-treated control lenses. Because these experiments utilized a matched-pair design (one drug-treated lens versus one vehicle-treated fellow lens per chicken), statistical comparisons were performed using two-tailed paired t-tests. Assumptions of normality were verified using the Shapiro-Wilk test.

5.2.1 Lens Treatment

Initial experiments evaluated the independent effect of temperature on lens stiffness and resilience using a paired contralateral design (n=13). For each bird, one lens was incubated in Tyrode's solution at room temperature while the fellow lens was incubated in Tyrode's solution at physiological temperature.

Subsequent experiments investigated whether the room temperature biomechanical changes observed in section 3.3 (Results) of Chapter 3 for aquaporin 0 (AQP0) and Na^+/K^+-ATPase (NKA) modulators persisted or shifted under physiological temperature. To modulate AQP0 function, lenses were incubated in Tyrode's solution (TS) for 15 mins at $36 - 37°C$ with either zinc chloride (80 µg/ml; n=14; 4906845001, Millipore Sigma, Oakville, Ontario, Canada) or the AQP0 antagonist, st-Ht31 (10µM; n=14; 6286, Bio-Techne Canada, Toronto, Ontario, Canada). To modulate NKA pump activity, lenses were treated with NKA agonist insulin (150 nM; n=13; I6634, Millipore Sigma, Oakville, Ontario, Canada) or NKA inhibitor ouabain (1 mM; n=14; O0200000, Millipore Sigma, Oakville, Ontario, Canada). The corresponding contralateral lenses were incubated in TS under identical thermal conditions. Solution osmolarity was verified prior to all experiments to ensure no significant shifts occurred with the addition of agonists or antagonists. Before microcompression testing, all lenses underwent a 1-minute rinse in fresh TS at physiological temperature to remove residual treatment drugs.

5.3 Results

5.3.1 The effect of temperature on the lens biomechanics

To assess the impact of temperature on lens biomechanics, the compression parameters (b-coefficient and resilience) of paired contralateral lenses were compared between room temperature and physiological temperature conditions. A paired t-test revealed that the b-coefficient was significantly higher under physiological temperature, increasing from 4.947 $\pm$ 0.364 at room temperature to 5.193 $\pm$ 0.366 at physiological temperature ($p = 0.040$). In contrast, lens resilience remained largely unaffected by thermal adjustments, showing no significant difference between the physiological temperature (76.727 $\pm$ 14.759) and room temperature (78.693 $\pm$ 8.594) with $p = 0.716$ (Fig. 5.1).

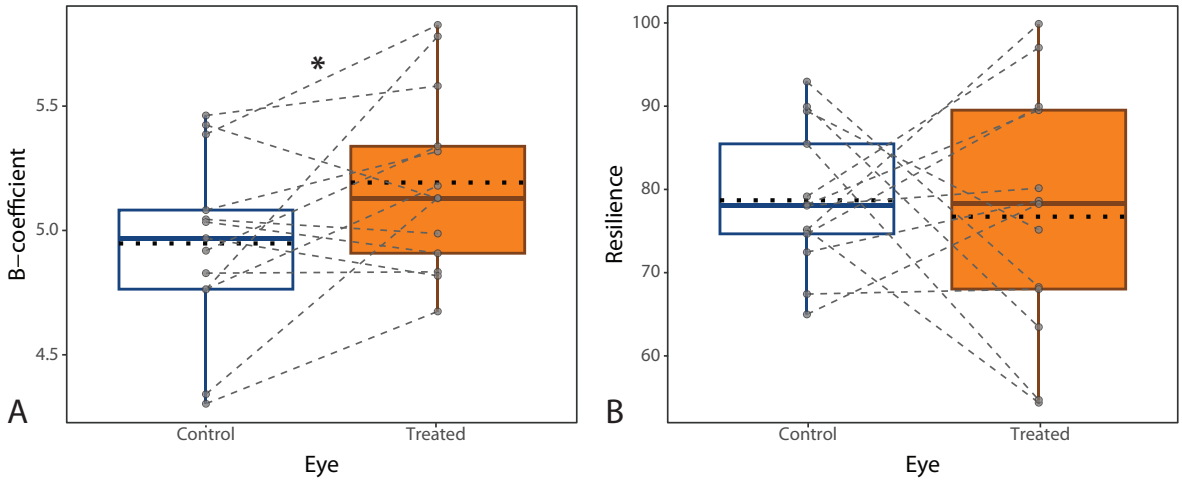


Figure 5.1: Box plots of the biomechanical responses of lenses in Tyrode's solution at physiological (filled boxes) or room temperature (empty boxes). **(A)** Exponential stiffness (b-coefficient) of lenses incubated at physiological temperature was significantly different compared to room temperature controls ($p = 0.040$). **(B)** Resilience values showed no significant difference between physiological and room temperature treatments ($p = 0.716$). Data are presented as mean ± sd ($n = 13$; paired t-test). Each pair of eyes is linked by dashed grey lines. Dotted black line = mean; dotted solid lines = median.

5.3.2 The effect of the modulators of the AQP0 and NKA pump on the lens biomechanics at physiological temperature

To evaluate the effects of AQP0 activation at physiological temperature, lenses were treated with the AQP0 agonist zinc chloride. The b-coefficient did not differ significantly between the zinc-treated (4.422 ± 0.311) and control lenses (4.441 ± 0.300; p = 0.075). Resilience of the lenses was also unaffected by zinc treatment, measuring 73.192 ± 11.165 compared to 72.035 ± 8.074 in the control group (p = 0.713)(Fig. 5.2).

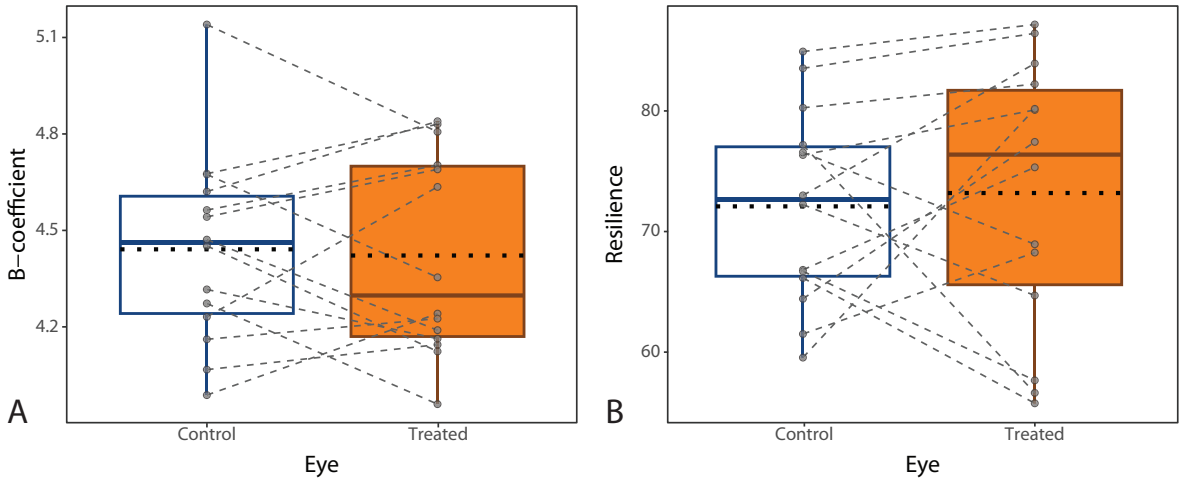


Figure 5.2: Box plots of the biomechanical responses of lenses treated with zinc (filled boxes) or vehicle (empty boxes) at physiological temperature. **(A)** Exponential stiffness (b-coefficient) of lenses treated with zinc (80μ/ml) showed no significant difference compared to vehicle control ($p = 0.075$). **(B)** Resilience values showed no significant difference between zinc and vehicle treatments ($p = 0.713$). Data are presented as mean ± sd ($n = 14$; paired t-test). Each pair of eyes is linked by dashed grey lines. Dotted black line = mean; dotted solid lines = median.

Targeted inhibition of AQP0 using the antagonist Ht31 did not yield statistically significant alterations in lens biomechanics at physiological temperature. No significant shifts were observed (Fig. 5.3) in the b-coefficient (4.555 ± 0.335 vs. control: 4.686 ± 0.365; p = 0.234) or lens resilience (80.383 ± 7.391 vs. control: 76.069 ± 9.621; p = 0.199).

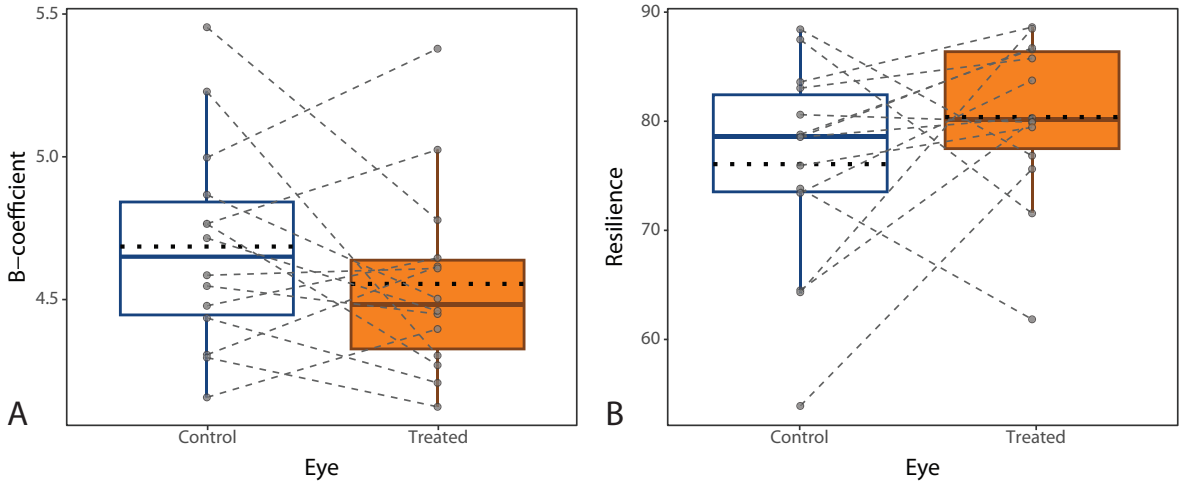


Figure 5.3: Box plots of the biomechanical responses of lenses treated with Ht31 (filled boxes) or vehicle (empty boxes) at physiological temperature. **(A)** Exponential stiffness (b-coefficient) of lenses treated with Ht31 (10μM) showed no significant difference compared to vehicle control ($p = 0.232$). **(B)** Resilience values showed no significant difference between Ht31 and vehicle treatments ($p = 0.199$). Data are presented as mean ± sd ($n = 14$; paired t-test). Each pair of eyes is linked by dashed grey lines. Dotted black line = mean; dotted solid lines = median.

Stimulation of NKA pump activity with insulin did not significantly modify any of the evaluated biomechanical properties at physiological temperature. The b-coefficient remained stable between groups (4.786 ± 0.594 vs. control: 4.718 ± 0.700; p = 0.610). Likewise, lens resilience under insulin treatment (77.131 ± 11.495) was statistically indistinguishable from control conditions (76.714 ± 9.184; p = 0.894) (Fig. 5.4).

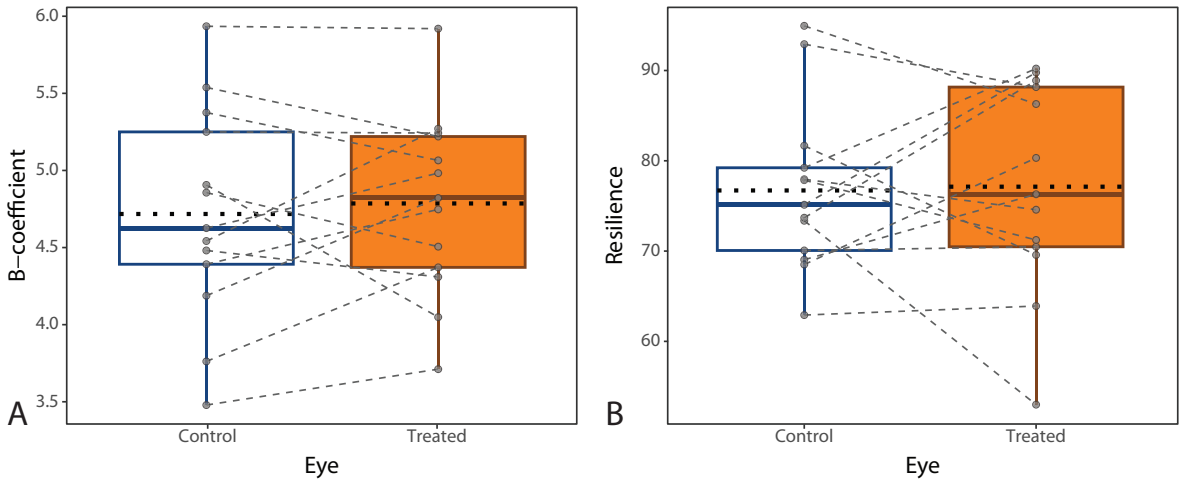


Figure 5.4: Box plots of the biomechanical responses of lenses treated with insulin (filled boxes) or vehicle (empty boxes) at physiological temperature. **(A)** Exponential stiffness (b-coefficient) of lenses treated with insulin ($100nM$) remained comparable to vehicle control ($p = 0.610$). **(B)** Resilience values showed no significant difference between insulin and vehicle treatments ($p = 0.894$). Data are presented as mean ± sd ($n = 13$; paired t-test). Each pair of eyes is linked by dashed grey lines. Dotted black line = mean; dotted solid lines = median.

Inhibition of the NKA pump using ouabain similarly failed to induce significant biomechanical changes at physiological temperature. No significant differences were detected in the b-coefficient (4.481 ± 0.716 vs. control: 4.621 ± 0.764; p = 0.442) or in lens resilience, which measured 49.516 ± 19.056 in the ouabain-treated group compared to 54.637 ± 21.828 in the controls (p = 0.329) (Fig. 5.5).

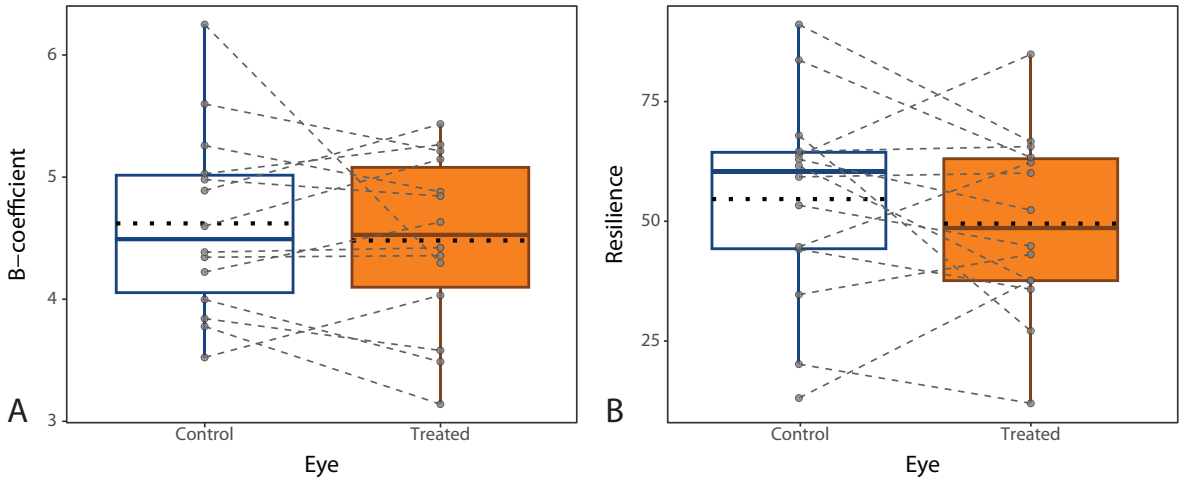


Figure 5.5: Box plots of the biomechanical responses of lenses treated with ouabain (filled boxes) or vehicle (empty boxes) at physiological temperature. **(A)** Exponential stiffness (b-coefficient) of lenses treated with ouabain remained comparable to vehicle control ($p = 0.442$). **(B)** Resilience values showing no significant difference between insulin and vehicle treatments ($p = 0.329$). Data are presented as mean ± sd ($n = 14$; paired t-test). Each pair of eyes is linked by dashed grey lines. Dotted black line = mean; dotted solid lines = median.

5.4 Discussion

The observed increase in stiffness of lenses at physiological temperature compared to room temperature (Fig. 5.1) without any modulators can be attributed to the baseline activation of polymodal, mechanosensitive TRPV4 channels. Previous studies have demonstrated that TRPV4 channels possess thermosensitivity and display baseline activity at normal physiological body temperature [Delamere et al., 2020, Nakazawa et al., 2021]. In the absence of an agonist, baseline TRPV4 activity triggers a sustained influx of Ca^{2+}, which has been shown to maintain the contractility of the actin cytoskeleton [Akepogu et al., 2026]. Additionally, TRPV4 can directly bind to the cytoskeletal network of tubulin and actin

proteins and physically stabilize the microtubule network under basal conditions in the dorsal root ganglion cells [Goswami et al., 2010]. Because TRPV4 (without any modulator) functions as a homeostatic thermostat linking fluid transport to the cytoskeletal organization, it plays a vital role in maintaining lens hydrostatic pressure. This may explain the elevated stiffness observed at physiological temperature while preserving biomechanical resilience. Additionally, given that TRPV4 physically colocalizes with intercellular junctional proteins such as N-cadherin and ZO-1 [Akepogu et al., 2026], enhanced thermal activation of TRPV4 may further stabilize junctional complexes, thereby increasing structural resistance to deformation. In parallel, temperature-dependent changes in the lipid bilayer may provide a complementary mechanism influencing AQP0 water permeability. Because AQP0 water permeability is fundamentally dependent on its surrounding lipid environment [Tong et al., 2013], elevated thermal energy at the physiological temperature increases membrane fluidity through alterations in lipid-cholesterol organization and phase behavior [de Almeida et al., 2003]. This enhanced fluidity can alter AQP0 conformation and transcellular water flux, thereby contributing to increased water content and elevated lens stiffness observed at the physiological temperature [de Almeida et al., 2003].

Activation of AQP0 by zinc at physiological temperature produced no significant change in lens stiffness and resilience (Fig. 5.2), suggesting that, at physiological temperature, compensatory homeostatic pathways, likely involving TRPV4-mediated calcium influx and hemichannel-dependent ATP signaling, are sufficiently active to buffer zinc-induced shifts in water permeability. These findings align with TRPV4's role in osmotic and thermal transduction in corneal epithelial cells [Lapajne et al., 2020]. Similarly, AQP0 inhibition with Ht31 (Fig. 5.3) failed to change lens stiffness and resilience at physiological temperature,

despite showing clear effects at room temperature. Although Ht31 is a known inhibitor of the AQP0 water permeability that acts by disrupting PKA-AKAP anchoring and preventing phosphorylation of AQP0 [Reichow et al., 2013, Reichow and Gonen, 2008], these findings can be explained by the hypothesis that increased temperature alters kinase and phosphatase activity [Oehler-Jänne et al., 2008]. Specifically, at physiological temperatures, accelerated enzymatic activity may sustain elevated levels of AQP0-phosphorylation, therefore overriding competitive inhibition normally imposed by Ht31 competition.

Additionally, the absence of significant changes in any of the lens biomechanical parameters at both room temperature and physiological temperature following NKA activation by insulin (Fig. 5.4) and inhibition by ouabain (Fig. 5.5), suggests that the lens possesses ionic homeostatic buffering capacities. This is likely maintained by reciprocal feedback between TRPV1 and TRPV4 signaling pathways involving NKCC1 and NKA, respectively. These findings align with the established role of the TRPV1/TRPV4 feedback loop in maintaining lens zero surface pressure and volume homeostasis [Delamere et al., 2020].

Chapter 6

Discussion and conclusion

The overall results of the thesis (Table 6.1) demonstrate that the chicken lens is an effective physiological model for evaluating biomechanical regulation via the microcirculatory system (MCS). Modulation of aquaporin 0 (AQP0) water channel activity at room temperature directly influenced lens hydrostatic pressure (water changes), indicating that AQP0-mediated water flow or volume redistribution underlies the lens's mechanical resistance to deformation. In contrast, changes in lens biomechanics driven by Na^+/K^+-ATPase (NKA) modulation appear to be connected to ionic and volume homeostasis. This suggests that the NKA pump may primarily become active when ionic or volume homeostasis within the lens is disturbed, as I observed in zinc-induced stress.

The confirmed protein expression of TRPV1 and TRPV4 in chicken lens tissue mirrors mammalian patterns [Delamere and Shahidullah, 2021, Shahidullah et al., 2020], identifying that TRPV1 and TRPV4 might operate through a reciprocal feedback loop to regulate

pressure and volume regulation like mammals. These findings suggest that NKA modulation operates through at least two distinct regulatory pathways: first, temperature-dependent changes in TRPV4 likely mediated by Ca^{2+} -triggered signaling cascades and hemichannels opening; insulin-stimulated NKA activation appears to function independently of this thermal modulation, pointing to a parallel mechanism for homeostatic buffering.

While TRPV4-mediated signaling was revealed by changing the experimental conditions from room temperature to physiological temperature, it remains unclear whether or how TRPV1 responds to noxious stimuli or osmotic imbalance. This study was restricted to non-noxious physiological conditions; baseline TRPV1 activity may have remained below its activation threshold. To evaluate TRPV1 function, future studies could investigate exposing lenses to hyperosmotic stress to test whether reciprocal TRPV1 activation counteracts cell shrinkage.

AQP0 and NKA modulation at physiological temperature failed to show any effect on lens biomechanics, suggesting that at body temperature, highly responsive, active homeostatic networks, likely involving the TRPV1-TRPV4 feedback loop or some other gating pathway, remain sufficiently active to buffer zinc-induced hydration changes or completely override the structural gating efficiency of calmodulin.

Limitations of this study: the lens compression was applied using a microtester oriented orthogonal to the lens's physiological accommodation, which occurs at the equatorial plane during zonule relaxation. While this directional loading aligns with previous studies [Cheng et al., 2016], it remains to be determined whether lens stiffness and resilience vary with the microbeam's compression direction, such as axial versus equatorial deformation.

Water permeability could not be measured directly following the application of AQP0 agonist or antagonist; instead, permeability changes were inferred indirectly by changing osmolarity and observing changes in subcapsular gap size. Therefore, changes in lens stiffness may reflect mechanisms independent of water permeability and hydrostatic pressure. Future investigations could address these limitations by measuring MCS permeability using magnetic resonance imaging [Lie et al., 2024], artificial proteoliposomes [Tong et al., 2013], or microelectrode-manometer hydrostatic pressure profiling [Gao et al., 2011]. Additionally, the current analyses largely rely on the assumption that the spatial distribution of key MCS components, TRPV1, TRPV4, AQP0, and AQP5 in avian lenses mirrors that of mammalian models, an expression profile that still requires confirmation in chicken lenses.

Moreover, intracellular calcium assays were not performed to directly verify whether TRPV4 agonist or antagonist treatments induced the anticipated fluctuations in intracellular calcium levels. The precise signaling cascades linking hydrostatic pressure variations to protein trafficking (e.g., TRPV4 distribution) and the broader functional impact of gap junction modulation on lens biomechanics also remain to be fully elucidated. Overall, while this study provides foundational insights, the exact molecular, spatial, and structural mechanisms governing these biomechanical responses require further elucidation.

In conclusion, given the presence of TRPV1, TRPV4, AQP0, and crystallins across vertebrate species, these insights provide a valuable foundation for understanding the precise cellular mechanisms and microcirculatory network that drive human lens stiffening and early-onset presbyopia, ultimately opening novel avenues for developing targeted, noninvasive therapeutic strategies for the aging lens. These findings highlight that the lens microcirculatory system is more dynamically regulated at physiological temperatures and

the importance of conducting biomechanical assessments under physiologically relevant temperature conditions to accurately capture the functional behavior of the living lens.

Table 6.1: Summary of the biomechanical changes in the lens as indicated by the b-coefficient and resilience under room and physiological temperatures (↑ indicates increase, ↓ indicates decrease, and = indicates no change)

Channel/target	**Temp**	**Modulator**	**B-coeff**	**Resilience**
Aquaporin 0 (AQP0)	20–22 °C	Zinc	↑	=
		Ht31	↓	=
Sodium–potassium ATPase pump (NKA)	20–22 °C	Insulin	=	=
		Ouabain	=	=
Transient receptor potential vanilloid 1 (TRPV1)	20–22 °C	Capsaicin	=	=
		AMG 9810	=	=
Transient receptor potential vanilloid 4 (TRPV4)	20–22 °C	GSK1016790A	=	=
		RN-1734	=	=
AQP0 + NKA	20–22 °C	Zinc + insulin	=	=
		Zinc + ouabain vs. ouabain	↑	↓
		Zinc + ouabain vs. zinc	=	↓
TRPV1	36–37 °C	Capsaicin	=	=
		AMG 9810	=	=
TRPV4	36–37 °C	GSK1016790A	↓	↓
		RN-1734	↑	=
AQP0	36–37 °C	Zinc	=	=
		Ht31	=	=
NKA	36–37 °C	Insulin	=	=
		Ouabain	=	=

Letter of Copyright Permission

The following page contains the copyright permission license from Elsevier for the reuse of figure (Fig. 2.3) in this thesis.

RightsLink



The physiological optics of the lens

Author: Paul J. Donaldson,Angus C. Grey,Bianca Maceo Heilman,Julie C. Lim,Ehsan Vaghefi
Publication: Progress in Retinal and Eye Research
Publisher: Elsevier
Date: January 2017

© 2016 Elsevier Ltd. All rights reserved.

Quick Price Estimate

This service provides permission for reuse only. If you do not have a copy of the content, you may be able to purchase a copy using RightsLink as an additional transaction. Simply select 'I would like to..... 'Purchase this content'.

Unclear about who you are?

A single table with multiple images should be treated as '1'. If you are using multiple unique figures, tables or illustrations, please enter the number being used.

Please note that, as the author of this Elsevier article, you retain the right to include it in a thesis or dissertation, provided it is not published commercially. Permission is not required, but please ensure that you reference the journal as the original source. For more information on this and on your other retained rights, please visit: https://www.elsevier.com/about/our-business/policies/copyright#Author-rights

I would like to...	reuse in a thesis/dissertation	I am the author of this Elsevier article...	Yes
I would like to use...	figures/tables/illustrations	I will be translating...	No
My number of figures/tables/illustra...	1	My currency is...	CAD - $
My format is...	both print and electronic		

This reuse is free of charge and does not require a license. Please print this page for your records.

PRICE: 0.00 CAD

CONTINUE

Publisher Terms and Conditions

To request permission for a type of use not listed, please contact Elsevier Global Rights Department.

Are you the author of this Elsevier journal article?

© 2026 Copyright - All Rights Reserved | Copyright Clearance Center, Inc. | Privacy statement | Data Security and Privacy | For California Residents | Terms and ConditionsComments? We would like to hear from you. E-mail us at customercare@copyright.com

References

Adams, D. R. (1929). The rôle of calcium in senile cataract. *Biochem J*, 23(5):902–912.

Aggett, P. J. and Comerford, J. G. (1995). Zinc and human health. *Nutr Rev*, 53(9 Pt 2):S16–22.

Agre, P., Sasaki, S., and Chrispeels, M. J. (1993). Aquaporins: A family of water channel proteins. *Am J Physiol*, 265(3 Pt 2):F461.

Aguado-Llera, D., Bacarizo, J., Gregorio-Teruel, L., Taberner, F. J., Cámara-Artigas, A., and Neira, J. L. (2012). Biophysical characterization of the isolated C-terminal region of the transient receptor potential vanilloid 1. *FEBS Letters*, 586(8):1154–1159.

Akepogu, J., Shikha, D., Kumar, B. K., Senthil, S., Bharadwaj, S. R., Goswami, C., and Ramachandran, C. (2026). Characterization of the functional transient receptor potential vanilloid channels 1 to 4 in human corneal endothelial cells. *Investigative Ophthalmology & Visual Science*, 67(1):20.

Al-Ghoul, K. J., Kirk, T., Kuszak, A. J., Zoltoski, R. K., Shiels, A., and Kuszak, J. R. (2003). Lens structure in mip-deficient mice. *Anat Rec A Discov Mol Cell Evol Biol*, 273(2):714–730.

Alamri, A., Bron, R., Brock, J. A., and Ivanusic, J. J. (2015). Transient receptor potential cation channel subfamily v member 1 expressing corneal sensory neurons can be subdivided into at least three subpopulations. *Frontiers in neuroanatomy*, 9:71.

Albal, M. V., Chandorkar, A. G., and Bulakh, P. M. (1987). Effect of inhibition of lens membrane Na+-K+ ATPase by ouabain pre-treatment–an in vitro study. *Indian Journal of Ophthalmology*, 35(5-6):214–216.

Alvarez, L. J., Candia, O. A., Zara, M., and Zamudio, A. C. (2001). Localization of a Na^+-K^+-$2Cl^-$ cotransporter in the rabbit lens. *Experimental Eye Research*, 73(5):657–667.

Andrews, R. K., Lopez, J. A., and Berndt, M. C. (1997). Molecular mechanisms of platelet adhesion and activation. *International Journal of Biochemistry & Cell Biology*, 29(1):91–105.

Ang, M. J. and Afshari, N. A. (2021). Cataract and systemic disease: A review. *Clinical and Experimental Ophthalmology*, 49(2):118–127.

Aoyagi, T., Takeuchi, T., Matsuzaki, A., Kawamura, K., Kondo, S., Hamada, M., Maeda, K., and Umezawa, H. (1969). Leupeptins, new protease inhibitors from actinomycetes. *The Journal of Antibiotics*, 22(6):283–286.

Artigas, J. M., Felipe, A., Navea, A., Fandiño, A., and Artigas, C. (2012). Spectral transmission of the human crystalline lens in adult and elderly persons: Color and total transmission of visible light. *Invest Ophthalmol Vis Sci*, 53(7):4076–4084.

Badheka, D., Yudin, Y., Borbiro, I., Hartle, C. M., Yazici, A., Mirshahi, T., and Rohacs, T. (2017). Inhibition of transient receptor potential melastatin 3 ion channels by g-protein $\beta\gamma$ subunits. *Elife*, 6:e26147.

Ball, E. E. (1977). Fine structure of the compound eyes of the midwater amphipod phronima in relation to behavior and habitat. *Tissue and Cell*, 9(3):521–536.

Ball, L. E., Little, M., Nowak, M. W., Garland, D. L., Crouch, R. K., and Schey, K. L. (2003). Water permeability of c-terminally truncated aquaporin 0 (aqp0 1-243) observed in the aging human lens. *Investigative ophthalmology & visual science*, 44(11):4820–4828.

Barandika, O., Ezquerra-Inchausti, M., Anasagasti, A., Vallejo-Illarramendi, A., Llarena, I., Bascaran, L., and Ruiz-Ederra, J. (2016). Increased aquaporin 1 and 5 membrane expression in the lens epithelium of cataract patients. *Biochim Biophys Acta*, 1862(10):2015–2021.

Baruch, A., Greenbaum, D., Levy, E. T., Nielsen, P. A., Gilula, N. B., Kumar, N. M., and Bogyo, M. (2001). Defining a link between gap junction communication, proteolysis, and cataract formation. *J Biol Chem*, 276(31):28999–29006.

Bassnett, S. and Beebe, D. C. (1992). Coincident loss of mitochondria and nuclei during lens fiber cell differentiation. *Developmental Dynamics*, 194(2):85–93.

Bassnett, S. and Mataic, D. (1997). Chromatin degradation in differentiating fiber cells of the eye lens. *The Journal of Cell Biology*, 137(1):37–49.

Becker, D., Blase, C., Bereiter-Hahn, J., and Jendrach, M. (2005). Trpv4 exhibits a functional role in cell-volume regulation. *J Cell Sci*, 118(Pt 11):2435–2440.

Beebe, D. C. (2008). Maintaining transparency: A review of the developmental physiology and pathophysiology of two avascular tissues. *Semin Cell Dev Biol*, 19(2):125–133.

Beebe, D. C., Compart, P. J., Johnson, M. C., Feagans, D. E., and Feinberg, R. N. (1982). The mechanism of cell elongation during lens fiber cell differentiation. *Dev Biol*, 92(1):54–59.

Bender, M. B. and Shanzer, S. (1964). Oculomotor pathways defined by electrical stimulation and lesions in the brainstem of the monkey. In Bender, M. B., editor, *The Oculomotor System*, pages 81–140. Harper & Row, New York.

Benedek, G. B. (1971). Theory of transparency of the eye. *Applied Optics*, 10(3):459–473.

Bennett, T. M., Mackay, D. S., Siegfried, C. J., and Shiels, A. (2014). Mutation of the melastatin-related cation channel, trpm3, underlies inherited cataract and glaucoma. *PLoS One*, 9(8):e104000.

Berry, V., Francis, P., Kaushal, S., Moore, A., and Bhattacharya, S. (2000). Missense mutations in mip underlie autosomal dominant 'polymorphic' and lamellar cataracts linked to 12q. *Nat Genet*, 25(1):15–17.

Berthoud, V. M. and Ngezahayo, A. (2017). Focus on lens connexins. *BMC Cell Biol*, 18(Suppl 1):6.

Berthoud, V. M., Westphale, E. M., Grigoryeva, A., and Beyer, E. C. (2000). Pkc isoenzymes in the chicken lens and tpa-induced effects on intercellular communication. *Invest Ophthalmol Vis Sci*, 41(3):850–858.

Bevan, S. and Szolcsányi, J. (1990). Sensory neuron-specific actions of capsaicin: mechanisms and applications. *Trends in Pharmacological Sciences*, 11(8):330–333.

Bienert, G. P., Møller, A. L., Kristiansen, K. A., Schulz, A., Møller, I. M., Schjoerring, J. K., and Jahn, T. P. (2007). Specific aquaporins facilitate the diffusion of hydrogen peroxide across membranes. *J Biol Chem*, 282(2):1183–1192.

Bloemendal, H. (1977). The vertebrate eye lens: A useful system for the study of fundamental biological processes on a molecular level. *Science*, 197(4299):127–138.

Bloemendal, H., Zweers, A., Vermorken, F., Dunia, I., and Benedetti, E. L. (1972). The plasma membranes of eye lens fibres. biochemical and structural characterization. *Cell Differ*, 1(2):91–106.

Bodendiek, S. B., Rubinos, C., Trelles, M. P., Coleman, N., Jenkins, D. P., Wulff, H., and Srinivas, M. (2012). Triarylmethanes, a new class of cx50 inhibitors. *Frontiers in Pharmacology*, 3:106.

Bok, D., Dockstader, J., and Horwitz, J. (1982). Immunocytochemical localization of the lens main intrinsic polypeptide (mip26) in communicating junctions. *The Journal of cell biology*, 92(1):213–220.

Bonting, S. L., Caravaggio, L. L., and Hawkins, N. M. (1963). Studies on sodium-potassium-activated adenosinetriphosphatase. vi. its role in cation transport in the lens of cat, calf and rabbit. *Arch Biochem Biophys*, 101:47–55.

Borges-Rodríguez, Y., Morales-Cueto, R., and Rivillas-Acevedo, L. (2023). Effect of the ultraviolet radiation on the lens. *Current Protein & Peptide Science*, 24(3):215–228.

Borin, M. and Siffert, W. (1991). Further characterization of the mechanisms mediating the rise in cytosolic free Na^+ in thrombin-stimulated platelets. evidence for inhibition of the Na^+, K^+-atpase and for Na^+ entry via a Ca^{2+} influx pathway. *Journal of Biological Chemistry*, 266(20):13153–13160.

Braga Ferreira, L. G., Faria, J. V., Dos Santos, J. P. S., and Faria, R. X. (2020). Capsaicin: Trpv1-independent mechanisms and novel therapeutic possibilities. *Eur J Pharmacol*, 887:173356.

Bridgeman, B. and Stark, L. (1977). *The theory of binocular vision: Ewald Hering (1868)*. Springer.

Bron, A. J. and Michael, R. (2011). The ageing lens and cataract: a model of normal and pathological ageing. *Philosophical Transactions of the Royal Society B: Biological Sciences*, 366(1568):1278–1292.

Brooks, H. L., Regan, J. W., and Yool, A. J. (2000). Inhibition of aquaporin-1 water permeability by tetraethylammonium: Involvement of the loop e pore region. *Mol Pharmacol*, 57(5):1021–1026.

Brown, N. (1974). The change in lens curvature with age. *Experimental Eye Research*, 19(2):175–183.

Budnar, P., Tangirala, R., Bakthisaran, R., and Rao, C. M. (2022). Protein aggregation and cataract: Role of age-related modifications and mutations in α-crystallins. *Biochemistry (Moscow)*, 87(3):225–241.

Campbell, F. W. and Gubisch, R. W. (1966). Optical quality of the human eye. *The Journal of Physiology*, 186(3):558–578.

Cao, E., Liao, M., Cheng, Y., and Julius, D. (2013). Trpv1 structures in distinct conformations reveal activation mechanisms. *Nature*, 504(7478):113–118.

Carr, D. W., Stofko-Hahn, R. E., Fraser, I. D., Bishop, S. M., Acott, T. S., Brennan, R. G., and Scott, J. D. (1991). Interaction of the regulatory subunit (rii) of camp-dependent protein kinase with rii-anchoring proteins occurs through an amphipathic helix binding motif. *J Biol Chem*, 266(22):14188–14192.

Carr, D. W., Stofko-Hahn, R. E., Fraser, I. D., Cone, R. D., and Scott, J. D. (1992). Localization of the camp-dependent protein kinase to the postsynaptic densities by a-kinase anchoring proteins. characterization of akap 79. *J Biol Chem*, 267(24):16816–16823.

Caterina, M. J., Schumacher, M. A., Tominaga, M., Rosen, T. A., Levine, J. D., and Julius, D. (1997). The capsaicin receptor: A heat-activated ion channel in the pain pathway. *Nature*, 389(6653):816–824.

Chee, K. N., Vorontsova, I., Lim, J. C., Kistler, J., and Donaldson, P. J. (2010). Expression of the sodium potassium chloride cotransporter (nkcc1) and sodium chloride cotransporter (ncc) and their effects on rat lens transparency. *Mol Vis*, 16:800–812.

Chen, G., Yao, C., Hasegawa, T., Akamatsu, T., Yoshimura, H., and Hosoi, K. (2014). Effects of isoproterenol on aquaporin 5 levels in the parotid gland of mice in vivo. *Am J Physiol Endocrinol Metab*, 306(1):E100–E108.

Chen, M. and Wu, Q. (2023). Roles and mechanisms of natural drugs on sinus node dysfunction. *Biomedicine & Pharmacotherapy*, 164:114777.

Chen, X., Sooch, G., Demaree, I. S., White, F. A., and Obukhov, A. G. (2020). Transient receptor potential canonical (trpc) channels: Then and now. *Cells*, 9(9):1983.

Chen, Y., Qiu, C., Donaldson, P. J., and Petrova, R. S. (2022). Intracellular hydrostatic pressure regulation in the bovine lens: a role in the regulation of lens optics? *American Journal of Physiology - Regulatory, Integrative and Comparative Physiology*, 322(3):R162–R172.

Chen, Y., Sagar, V., Len, H.-S., Peterson, K., Fan, J., Mishra, S., McMurtry, J., Wilmarth, P. A., David, L. L., and Wistow, G. (2017). γ-crystallins of the chicken lens: remnants of an ancient vertebrate gene family in birds. *FEBS Journal*, 283(8):1516–1530.

Cheng, C., Gokhin, D. S., Nowak, R. B., and Fowler, V. M. (2016). Sequential application of glass coverslips to assess the compressive stiffness of the mouse lens: Strain and morphometric analyses. *Journal of Visualized Experiments*, (111):e53986.

Cheng, C., Parreno, J., Nowak, R. B., Biswas, S. K., Wang, K., Hoshino, M., and Fowler, V. M. (2019). Age-related changes in eye lens biomechanics, morphology, refractive index and transparency. *Aging (Albany NY)*, 11(24):12497–12531.

Chijiwa, T., Mishima, A., Hagiwara, M., Sano, M., Hayashi, K., Inoue, T., and Hidaka, H. (1990). Inhibition of forskolin-induced neurite outgrowth and protein phosphorylation by a newly synthesized selective inhibitor of cyclic amp-dependent protein kinase, h-89, of pc12d pheochromocytoma cells. *J Biol Chem*, 265(9):5267–5272.

Chiu, C. J. and Taylor, A. (2007). Nutritional antioxidants and age-related cataract and maculopathy. *Exp Eye Res*, 84(2):229–245.

Choh, V., Sivak, J. G., and Meriney, S. D. (2002). A physiological model to measure effects of age on lenticular accommodation and spherical aberration in chickens. *Investigative ophthalmology & visual science*, 43(1):92–98.

Clapham, D. E. (2003). Trp channels as cellular sensors. *Nature*, 426(6966):517–524.

Clausen, M. V., Hilbers, F., and Poulsen, H. (2017). The structure and function of the na,k-atpase isoforms in health and disease. *Front Physiol*, 8:371.

Clausen, T. (2003). Na+-k+ pump regulation and skeletal muscle contractility. *Physiol Rev*, 83(4):1269–1324.

Coghlan, S. D. and Augusteyn, R. C. (1977). Changes in the distribution of proteins in the aging human lens. *Exp Eye Res*, 25(6):603–611.

Comellas, A. P., Kelly, A. M., Trejo, H. E., Briva, A., Lee, J., Sznajder, J. I., and Dada, L. A. (2010). Insulin regulates alveolar epithelial function by inducing Na^+/K^+-ATPase translocation to the plasma membrane in a process mediated by the action of Akt. *Journal of Cell Science*, 123(8):1343–1351.

Contreras, R. G., Shoshani, L., Flores-Maldonado, C., Lázaro, A., and Cereijido, M. (1999). Relationship between na(+),k(+)-atpase and cell attachment. *J Cell Sci*, 112(Pt 23):4223–4232.

Cornelius, F. and Mahmmoud, Y. A. (2009). Interaction between cardiotonic steroids and na,k-atpase. effects of ph and ouabain-induced changes in enzyme conformation. *Biochemistry*, 48(42):10056–10065.

Cosens, D. and Manning, A. (1969). Abnormal electroretinogram from a drosophila mutant. *Nature*, 224(5216):285–287.

Crewther, S. G., Murphy, M. J., and Crewther, D. P. (2008). Potassium channel and nkcc cotransporter involvement in ocular refractive control mechanisms. *PLoS One*, 3(7):e2839.

Cristina-Silva, C., Amaral-Silva, L., Santos, K. M., Correa, G. M., da Silva, W. C., Fernandes, M. H. M. R., da Silva, G. S. F., Gargaglioni, L. H., Almeida, M. C., and Bicego, K. C. (2022). Cutaneous TRPV4 channels activate warmth-defense responses in young and adult birds. *Frontiers in Physiology*, 13:892828.

Cvekl, A., McGreal, R., and Liu, W. (2015). Lens development and crystallin gene expression. *Progress in Molecular Biology and Translational Science*, 134:129–167.

D'Andrea, L., Lytle, C., Matthews, J. B., Hofman, P., Forbush, B., and Madara, J. L. (1996). Na:k:2cl cotransporter (nkcc) of intestinal epithelial cells. surface expression in response to camp. *J Biol Chem*, 271(46):28969–28976.

Darman, R. B., Flemmer, A., and Forbush, B. (2001). Modulation of ion transport by direct targeting of protein phosphatase type 1 to the na-k-cl cotransporter. *J Biol Chem*, 276(37):34359–34362.

Darwin, C. (1859). *On the Origin of Species by Means of Natural Selection, or the Preservation of Favoured Races in the Struggle for Life*. John Murray, London.

de Almeida, R. F. M., Fedorov, A., and Prieto, M. (2003). Sphingomyelin/phosphatidylcholine/cholesterol phase diagram: boundaries and composition of lipid rafts. *Biophysical Journal*, 85(4):2406–2416.

Deachapunya, C., Palmer-Densmore, M., and O'Grady, S. M. (1999). Insulin stimulates transepithelial sodium transport by activation of a protein phosphatase that increases na-k atpase activity in endometrial epithelial cells. *J Gen Physiol*, 114(4):561–574.

Delamere, N. A. and Dean, W. L. (1993). Distribution of lens sodium-potassium-adenosine triphosphatase. *Invest Ophthalmol Vis Sci*, 34(7):2159–2163.

Delamere, N. A. and Shahidullah, M. (2021). Ion transport regulation by trpv4 and trpv1 in lens and ciliary epithelium. *Front Physiol*, 12:834916.

Delamere, N. A. and Shahidullah, M. (2022). Ion transport regulation by trpv4 and trpv1 in lens and ciliary epithelium. *Frontiers in Physiology*, 12:834916.

Delamere, N. A., Shahidullah, M., Mathias, R. T., Gao, J., Sun, X., Sellitto, C., and White, T. W. (2020). Signaling between trpv1/trpv4 and intracellular hydrostatic pressure in the mouse lens. *Invest Ophthalmol Vis Sci*, 61(6):58.

Delamere, N. A. and Tamiya, S. (2004). Expression, regulation and function of na,k-atpase in the lens. *Prog Retin Eye Res*, 23(6):593–615.

Delamere, N. A. and Tamiya, S. (2009). Lens ion transport: From basic concepts to regulation of na,k-atpase activity. *Exp Eye Res*, 88(2):140–143.

Delaye, M. and Tardieu, A. (1983). Short-range order of crystallin proteins accounts for eye lens transparency. *Nature*, 302(5907):415–417.

Deretic, D., Aebersold, R. H., Morrison, H. D., and Papermaster, D. S. (1994). Alpha a- and alpha b-crystallin in the retina. association with the post-golgi compartment of frog retinal photoreceptors. *Journal of Biological Chemistry*, 269(23):16853–16861.

DeRosa, A. M., Martinez-Wittinghan, F. J., Mathias, R. T., and White, T. W. (2005). Intercellular communication in lens development and disease. In Winterhager, E., editor, *Gap Junctions in Development and Disease*, pages 173–195. Springer Berlin Heidelberg, Berlin, Heidelberg.

DeTomaso, A. W., Blanco, G., and Mercer, R. W. (1994). The alpha and beta subunits of the na,k-atpase can assemble at the plasma membrane into functional enzyme. *J Cell Biol*, 127(1):55–69.

Dismuke, W. M., Mbadugha, C. C., Faison, D., and Ellis, D. Z. (2009). Ouabain-induced changes in aqueous humour outflow facility and trabecular meshwork cytoskeleton. *Br J Ophthalmol*, 93(1):104–109.

Donaldson, P., Kistler, J., and Mathias, R. T. (2001). Molecular solutions to mammalian lens transparency. *News Physiol Sci*, 16:118–123.

Donaldson, P. J., Grey, A. C., and Maceo Heilman, B. (2017). The physiological optics of the lens. *Progress in Retinal and Eye Research*, 56:e1–e24.

Donaldson, P. J., Musil, L. S., and Mathias, R. T. (2010). Point: A critical appraisal of the lens circulation model–an experimental paradigm for understanding the maintenance of lens transparency? *Invest Ophthalmol Vis Sci*, 51(5):2303–2306.

Donders, F. C. and Moore, W. D. (1864). *On the anomalies of accommodation and refraction of the eye: With a preliminary essay on physiological dioptrics*, volume 22. New Sydenham Society.

Dorward, H. S., Du, A., Bruhn, M. A., Wrin, J., Pei, J. V., Evdokiou, A., and Hardingham, J. E. (2016). Pharmacological blockade of aquaporin-1 water channel by aqb013 restricts migration and invasiveness of colon cancer cells and prevents endothelial tube formation in vitro. *J Exp Clin Cancer Res*, 35:36.

Dowd, B. F. and Forbush, B. (2003). Pask (proline-alanine-rich ste20-related kinase), a regulatory kinase of the na-k-cl cotransporter (nkcc1). *J Biol Chem*, 278(30):27347–27353.

Drews, A., Mohr, F., Rizun, O., Wagner, T. F., Dembla, S., Rudolph, S., and Oberwinkler, J. (2014). Structural requirements of steroidal agonists of transient receptor potential melastatin 3 (trpm3) cation channels. *Br J Pharmacol*, 171(4):1019–1032.

Duane, A. (1897). *A New Classification of the Motor Anomalies of the Eye*. J. H. Vail.

Duncan, G. and Bushell, A. R. (1975). Ion analyses of human cataractous lenses. *Exp Eye Res*, 20(3):223–230.

Duncan, G. and Croghan, P. C. (1969). Mechanisms for the regulation of cell volume with particular reference to the lens. *Experimental Eye Research*, 8(4):421–428.

Duncan, G., Marcantonio, J. M., and Tomlinson, J. (1991). Lens calcium and cataract. In Obrecht, G. and Stark, L. W., editors, *Presbyopia Research*, Perspectives in Vision Research, pages 33–40. Springer, Boston, MA.

Dzhala, V. I., Brumback, A. C., and Staley, K. J. (2008). Bumetanide enhances phenobarbital efficacy in a neonatal seizure model. *Ann Neurol*, 63(2):222–235.

Dzhala, V. I., Talos, D. M., Sdrulla, D. A., Brumback, A. C., Mathews, G. C., Benke, T. A., and Staley, K. J. (2005). Nkcc1 transporter facilitates seizures in the developing brain. *Nat Med*, 11(11):1205–1213.

Evans, W. H. and Martin, P. E. M. (2002). Gap junctions: structure and function (review). *Molecular Membrane Biology*, 19(2):121–136.

Fambrough, D. M., Lemas, M. V., Hamrick, M., Emerick, M., Renaud, K. J., Inman, E. M., and Takeyasu, K. (1994). Analysis of subunit assembly of the na-k-atpase. *Am J Physiol*, 266(3 Pt 1):C579–C589.

Faure, P., Benhamou, P. Y., Perard, A., Halimi, S., and Roussel, A. M. (1995). Lipid peroxidation in insulin-dependent diabetic patients with early retina degenerative lesions: Effects of an oral zinc supplementation. *Eur J Clin Nutr*, 49(4):282–288.

Fedosova, N. U., Habeck, M., and Nissen, P. (2021). Structure and function of na,k-atpase—the sodium-potassium pump. *Compr Physiol*, 12(1):2659–2679.

Feldman, S. T., Gately, D., Seely, B. L., Schonthal, A., and Feramisco, J. R. (1993). Stimulation of dna synthesis and c-fos expression in corneal endothelium by insulin or insulin-like growth factor-i. *Invest Ophthalmol Vis Sci*, 34(6):2105–2111.

Feldmann, T., Glukmann, V., Medvenev, E., Shpolansky, U., Galili, D., Lichtstein, D., and Rosen, H. (2007). Role of endosomal Na^+-K^+-ATPase and cardiac steroids in the regulation of endocytosis. *American Journal of Physiology-Cell Physiology*, 293(3):C885–C896.

Fernald, R. D. and Wright, S. E. (1983). Maintenance of optical quality during crystalline lens growth. *Nature*, 301(5901):618–620.

Fisher, R. (1973). Human lens fibre transparency and mechanical stress. *Experimental Eye Research*, 16(1):41–49.

Fisher, R. F. (1971). The elastic constants of the human lens. *The Journal of Physiology*, 212(1):147–180.

Fitzgerald, P. G., Bok, D., and Horwitz, J. (1983). Immunocytochemical localization of the main intrinsic polypeptide (mip) in ultrathin frozen sections of rat lens. *J Cell Biol*, 97(5 Pt 1):1491–1499.

Flemmer, A. W., Monette, M. Y., Djurisic, M., Dowd, B., Darman, R., Gimenez, I., and Forbush, B. (2010). Phosphorylation state of the na+-k+-cl- cotransporter (nkcc1) in the gills of atlantic killifish (fundulus heteroclitus) during acclimation to water of varying salinity. *J Exp Biol*, 213(Pt 9):1558–1566.

Frick, K. D. (2012). What the comprehensive economics of blindness and visual impairment can help us understand. *Indian J Ophthalmol*, 60(5):406–410.

Frick, K. D., Joy, S. M., Wilson, D. A., Naidoo, K. S., and Holden, B. A. (2015). The global burden of potential productivity loss from uncorrected presbyopia. *Ophthalmology*, 122(8):1706–1710.

Fricke, T. R., Tahhan, N., Resnikoff, S., Papas, E., Burnett, A., Ho, S. M., Naduvilath, T., and Naidoo, K. S. (2018). Global prevalence of presbyopia and vision impairment from uncorrected presbyopia: systematic review, meta-analysis, and modelling. *Ophthalmology*, 125(10):1492–1499.

Galin, M. A., Nano, H. D., and Hall, T. (1962). Ocular zinc concentration. *Invest Ophthalmol*, 1:142–148.

Gamba, G., Miyanoshita, A., Lombardi, M., Lytton, J., Lee, W. S., Hediger, M. A., and Hebert, S. C. (1994). Molecular cloning, primary structure, and characterization of two members of the mammalian electroneutral sodium-(potassium)-chloride cotransporter family expressed in kidney. *J Biol Chem*, 269(26):17713–17722.

Gao, J., Mathias, R. T., Varadaraj, K., Shahidullah, M., Mei, J., and Delamere, N. A. (2025). Studies on hydrostatic pressure responses to piezo1 and trpv4 in the mouse lens. *Investigative Ophthalmology & Visual Science*, 66(1):5.

Gao, J., Sun, X., Moore, L. C., White, T. W., Brink, P. R., and Mathias, R. T. (2011). Lens intracellular hydrostatic pressure is generated by the circulation of sodium and modulated by gap junction coupling. *J Gen Physiol*, 137(6):507–520.

Gao, J., Sun, X., White, T. W., Delamere, N. A., and Mathias, R. T. (2015). Feedback regulation of intracellular hydrostatic pressure in surface cells of the lens. *Biophys J*, 109(9):1830–1839.

Gao, J., Wang, H., Sun, X., Varadaraj, K., Li, L., White, T. W., and Mathias, R. T. (2013). The effects of age on lens transport. *Investigative Ophthalmology & Visual Science*, 54(12):7174–7187.

Garcia-Elias, A., Mrkonjić, S., Jung, C., Pardo-Pastor, C., Vicente, R., and Valverde, M. A. (2014). The TRPV4 channel. In Nilius, B. and Flockerzi, V., editors, *Mammalian Transient Receptor Potential (TRP) Channels*, volume 222 of *Handbook of Experimental Pharmacology*, pages 293–319. Springer, Berlin, Heidelberg.

Garm, A., Oskarsson, M., and Nilsson, D.-E. (2011). Box jellyfish use terrestrial visual cues for navigation. *Current Biology*, 21(9):798–803.

Garner, M. H. and Kong, Y. (1999). Lens epithelium and fiber na,k-atpases: Distribution and localization by immunocytochemistry. *Invest Ophthalmol Vis Sci*, 40(10):2291–2298.

Gavva, N. R., Tamir, R., Qu, Y., Klionsky, L., Zhang, T. J., Immke, D., Wang, J., Zhu, D., Vanderah, T. W., Porreca, F., Doherty, E. M., Norman, M. H., Wild, K. D., Bannon, A. W., Louis, J.-C., and Treanor, J. J. S. (2005). AMG 9810 [(E)-3-(4-t-butylphenyl)-N-(2,3-dihydrobenzo[b][1,4] dioxin-6-yl)acrylamide], a novel vanilloid receptor 1 (TRPV1) antagonist with antihyperalgesic properties. *Journal of Pharmacology and Experimental Therapeutics*, 313(1):474–484.

Geck, P., Pietrzyk, C., Burckhardt, B. C., Pfeiffer, B., and Heinz, E. (1980). Electrically silent cotransport of Na+, K+ and Cl- in Ehrlich cells. *Biochimica et Biophysica Acta (BBA) - Biomembranes*, 600(2):432–447.

Geering, K. (2001). The functional role of beta subunits in oligomeric p-type atpases. *J Bioenerg Biomembr*, 33(5):425–438.

Gerometta, R. and Candia, O. A. (2016). A decrease in the permeability of aquaporin zero as a possible cause for presbyopia. *Medical Hypotheses*, 86:132–134.

Gerometta, R., Zamudio, A. C., Escobar, D. P., and Candia, O. A. (2007). Volume change of the ocular lens during accommodation. *Am J Physiol Cell Physiol*, 293(2):C797–C804.

Giannone, A. A., Li, L., Sellitto, C., and White, T. W. (2021). Physiological mechanisms regulating lens transport. *Frontiers in Physiology*, 12:818649.

Gladkikh, I. N., Sintsova, O. V., Leychenko, E. V., and Kozlov, S. A. (2021). Trpv1 ion channel: Structural features, activity modulators, and therapeutic potential. *Biochemistry (Moscow)*, 86(1):S50–S70. Suppl 1.

Glasser, A., Murphy, C. J., Troilo, D., and Howland, H. C. (1995). The mechanism of lenticular accommodation in chicks. *Vision Research*, 35(11):1525–1540.

Glasser, A., Pardue, M. T., Andison, M. E., and Sivak, J. G. (1997). A behavioral study of refraction, corneal curvature, and accommodation in raptor eyes. *Canadian Journal of Zoology*, 75(12):2010–2020.

Gletten, R. B., Cantrell, L. S., Bhattacharya, S., and Schey, K. L. (2022). Lens aquaporin-5 inserts into bovine fiber cell plasma membranes via unconventional protein secretion. *Invest Ophthalmol Vis Sci*, 63(8):5.

Glynn, I. M. (1957). The action of cardiac glycosides on sodium and potassium movements in human red cells. *J Physiol*, 136(1):148–173.

Gold, M. G., Reichow, S. L., O'Neill, S. E., Weisbrod, C. R., Langeberg, L. K., Bruce, J. E., and Scott, J. D. (2012). Akap2 anchors pka with aquaporin-0 to support ocular lens transparency. *EMBO Mol Med*, 4(1):15–26.

Golestaneh, N., Fan, J., Zelenka, P., and Chepelinsky, A. B. (2008). Pkc putative phosphorylation site ser235 is required for mip/aqp0 translocation to the plasma membrane. *Molecular Vision*, 14:1006–1014.

Gong, X., Li, E., Klier, G., Huang, Q., Wu, Y., Lei, H., Kumar, N. M., Horwitz, J., and Gilula, N. B. (1997). Disruption of alpha3 connexin gene leads to proteolysis and cataractogenesis in mice. *Cell*, 91(6):833–843.

Gong, Y., Wu, M., Shen, J., Tang, J., Li, J., Xu, J., and Chen, G. (2021). Inhibition of the nkcc1/nf-κb signaling pathway decreases inflammation and improves brain edema and nerve cell apoptosis in an sbi rat model. *Front Mol Neurosci*, 14:641993.

González-Iglesias, H., Petrash, C., Rodríguez-Menéndez, S., García, M., Álvarez, L., Fernandez-Vega Cueto, L., Fernández, B., Pereiro, R., Sanz-Medel, A., and Coca-Prados, M. (2017). Quantitative distribution of zn, fe and cu in the human lens and study of the zn–metallothionein redox system in cultured lens epithelial cells by elemental ms. *Journal of Analytical Atomic Spectrometry*, 32(9):1746–1756.

Goodenough, D. A. (1979). Lens gap junctions: A structural hypothesis for nonregulated low-resistance intercellular pathways. *Invest Ophthalmol Vis Sci*, 18(11):1104–1122.

Goodenough, D. A. and Paul, D. L. (2003). Beyond the gap: Functions of unpaired connexon channels. *Nat Rev Mol Cell Biol*, 4(4):285–294.

Goretzki, B., Tebbe, F., Mitrovic, S.-A., and Hellmich, U. A. (2022). Backbone nmr assignments of the extensive human and chicken trpv4 n-terminal intrinsically disordered regions as important players in ion channel regulation. *Biomolecular NMR Assignments*, 16(2):205–212.

Gorin, M. B., Yancey, S. B., Cline, J., Revel, J.-P., and Horwitz, J. (1984). The major intrinsic protein (mip) of the bovine lens fiber membrane: characterization and structure based on cdna cloning. *Cell*, 39(1):49–59.

Gosmanov, A. R. and Thomason, D. B. (2002). Insulin and isoproterenol differentially regulate mitogen-activated protein kinase-dependent Na+-K+-2Cl- cotransporter activity in skeletal muscle. *Diabetes*, 51(3):615–623.

Goswami, C., Kuhn, J., Heppenstall, P. A., and Hucho, T. (2010). Importance of non-selective cation channel trpv4 interaction with cytoskeleton and their reciprocal regulations in cultured cells. *PLoS One*, 5(7):e11654.

Grahn, B. H., Paterson, P. G., Gottschall-Pass, K. T., and Zhang, Z. (2001). Zinc and the eye. *Journal of the American College of Nutrition*, 20(2 Suppl):106–118.

Greiner, J. V., Kopp, S. J., Gillette, T. E., and Glonek, T. (1983). Phosphatic metabolites of the intact cornea by phosphorus-31 nuclear magnetic resonance. *Investigative Ophthalmology & Visual Science*, 24(5):535–542.

Grey, A. C., Li, L., Jacobs, M. D., Schey, K. L., and Donaldson, P. J. (2009). Differentiation-dependent modification and subcellular distribution of aquaporin-0 suggests multiple functional roles in the rat lens. *Differentiation*, 77(1):70–83.

Grey, A. C., Walker, K. L., Petrova, R. S., Han, J., Wilmarth, P. A., David, L. L., and Schey, K. L. (2013). Verification and spatial localization of aquaporin-5 in the ocular lens. *Exp Eye Res*, 108:94–102.

Grimm, C., Kraft, R., Sauerbruch, S., Schultz, G., and Harteneck, C. (2003). Molecular and functional characterization of the melastatin-related cation channel trpm3. *J Biol Chem*, 278(24):21493–21501.

Group, A.-R. E. D. S. R. (2001). A randomized, placebo-controlled, clinical trial of high-dose supplementation with vitamins c and e, beta carotene, and zinc for age-related macular degeneration and vision loss: Areds report no. 8. *Arch Ophthalmol*, 119(10):1417–1436.

Güler, A. D., Lee, H., Iida, T., Shimizu, I., Tominaga, M., and Caterina, M. (2002). Heat-evoked activation of the ion channel, trpv4. *The Journal of Neuroscience*, 22(15):6408–6414.

Harding, J. J. (1970). Free and protein-bound glutathione in normal and cataractous human lenses. *Biochemical Journal*, 117(5):957–960.

Harding, J. J. (1973). Disulphide cross-linked protein of high molecular weight in human cataractous lens. *Experimental Eye Research*, 17(4):377–383.

Harding, J. J. and van Heyningen, R. (1987). Epidemiology and risk factors for cataract. *Eye (Lond)*, 1(Pt 5):537–541.

Harteneck, C. (2013). Pregnenolone sulfate: From steroid metabolite to trp channel ligand. *Molecules*, 18(10):12012–12028.

Hartmann, A. M., Tesch, D., Nothwang, H. G., and Bininda-Emonds, O. R. (2014). Evolution of the cation chloride cotransporter family: Ancient origins, gene losses, and subfunctionalization through duplication. *Mol Biol Evol*, 31(2):434–447.

Hatou, S. (2011). Hormonal regulation of Na+/K+-dependent ATPase activity and pump function in corneal endothelial cells. *Cornea*, 30:S60–S66.

Hatou, S., Yamada, M., Akune, Y., Mochizuki, H., Shiraishi, A., Joko, T., and Tsubota, K. (2010). Role of insulin in regulation of Na+/K+-dependent ATPase activity and pump function in corneal endothelial cells. *Investigative Ophthalmology & Visual Science*, 51(8):3935–3942.

Hayashi, R., Hayashi, S., Fukuda, K., Sakai, M., and Machida, S. (2017). Immunolocation of aquaporin 8 in human cataractous lenticular epithelial cells. *Biomed Hub*, 2(3):1–5.

Hebert, S. C., Mount, D. B., and Gamba, G. (2004). Molecular physiology of cation-coupled cl- cotransport: The slc12 family. *Pflugers Arch*, 447(5):580–593.

Held, K., Kichko, T., De Clercq, K., Klaassen, H., Van Bree, R., Vanherck, J. C., and Vriens, J. (2015). Activation of trpm3 by a potent synthetic ligand reveals a role in peptide release. *Proc Natl Acad Sci U S A*, 112(11):E1363–1372.

Helmholtz, H. v. (1855). Ueber die accommodation des auges. *Archiv für Ophthalmologie*, 1(2):1–74.

Hernandez, M., Shao, Q., Yang, X. J., Luh, S. P., Kandouz, M., Batist, G., and Alaoui-Jamali, M. A. (2006). A histone deacetylation-dependent mechanism for transcriptional repression of the gap junction gene cx43 in prostate cancer cells. *Prostate*, 66(11):1151–1161.

Heymann, J. B. and Engel, A. (1999). Aquaporins: Phylogeny, structure, and physiology of water channels. *News Physiol Sci*, 14:187–193.

Hightower, K. R., Leverenz, V., and Reddy, V. N. (1980). Calcium transport in the lens. *Investigative Ophthalmology & Visual Science*, 19(9):1059–1066.

Hilbers, F., Kopec, W., Isaksen, T. J., Holm, T. H., Lykke-Hartmann, K., Nissen, P., Khandelia, H., and Poulsen, H. (2016). Tuning of the na,k-atpase by the beta subunit. *Sci Rep*, 6:20442.

Hirano, Y., Okimoto, N., Kadohira, I., Suematsu, M., Yasuoka, K., and Yasui, M. (2010). Molecular mechanisms of how mercury inhibits water permeation through aquaporin-1: understanding by molecular dynamics simulation. *Biophysical Journal*, 98(8):1512–1519.

His, W. (1880). *Anatomie menschlicher Embryonen: Embryonen des ersten Monats*, volume 1. Vogel.

Hodeify, R., Kreydiyyeh, S., and Zaid, L. M. J. (2024). Identified and potential internalization signals involved in trafficking and regulation of Na^+/K^+ ATPase activity. *Molecular and Cellular Biochemistry*, 479:1583–1598.

Holden, B. A., Fricke, T. R., Ho, S. M., Wong, R., Schlenther, G., Cronjé, S., and Frick, K. D. (2008). Global vision impairment due to uncorrected presbyopia. *Arch Ophthalmol*, 126(12):1731–1739.

Horwitz, J. (1992). Alpha-crystallin can function as a molecular chaperone. *Proceedings of the National Academy of Sciences USA*, 89:10449–10453.

Hosoi, K., Yao, C., Hasegawa, T., Yoshimura, H., and Akamatsu, T. (2020). Dynamics of salivary gland aqp5 under normal and pathologic conditions. *Int J Mol Sci*, 21(4).

Hossain Saad, M. Z., Xiang, L., Liao, Y. S., Reznikov, L. R., and Du, J. (2021). The underlying mechanism of modulation of transient receptor potential melastatin 3 by protons. *Front Pharmacol*, 12:632711.

Hu, Z., Shi, W., Riquelme, M. A., Shi, Q., Biswas, S., Lo, W.-K., White, T. W., Gu, S., and Jiang, J. X. (2017). Connexin 50 functions as an adhesive molecule and promotes lens cell differentiation. *Scientific Reports*, 7:5298.

Hua, Y., Ying, X., Qian, Y., Liu, H., Lan, Y., Xie, A., and Zhu, X. (2019). Physiological and pathological impact of aqp1 knockout in mice. *Biosci Rep*, 39(5).

Huang, L., Grami, V., Marrero, Y., Tang, D., Yappert, M. C., Rasi, V., and Borchman, D. (2005). Human lens phospholipid changes with age and cataract. *Invest Ophthalmol Vis Sci*, 46(5):1682–1689.

Husøy, T., Cruciani, V., Sanner, T., and Mikalsen, S.-O. (2001). Phosphorylation of connexin43 and inhibition of gap junctional communication in 12-o-tetradecanoylphorbol-13-acetate-exposed r6 fibroblasts: Minor role of protein kinase cβi and μ. *Carcinogenesis*, 22(2):221–231.

Ingolia, T. D. and Craig, E. A. (1982). Four small drosophila heat shock proteins are related to each other and to mammalian alpha-crystallin. *Proceedings of the National Academy of Sciences*, 79(7):2360–2364.

Inoue, T., Kumamoto, H., Okamoto, K., Umesono, Y., Sakai, M., Sánchez Alvarado, A., and Agata, K. (2004). Morphological and functional recovery of the planarian photosensing system during head regeneration. *Zoological Science*, 21(3):275–283.

Ishibashi, K., Kuwahara, M., Gu, Y., Kageyama, Y., Tohsaka, A., Suzuki, F., and Sasaki, S. (1997a). Cloning and functional expression of a new water channel abundantly expressed in the testis permeable to water, glycerol, and urea. *J Biol Chem*, 272(33):20782–20786.

Ishibashi, K., Kuwahara, M., Kageyama, Y., Tohsaka, A., Marumo, F., and Sasaki, S. (1997b). Cloning and functional expression of a second new aquaporin abundantly expressed in testis. *Biochem Biophys Res Commun*, 237(3):714–718.

Isokpehi, R. D., Rajnarayanan, R. V., Jeffries, C. D., Oyeleye, T. O., and Cohly, H. H. P. (2009). Integrative sequence and tissue expression profiling of chicken and mammalian aquaporins. *BMC Genomics*, 10(Suppl 2):S7.

Jagielnicki, M., Kucharska, I., Bennett, B. C., Harris, A. L., and Yeager, M. (2024). Connexin gap junction channels and hemichannels: Insights from high-resolution structures. *Biology (Basel)*, 13(5).

Jara, O., Minogue, P. J., Berthoud, V. M., and Beyer, E. C. (2018). Chemical chaperone treatment improves levels and distributions of connexins in cx50d47a mouse lenses. *Exp Eye Res*, 175:192–198.

Jensen, M. Ø., Dror, R. O., Xu, H., Borhani, D. W., Arkin, I. T., Eastwood, M. P., and Shaw, D. E. (2008). Dynamic control of slow water transport by aquaporin 0: Implications for hydration and junction stability in the eye lens. *Proceedings of the National Academy of Sciences*, 105(38):14430–14435.

Jiang, J. X., White, T. W., Goodenough, D. A., and Paul, D. L. (1994). Molecular cloning and functional characterization of chick lens fiber connexin45.6. *Molecular Biology of the Cell*, 5(3):363–373.

Jiang, X., Xu, B., Zhai, J., Huang, S., Cheng, H., Ma, L., and Zhao, Y.-E. (2026). Global trends in cataract burden: a 30-year epidemiological analysis and prediction of 2050 from the global burden of disease 2021 study. *British Journal of Ophthalmology*, 110(2):139–147.

Jiao, H., Ivanusic, J. J., McMenamin, P. G., and Chinnery, H. R. (2021). Distribution of corneal TRPV1 and its association with immune cells during homeostasis and injury. *Investigative Ophthalmology & Visual Science*, 62(9):6.

Johnson, R. (1997). The differential effects of 12-o-tetradecanoylphorbol-13-acetate on the gap junctions and connexins of the developing mammalian lens. *Developmental Biology*, 192(1):1–16.

Kalman, K., Németh-Cahalan, K. L., Froger, A., and Hall, J. E. (2008). Phosphorylation determines the calmodulin-mediated ca2+ response and water permeability of aqp0. *J Biol Chem*, 283(30):21278–21283.

Kaplan, J. H. (2002). Biochemistry of na,k-atpase. *Annu Rev Biochem*, 71:511–535.

Kassambara, A. (2026). *rstatix: Pipe-Friendly Framework for Basic Statistical Tests*. R package version 1.1.0.

Kaufman, J., Gordon, C., Bergamaschi, R., Wang, H. Z., Cohen, I. S., Valiunas, V., and Brink, P. R. (2013). The effects of the histone deacetylase inhibitor 4-phenylbutyrate on gap junction conductance and permeability. *Front Pharmacol*, 4:111.

Ketola, H. G. (1979). Influence of dietary zinc on cataracts in rainbow trout (salmo gairdneri). *The Journal of Nutrition*, 109(6):965–969.

Khan, Z., Akhtar, M., Asklund, T., Juliusson, B., Almqvist, P. M., and Ekström, T. J. (2007). Hdac inhibition amplifies gap junction communication in neural progenitors: Potential for cell-mediated enzyme prodrug therapy. *Exp Cell Res*, 313(13):2958–2967.

Kinoshita, J. H. (1974). Mechanisms initiating cataract formation. proctor lecture. *Invest Ophthalmol*, 13(10):713–724.

Kinsey, V. E. and Reddy, D. V. (1965). Studies on the crystalline lens. XI. the relative role of the epithelium and capsule in transport. *Investigative Ophthalmology*, 4(1):104–116.

Kourghi, M., De Ieso, M. L., Nourmohammadi, S., Pei, J. V., and Yool, A. J. (2018). Identification of loop d domain amino acids in the human aquaporin-1 channel involved in activation of the ionic conductance and inhibition by aqb011. *Front Chem*, 6:142.

Kreida, S., Roche, J. V., Missel, J. W., Al-Jubair, T., Hagströmer, C. J., Wittenbecher, V., and Törnroth-Horsefield, S. (2024). The role of phosphorylation in calmodulin-mediated gating of human aqp0. *Biochem J*, 481(1):17–32.

Kreida, S., Roche, J. V., Olsson, C., Linse, S., and Törnroth-Horsefield, S. (2018). Protein-protein interactions in aqp regulation - biophysical characterization of aqp0-cam and aqp2-lip5 complex formation. *Faraday Discuss*, 209:35–54.

Krüger, C., Waldeck-Weiermair, M., Kaynert, J., Pokrant, T., Komaragiri, Y., Otto, O., Michel, T., and Elsner, M. (2021). AQP8 is a crucial H2O2 transporter in insulin-producing RINm5F cells. *Redox Biology*, 43:101962.

Kumar, H., Lee, S.-H., Kim, K.-T., Zeng, X., and Han, I. (2018). TRPV4: a sensor for homeostasis and pathological events in the CNS. *Molecular Neurobiology*, 55(11):8695–8708.

Kumar, S., Jin, F., Park, S. J., Choi, W., Keuning, S. I., Massimino, R. P., Vu, S., Lü, W., and Du, J. (2026). Structural basis for agonist and heat activation of nociceptor TRPM3. *Nature Structural & Molecular Biology*, 33(1):34–42.

Kumari, S. S. and Varadaraj, K. (2009). Intact aqp0 performs cell-to-cell adhesion. *Biochem Biophys Res Commun*, 390(3):1034–1039.

Kumari, S. S., Varadaraj, M., Yerramilli, V. S., Menon, A. G., and Varadaraj, K. (2012). Spatial expression of aquaporin 5 in mammalian cornea and lens, and regulation of its localization by phosphokinase a. *Mol Vis*, 18:957–967.

Kuwabara, T. (1975). The maturation of the lens cell: a morphological study. *Experimental Eye Research*, 20(5):427–443.

Kuwabara, T. and Imaizumi, M. (1974). Denucleation process of the lens. *Investigative Ophthalmology & Visual Science*, 13(12):973–981.

Lampe, P. D., TenBroek, E. M., Burt, J. M., Kurata, W. E., Johnson, R. G., and Lau, A. F. (2000). Phosphorylation of connexin43 on serine368 by protein kinase c regulates gap junctional communication. *J Cell Biol*, 149(7):1503–1512.

Lampi, K. J., Ma, Z., Hanson, S. R., Azuma, M., Shih, M., Shearer, T. R., Smith, D. L., Smith, J. B., and David, L. L. (1998). Age-related changes in human lens crystallins identified by two-dimensional electrophoresis and mass spectrometry. *Experimental Eye Research*, 67(1):31–43.

Land, M. F. and Fernald, R. D. (1992). The evolution of eyes. *Annual Review of Neuroscience*, 15:1–29.

Land, M. F. and Nilsson, D.-E. (2002). *Animal Eyes*. Oxford University Press, New York.

Land, M. F. and Nilsson, D.-E. (2012). *Animal Eyes*. OUP Oxford, 2 edition.

Lapajne, L., Lakk, M., Yarishkin, O., Gubeljak, L., Hawlina, M., and Križaj, D. (2020). Polymodal sensory transduction in mouse corneal epithelial cells. *Investigative Ophthalmology & Visual Science*, 61(4):6.

Lauf, P. K., Chimote, A. A., and Adragna, N. C. (2008). Lithium fluxes indicate presence of na-cl cotransport (ncc) in human lens epithelial cells. *Cellular Physiology and Biochemistry*, 21(1–3):335–346.

Leithe, E. and Rivedal, E. (2004). Ubiquitination and down-regulation of gap junction protein connexin-43 in response to 12-o-tetradecanoylphorbol 13-acetate treatment. *J Biol Chem*, 279(48):50089–50096.

Lewis, W. H. (1904). Experimental studies on the development of the eye in amphibia. i. on the origin of the lens. rana palustris. *American Journal of Anatomy*, 3(4):505–536.

Li, C. and Wang, W. (2014). Urea transport mediated by aquaporin water channel proteins. In *Urea Transporters*, pages 227–265. Springer.

Li, Z., Quan, Y., Gu, S., and Jiang, J. X. (2022). Beyond the channels: Adhesion functions of aquaporin 0 and connexin 50 in lens development. *Front Cell Dev Biol*, 10:866980.

Liao, M., Cao, E., Julius, D., and Cheng, Y. (2013). Structure of the trpv1 ion channel determined by electron cryo-microscopy. *Nature*, 504(7478):107–112.

Lie, A. L., Pan, X., Vaghefi, E., White, T. W., and Donaldson, P. J. (2024). Alterations in lens free water distribution are associated with shape deformation in accommodation. *Ophthalmol Sci*, 4(1):100404.

Liedtke, W., Choe, Y., Martí-Renom, M. A., Bell, A. M., Denis, C. S., Sali, A., and Heller, S. (2000). Vanilloid receptor-related osmotically activated channel (vr-oac), a candidate vertebrate osmoreceptor. *Cell*, 103(3):525–535.

Liedtke, W. B. and Heller, S., editors (2007). *TRP Ion Channel Function in Sensory Transduction and Cellular Signaling Cascades*. Frontiers in Neuroscience. CRC Press/Taylor & Francis, Boca Raton (FL).

Lin, L., Liang, Y., Jiang, G., Gan, Q., Yang, T., Liao, P., and Liang, H. (2025). Global, regional, and national burden of cataract: A comprehensive analysis and projections from 1990 to 2021. *PLoS One*, 20(6):e0326263.

Lindsey Rose, K. M., Gourdie, R. G., Prescott, A. R., Quinlan, R. A., Crouch, R. K., and Schey, K. L. (2006). The c terminus of lens aquaporin 0 interacts with the cytoskeletal proteins filensin and cp49. *Invest Ophthalmol Vis Sci*, 47(4):1562–1570.

Liu, J., Ek Vitorin, J. F., Weintraub, S. T., Gu, S., Shi, Q., Burt, J. M., and Jiang, J. X. (2011). Phosphorylation of connexin 50 by protein kinase a enhances gap junction and hemichannel function. *Journal of Biological Chemistry*, 286(19):16914–16928.

Lo, W. K., Biswas, S. K., Brako, L., Shiels, A., Gu, S., and Jiang, J. X. (2014). Aquaporin-0 targets interlocking domains to control the integrity and transparency of the eye lens. *Invest Ophthalmol Vis Sci*, 55(3):1202–1212.

Lo, W.-K., Biswas, S. K., and Haroun, K. (2020). Two distinct patterns of epithelial aqp1 expression during lens development with their unique upregulations in aqp0-deficient cataractous mouse lenses. *Investigative Ophthalmology & Visual Science*, 61(7):2851.

Lochner, A. and Moolman, J. A. (2006). The many faces of h89: A review. *Cardiovasc Drug Rev*, 24(3-4):261–274.

Löhn, M. and Wirth, K. J. (2024). Potential pathophysiological role of the ion channel trpm3 in myalgic encephalomyelitis/chronic fatigue syndrome (me/cfs) and the therapeutic effect of low-dose naltrexone. *Journal of Translational Medicine*, 22:630.

Lou, M. F. (2003). Redox regulation in the lens. *Progress in Retinal and Eye Research*, 22(5):657–682.

Lytle, C. and Forbush, B. (1992). The na-k-cl cotransport protein of shark rectal gland. ii. regulation by direct phosphorylation. *J Biol Chem*, 267(35):25438–25443.

Lytle, C. and Forbush, B. (1996). Regulatory phosphorylation of the secretory na-k-cl cotransporter: Modulation by cytoplasmic cl. *Am J Physiol*, 270(2 Pt 1):C437–C448.

Ma, L., Dong, F., Denis, M., Feng, Y., Wang, M.-D., and Zha, X. (2011). Ht31, a protein kinase a anchoring inhibitor, induces robust cholesterol efflux and reverses macrophage foam cell formation through atp-binding cassette transporter a1. *Journal of Biological Chemistry*, 286(5):3370–3378.

Ma, T., Yang, B., and Verkman, A. S. (1997). Cloning of a novel water and urea-permeable aquaporin from mouse expressed strongly in colon, placenta, liver, and heart. *Biochem Biophys Res Commun*, 240(2):324–328.

Mandal, A., Shahidullah, M., and Delamere, N. A. (2018). Trpv1-dependent erk1/2 activation in porcine lens epithelium. *Exp Eye Res*, 172:128–136.

Mathias, R. T., Kistler, J., and Donaldson, P. (2007). The lens circulation. *J Membr Biol*, 216(1):1–16.

Mathias, R. T. and Rae, J. L. (2004). The lens: Local transport and global transparency. *Exp Eye Res*, 78(3):689–698.

Mathias, R. T., Rae, J. L., and Baldo, G. J. (1997). Physiological properties of the normal lens. *Physiol Rev*, 77(1):21–50.

McArthur, J. R., Finol-Urdaneta, R. K., and Adams, D. J. (2019). Analgesic transient receptor potential vanilloid-1-active compounds inhibit native and recombinant t-type calcium channels. *British Journal of Pharmacology*, 176(13):2264–2278.

McGaraughty, S., Chu, K. L., Brown, B. S., Zhu, C. Z., Zhong, C., Joshi, S. K., and Jarvis, M. F. (2008). Contributions of central and peripheral trpv1 receptors to mechanically evoked and spontaneous firing of spinal neurons in inflamed rats. *J Neurophysiol*, 100(6):3158–3166.

McKenna, M. J., Renaud, J.-M., Ørtenblad, N., and Overgaard, K. (2024). A century of exercise physiology: effects of muscle contraction and exercise on skeletal muscle Na+, K+-atpase, Na+ and K+ ions, and on plasma K+ concentration—historical developments. *European Journal of Applied Physiology*, 124(3):681–751.

Michalick, L. and Kuebler, W. M. (2020). TRPV4—A missing link between mechanosensation and immunity. *Frontiers in Immunology*, 11:413.

Michea, L. F., de la Fuente, M., and Lagos, N. (1994). Lens major intrinsic protein (mip) promotes adhesion when reconstituted into large unilamellar liposomes. *Biochemistry*, 33(24):7663–7669.

Migliati, E., Meurice, N., DuBois, P., Fang, J. S., Somasekharan, S., Beckett, E., and Yool, A. J. (2009). Inhibition of aquaporin-1 and aquaporin-4 water permeability by a derivative of the loop diuretic bumetanide acting at an internal pore-occluding binding site. *Mol Pharmacol*, 76(1):105–112.

Mihara, H., Boudaka, A., Sugiyama, T., Moriyama, Y., and Tominaga, M. (2011). Transient receptor potential vanilloid 4 (trpv4)-dependent calcium influx and atp release in mouse oesophageal keratinocytes. *J Physiol*, 589(Pt 14):3471–3482.

Mihara, H., Suzuki, N., Boudaka, A. A., Muhammad, J. S., Tominaga, M., Tabuchi, Y., and Sugiyama, T. (2016). Transient receptor potential vanilloid 4-dependent calcium influx and ATP release in mouse and rat gastric epithelia. *World Journal of Gastroenterology*, 22(24):5512–5519.

Minke, B., Wu, C.-F., and Pak, W. L. (1975). Induction of photoreceptor voltage noise in the dark in drosophila mutant. *Nature*, 258(5530):84–87.

Moiseenkova-Bell, V. Y., Stanciu, L. A., Serysheva, I. I., Tobe, B. J., and Wensel, T. G. (2008). Structure of trpv1 channel revealed by electron cryomicroscopy. *Proceedings of the National Academy of Sciences*, 105(21):7451–7455.

Mom, R., Réty, S., Mocquet, V., and Auguin, D. (2024). Deciphering molecular mechanisms involved in the modulation of human aquaporins' water permeability by zinc cations: A molecular dynamics approach. *International Journal of Molecular Sciences*, 25(4):2267.

Montell, C. and Rubin, G. M. (1989). Molecular characterization of the drosophila trp locus: a putative integral membrane protein required for phototransduction. *Neuron*, 2(4):1313–1323.

Moore, R. D. (1983). Effects of insulin upon ion transport. *Biochim Biophys Acta*, 737(1):1–49.

Morth, J. P., Pedersen, B. P., Toustrup-Jensen, M. S., Sørensen, T. L., Petersen, J., Andersen, J. P., and Nissen, P. (2007). Crystal structure of the sodium-potassium pump. *Nature*, 450(7172):1043–1049.

Murata, K., Mitsuoka, K., Hirai, T., Walz, T., Agre, P., Heymann, J. B., and Fujiyoshi, Y. (2000). Structural determinants of water permeation through aquaporin-1. *Nature*, 407(6804):599–605.

Murphy, M. J. and Crewther, S. G. (2013). Ouabain inhibition of na/k-atpase across the retina prevents signed refractive compensation to lens-induced defocus, but not default ocular growth in young chicks. *F1000Res*, 2:97.

Møller, B., Vaag, A., and Johansen, T. (1990). Ouabain inhibition of the sodium-potassium pump: Estimation of ed50 in different types of human leucocytes in vitro. *Br J Clin Pharmacol*, 29(1):93–100.

Müller, E. M., Hub, J. S., Grubmüller, H., and de Groot, B. L. (2008). Is tea an inhibitor for human aquaporin-1? *Pflugers Arch*, 456(4):663–669.

Nakamura, Y., Fukiage, C., Shih, M., Ma, H., David, L. L., Azuma, M., and Shearer, T. R. (2000). Contribution of calpain lp82-induced proteolysis to experimental cataractogenesis in mice. *Invest Ophthalmol Vis Sci*, 41(6):1460–1466.

Nakazawa, Y., Donaldson, P. J., and Petrova, R. S. (2019). Verification and spatial mapping of trpv1 and trpv4 expression in the embryonic and adult mouse lens. *Exp Eye Res*, 186:107707.

Nakazawa, Y., Petrova, R. S., Sugiyama, Y., Nagai, N., Tamura, H., and Donaldson, P. J. (2021). Regulation of the Membrane Trafficking of the Mechanosensitive Ion Channels TRPV1 and TRPV4 by Zonular Tension, Osmotic Stress and Activators in the Mouse Lens. *International Journal of Molecular Sciences*, 22(23):12658.

Nielsen, S., Maunsbach, A. B., Ecelbarger, C. A., and Knepper, M. A. (1998). Ultrastructural localization of na-k-2cl cotransporter in thick ascending limb and macula densa of rat kidney. *American Journal of Physiology-Renal Physiology*, 275(6):F885–F893.

Nilsson, D.-E. (2009). The evolution of eyes and visually guided behaviour. *Philosophical Transactions of the Royal Society B: Biological Sciences*, 364(1531):2833–2847.

Nishihara, E., Hiyama, T. Y., and Noda, M. (2011). Osmosensitivity of transient receptor potential vanilloid 1 is synergistically enhanced by distinct activating stimuli such as temperature and protons. *PLoS One*, 6(7):e22246.

Németh-Cahalan, K. L. and Hall, J. E. (2000). ph and calcium regulate the water permeability of aquaporin 0. *J Biol Chem*, 275(10):6777–6782.

Németh-Cahalan, K. L., Kalman, K., Froger, A., and Hall, J. E. (2007). Zinc modulation of water permeability reveals that aquaporin 0 functions as a cooperative tetramer. *J Gen Physiol*, 130(5):457–464.

Oehler-Jänne, C., von Bueren, A. O., Vuong, V., Hollenstein, A., Grotzer, M. A., and Pruschy, M. (2008). Temperature sensitivity of phospho-ser473-pkb/akt. *Biochemical and Biophysical Research Communications*, 375(3):399–404.

O'Grady, S. M., Palfrey, H. C., and Field, M. (1987). Na-K-2Cl cotransport in winter flounder intestine and bovine kidney outer medulla: [3H] bumetanide binding and effects of furosemide analogues. *The Journal of Membrane Biology*, 96(1):11–18.

Okafor, M. C., Dean, W. L., and Delamere, N. A. (1999). Thrombin inhibits active sodium–potassium transport in porcine lens. *Investigative Ophthalmology & Visual Science*, 40(9):2033–2038.

O'Rahilly, R. (1975). The prenatal development of the human eye. *Experimental Eye Research*, 21(2):93–112.

Paine, T. A., Neve, R. L., and Carlezon, W. A. (2009). Attention deficits and hyperactivity following inhibition of camp-dependent protein kinase within the medial prefrontal cortex of rats. *Neuropsychopharmacology*, 34(9):2143–2155.

Pardue, M. T. and Sivak, J. G. (1997). The functional anatomy of the ciliary muscle in four avian species. *Brain, Behavior and Evolution*, 49(6):295–311.

Parmelee, J. T. and Beebe, D. C. (1988). Decreased membrane permeability to potassium is responsible for the cell volume increase that drives lens fiber cell elongation. *J Cell Physiol*, 134(3):491–496.

Paul, D. L., Ebihara, L., Takemoto, L. J., Swenson, K. I., and Goodenough, D. A. (1991). Connexin46, a novel lens gap junction protein, induces voltage-gated currents in nonjunctional plasma membrane of xenopus oocytes. *J Cell Biol*, 115(4):1077–1089.

Pellegrino de Iraldi, A., Peña, C., and Rodríguez de Lores Arnaiz, G. (2003). The effect of an endogenous na+, k+-atpase inhibitor on rat lens transparency and ultrastructure. *Cell Mol Neurobiol*, 23(2):131–141.

Petrova, R. S., Francis, N., Schey, K. L., and Donaldson, P. J. (2024). Verification of the gene and protein expression of the aquaglyceroporin aqp3 in the mammalian lens. *Experimental Eye Research*, 240:109828.

Petrova, R. S., Nair, N., Bavana, N., Chen, Y., Schey, K. L., and Donaldson, P. J. (2023). Modulation of membrane trafficking of aqp5 in the lens in response to changes in zonular tension is mediated by the mechanosensitive channel trpv1. *International Journal of Molecular Sciences*, 24(10):9080.

Petrova, R. S., Schey, K. L., Donaldson, P. J., and Grey, A. C. (2015). Spatial distributions of aqp5 and aqp0 in embryonic and postnatal mouse lens development. *Exp Eye Res*, 132:124–135.

Petrova, R. S., Webb, K. F., Vaghefi, E., Walker, K., Schey, K. L., and Donaldson, P. J. (2018). Dynamic functional contribution of the water channel aqp5 to the water permeability of peripheral lens fiber cells. *Am J Physiol Cell Physiol*, 314(2):C191–C201.

Piatigorsky, J. (1984). Delta crystallins and their nucleic acids. *Molecular and cellular biochemistry*, 59(1):33–56.

Piechotta, K., Lu, J., and Delpire, E. (2002). Cation chloride cotransporters interact with the stress-related kinases ste20-related proline-alanine-rich kinase (spak) and oxidative stress response 1 (osr1). *J Biol Chem*, 277(52):50812–50819.

Pierscionek, B. K. (2021). Anti-cataract therapies: is there a need for a new approach based on targeting of aquaporins? *Expert Opinion on Therapeutic Targets*, 25(12):1027–1031.

Pierscionek, B. K. and Chan, D. Y. C. (1989). Refractive index gradient of the human lens. *Optometry and Vision Science*, 66(12):822–829.

Pierscionek, B. K. and Regini, S. (2012). The gradient index lens of the eye: An opto-biological synchrony. *Progress in Retinal and Eye Research*, 31(4):332–349.

Pirkmajer, S. and Chibalin, A. V. (2016). Na,k-atpase regulation in skeletal muscle. *Am J Physiol Endocrinol Metab*, 311(1):E1–E31.

Poggio, G. F. and Fischer, B. (1977). Binocular interaction and depth sensitivity in striate and prestriate cortex of behaving rhesus monkey. *Journal of Neurophysiology*, 40(6):1392–1405.

Ponto, L. L. and Schoenwald, R. D. (1990). Furosemide (frusemide). a pharmacokinetic/pharmacodynamic review (part i). *Clin Pharmacokinet*, 18(5):381–408.

Posit Team (2026). *RStudio: Integrated Development Environment for R*. Posit Software, PBC, Boston, MA.

Prassas, I. and Diamandis, E. P. (2008). Novel therapeutic applications of cardiac glycosides. *Nat Rev Drug Discov*, 7(11):926–935.

Preston, G. M., Carroll, T. P., Guggino, W. B., and Agre, P. (1992). Appearance of water channels in xenopus oocytes expressing red cell chip28 protein. *Science*, 256(5055):385–387.

Preston, G. M., Jung, J. S., Guggino, W. B., and Agre, P. (1993). The mercury-sensitive residue at cysteine 189 in the chip28 water channel. *J Biol Chem*, 268(1):17–20.

Pun, R., Kim, M. H., and North, B. J. (2023). Role of connexin 43 phosphorylation on serine-368 by pkc in cardiac function and disease. *Frontiers in Cardiovascular Medicine*, 9:1080131.

Quallo, T., Alkhatib, O., Gentry, C., Andersson, D. A., and Bevan, S. (2017). G protein $\beta\gamma$ subunits inhibit TRPM3 ion channels in sensory neurons. *eLife*, 6:e26138.

R Core Team (2026). *R: A Language and Environment for Statistical Computing*. R Foundation for Statistical Computing, Vienna, Austria.

Ramaekers, F. C. S., Boomkens, T. R., and Bloemendal, H. (1981). Cytoskeletal and contractile structures in bovine lens cell differentiation. *Experimental Cell Research*, 135(2):454–461.

Ramón y Cajal, S. (1972). *The Structure of the Retina*. Charles C Thomas, Springfield, IL.

Reichow, S. L., Clemens, D. M., Freites, J. A., Németh-Cahalan, K. L., Heyden, M., Tobias, D. J., and Gonen, T. (2013). Allosteric mechanism of water-channel gating by ca2+-calmodulin. *Nat Struct Mol Biol*, 20(9):1085–1092.

Reichow, S. L. and Gonen, T. (2008). Noncanonical binding of calmodulin to aquaporin-0: Implications for channel regulation. *Structure*, 16(9):1389–1398.

Revel, J. P. and Karnovsky, M. J. (1967). Hexagonal array of subunits in intercellular junctions of the mouse heart and liver. *J Cell Biol*, 33(3):C7–C12.

Ruan, X., Liu, Z., Luo, L., and Liu, Y. (2020). The structure of the lens and its associations with the visual quality. *BMJ Open Ophthalmol*, 5(1):e000459.

Rubinos, C., Sánchez, H. A., Verselis, V. K., and Srinivas, M. (2012). Mechanism of inhibition of connexin channels by the quinine derivative n-benzylquininium. *Journal of General Physiology*, 139(1):69–82.

Ruiz-Ederra, J. and Verkman, A. S. (2006). Accelerated cataract formation and reduced lens epithelial water permeability in aquaporin-1-deficient mice. *Invest Ophthalmol Vis Sci*, 47(9):3960–3967.

Rump, K., Koos, B., Ziehe, D., Thon, P., Rahmel, T., Palmowski, L., Marko, B., Wolf, A., Witowski, A., Bazzi, Z., Bazzi, M., Orlowski, J., Adamzik, M., Bergmann, L., and Unterberg, M. (2024). Methazolamide reduces the aqp5 mrna expression and immune cell migration—a new potential drug in sepsis therapy? *International Journal of Molecular Sciences*, 25(1):610.

Rup, D. M., Veenstra, R. D., Wang, H. Z., Brink, P. R., and Beyer, E. C. (1993). Chick connexin-56, a novel lens gap junction protein. molecular cloning and functional expression. *Journal of Biological Chemistry*, 268(1):706–712.

Russell, J. M. (2000). Sodium-potassium-chloride cotransport. *Physiol Rev*, 80(1):211–276.

Ryskamp, D. A., Frye, A. M., Phuong, T. T. T., Yarishkin, O., Jo, A. O., Xu, Y., Lakk, M., Iuso, A., Redmon, S. N., Ambati, B., Hageman, G., Prestwich, G. D., Torrejon, K. Y., and Križaj, D. (2016). Trpv4 regulates calcium homeostasis, cytoskeletal remodeling, conventional outflow and intraocular pressure in the mammalian eye. *Scientific Reports*, 6:30583.

Ryskamp, D. A., Witkovsky, P., Barabas, P., Huang, W., Koehler, C., Akimov, N. P., Lee, S. H., Chauhan, S., Xing, W., Rentería, R. C., et al. (2011). The polymodal ion channel transient receptor potential vanilloid 4 modulates calcium flux, spiking rate, and apoptosis of mouse retinal ganglion cells. *Journal of Neuroscience*, 31(19):7089–7101.

Saboe, P. O., Rapisarda, C., Kaptan, S., Hsiao, Y.-S., Summers, S. R., De Zorzi, R., Dukovski, D., Yu, J., de Groot, B. L., Kumar, M., and Walz, T. (2017). Role of pore-lining residues in defining the rate of water conduction by aquaporin-0. *Biophysical Journal*, 112(5):953–965.

Sackin, H. (1995). Mechanosensitive channels. *Annual Review of Physiology*, 57(1):333–353.

Salminen, A. (1984). Effects of the protease inhibitor leupeptin on proteolytic activities and regeneration of mouse skeletal muscles after exercise injuries. *Am J Pathol*, 117(1):64–70.

Saltiel, A. R. and Kahn, C. R. (2001). Insulin signalling and the regulation of glucose and lipid metabolism. *Nature*, 414(6865):799–806.

Sanderson, J., Marcantonio, J. M., and Duncan, G. (1996). Calcium ionophore induced proteolysis and cataract: Inhibition by cell permeable calpain antagonists. *Biochemical and Biophysical Research Communications*, 218(3):893–901.

Sappington, R. M., Sidorova, T., Long, D. J., and Calkins, D. J. (2009). Trpv1: contribution to retinal ganglion cell apoptosis and increased intracellular ca2+ with exposure to hydrostatic pressure. *Investigative ophthalmology & visual science*, 50(2):717–728.

Schaeffel, F. and Howland, H. C. (1987). Corneal accommodation in chick and pigeon. *Journal of Comparative Physiology A*, 160(3):375–384.

Schey, K. L., Gletten, R. B., O'Neale, C. V. T., Wang, Z., Petrova, R. S., and Donaldson, P. J. (2022). Lens aquaporins in health and disease: Location is everything! *Front Physiol*, 13:882550.

Schey, K. L., Little, M., Fowler, J. G., and Crouch, R. K. (2000). Characterization of human lens major intrinsic protein structure. *Invest Ophthalmol Vis Sci*, 41(1):175–182.

Schey, K. L., Petrova, R. S., Gletten, R. B., and Donaldson, P. J. (2017). The role of aquaporins in ocular lens homeostasis. *International Journal of Molecular Sciences*, 18(12):2693.

Schneider, C. A., Rasband, W. S., and Eliceiri, K. W. (2012). Nih image to imagej: 25 years of image analysis. *Nature Methods*, 9(7):671–675.

Shahidullah, M. and Delamere, N. A. (2023). Mechanical stretch activates trpv4 and hemichannel responses in the nonpigmented ciliary epithelium. *International Journal of Molecular Sciences*, 24(2):1673.

Shahidullah, M., Lopez Rosales, J., and Delamere, N. (2022). Activation of piezo1 increases na,k-atpase-mediated ion transport in mouse lens. *International Journal of Molecular Sciences*, 23(21):12870.

Shahidullah, M., Mandal, A., Beimgraben, C., and Delamere, N. A. (2012a). Hyposmotic stress causes atp release and stimulates na,k-atpase activity in porcine lens. *J Cell Physiol*, 227(4):1428–1437.

Shahidullah, M., Mandal, A., and Delamere, N. A. (2012b). Trpv4 in porcine lens epithelium regulates hemichannel-mediated atp release and na-k-atpase activity. *American Journal of Physiology-Cell Physiology*, 302(12):C1751–C1761.

Shahidullah, M., Mandal, A., and Delamere, N. A. (2017). A role for calcium-activated adenylate cyclase and protein kinase a in the lens src family kinase and na,k-atpase response to hyposmotic stress. *Investigative Ophthalmology & Visual Science*, 58(11):4447–4456.

Shahidullah, M., Mandal, A., and Delamere, N. A. (2018). Activation of trpv1 channels leads to stimulation of nkcc1 cotransport in the lens. *Am J Physiol Cell Physiol*, 315(6):C793–C802.

Shahidullah, M., Mandal, A., Mathias, R. T., Gao, J., Križaj, D., Redmon, S., and Delamere, N. A. (2020). Trpv1 activation stimulates nkcc1 and increases hydrostatic pressure in the mouse lens. *Am J Physiol Cell Physiol*, 318(5):C969–C980.

Shiels, A. (2020). $trpm3_mir - 204$: A complex locus for eye development and disease. *Hum Genomics*, 14(1):7.

Shull, G. E., Greeb, J., and Lingrel, J. B. (1986). Molecular cloning of three distinct forms of the na+,k+-atpase alpha-subunit from rat brain. *Biochemistry*, 25(25):8125–8132.

Siezen, R. J., Fisch, M. R., Slingsby, C., and Benedek, G. B. (1985). Opacification of gamma-crystallin solutions from calf lens in relation to cold cataract formation. *Proceedings of the National Academy of Sciences*, 82(6):1701–1705.

Sindhu Kumari, S. and Varadaraj, K. (2013). Aquaporin 5 knockout mouse lens develops hyperglycemic cataract. *Biochem Biophys Res Commun*, 441(2):333–338.

Sivak, J., Hildebrand, T., Lebert, C., Myshak, L., and Ryall, L. (1986). Ocular accommodation in chickens: Corneal vs lenticular accommodation and effect of age. *Vision Research*, 26(11):1865–1872.

Sivak, J. G. (2004). Through the lens clearly: Phylogeny and development. *Investigative Ophthalmology & Visual Science*, 45(3):740–747.

Sivak, J. G., Hildebrand, T., and Lebert, C. (1985). Magnitude and rate of accommodation in diving and nondiving birds. *Vision Research*, 25(7):925–933.

Sivak, J. G. and Kreuzer, R. O. (1983). Spherical aberration of the crystalline lens. *Vision Research*, 23(1):59–70.

SKOU, J. C. (1957). The influence of some cations on an adenosine triphosphatase from peripheral nerves. *Biochim Biophys Acta*, 23(2):394–401.

Sohara, E., Uchida, S., and Sasaki, S. (2009). Function of aquaporin-7 in the kidney and the male reproductive system. *Aquaporins*, pages 219–231.

Spector, A. (1995). Oxidative stress-induced cataract: mechanism of action. *The FASEB Journal*, 9(12):1173–1182.

Srinivasan, A. N., Nagineni, C. N., and Bhat, S. P. (1992). alpha a-crystallin is expressed in non-ocular tissues. *Journal of Biological Chemistry*, 267(33):23337–23341.

Streeter, G. L. (1912). The development of the nervous system. In Keibel, F. and Mall, F. P., editors, *Manual of Human Embryology*, volume 2, chapter 14. J. B. Lippincott Company, Philadelphia.

Susa, T., Sawai, N., Aoki, T., Iizuka-Kogo, A., Kogo, H., Negishi, A., Yokoo, S., Takata, K., and Matsuzaki, T. (2013). Effects of repeated administration of pilocarpine and isoproterenol on aquaporin-5 expression in rat salivary glands. *Acta Histochemica et Cytochemica*, 46(6):187–197.

Swanson, A. A. and Truesdale, A. W. (1971). Elemental analysis in normal and cataractous human lens tissue. *Biochem Biophys Res Commun*, 45(6):1488–1496.

Sweadner, K. J. and Goldin, S. M. (1980). Active transport of sodium and potassium ions: Mechanism, function, and regulation. *N Engl J Med*, 302(14):777–783.

Sweeney, G., Niu, W., Canfield, V. A., Levenson, R., and Klip, A. (2001). Insulin increases plasma membrane content and reduces phosphorylation of na(+)-k(+) pump alpha(1)-subunit in hek-293 cells. *Am J Physiol Cell Physiol*, 281(6):C1797–1803.

Takata, K., Matsuzaki, T., and Tajika, Y. (2004). Aquaporins: Water channel proteins of the cell membrane. *Prog Histochem Cytochem*, 39(1):1–83.

Takemoto, L. J., Hansen, J. S., and Hokin, L. E. (1982). Biochemical and immunological characterization of na+, k+-atpase from lens membrane and other tissues. *Exp Eye Res*, 35(4):337–349.

Tamiya, S. and Delamere, N. A. (2006). The influence of sodium-calcium exchange inhibitors on rabbit lens ion balance and transparency. *Exp Eye Res*, 83(5):1089–1095.

Tang, S., Di, G., Hu, S., Liu, Y., Dai, Y., and Chen, P. (2021). Aqp5 regulates vimentin expression via mir-124-3p.1 to protect lens transparency. *Exp Eye Res*, 205:108485.

Tate, D. J., Miceli, M. V., and Newsome, D. A. (1999). Zinc protects against oxidative damage in cultured human retinal pigment epithelial cells. *Free Radic Biol Med*, 26(5-6):704–713.

Tedesco, R. C., Calabrese, K. D. S., and Smith, R. L. (2005). Architecture of the ciliary muscle of Gallus domesticus. *The Anatomical Record Part A: Discoveries in Molecular, Cellular, and Evolutionary Biology*, 284(2):544–549.

Teichert, C. and Matsumoto, T. (2010). The ancestry of the genus Nautilus. In Saunders, W. B. and Landman, N. H., editors, *Nautilus: The Biology and Paleobiology of a Living Fossil*, volume 6 of *Topics in Geobiology*, pages 25–32. Springer, Dordrecht.

Therien, A. G. and Blostein, R. (2000). Mechanisms of sodium pump regulation. *Am J Physiol Cell Physiol*, 279(3):C541–566.

Thomas, B. C., Minogue, P. J., Valiunas, V., Kanaporis, G., Brink, P. R., Berthoud, V. M., and Beyer, E. C. (2008). Cataracts are caused by alterations of a critical n-terminal positive charge in connexin50. *Invest Ophthalmol Vis Sci*, 49(6):2549–2556.

Thorneloe, K. S., Sulpizio, A. C., Lin, Z., Figueroa, D. J., Clouse, A. K., McCafferty, G. P., Chendrimada, T. P., Lashinger, E. S., Gordon, E., Evans, L., et al. (2008). N-((1 s)-1-{[4-((2 S)-2-{[(2, 4-dichlorophenyl) sulfonyl] amino}-3-hydroxypropanoyl)-1-piperazinyl] carbonyl}-3-methylbutyl)-1-benzothiophene-2-carboxamide (gsk1016790a), a novel and potent transient receptor potential vanilloid 4 channel agonist induces urinary bladder contraction and hyperactivity: part i. *The Journal of pharmacology and experimental therapeutics*, 326(2):432–442.

Timpl, R., Rohde, H., Robey, P. G., Rennard, S. I., Foidart, J.-M., and Martin, G. R. (1979). Laminin—a glycoprotein from basement membranes. *Journal of Biological Chemistry*, 254(19):9933–9937.

Tominaga, M., Caterina, M. J., Malmberg, A. B., Rosen, T. A., Gilbert, H., Skinner, K., and Julius, D. (1998). The cloned capsaicin receptor integrates multiple pain-producing stimuli. *Neuron*, 21(3):531–543.

Tong, J., Canty, J. T., Briggs, M. M., and McIntosh, T. J. (2013). The water permeability of lens aquaporin-0 depends on its lipid bilayer environment. *Experimental Eye Research*, 110:80–86.

Tran, T. L., Bek, T., Holm, L., la Cour, M., Nielsen, S., Prause, J. U., and Heegaard, S. (2013). Aquaporins 6–12 in the human eye. *Acta Ophthalmol*, 91(6):557–563.

Truscott, R. J. (2005). Age-related nuclear cataract—oxidation is the key. *Exp Eye Res*, 80(5):709–725.

Truscott, R. J. and Friedrich, M. G. (2019). Molecular processes implicated in human age-related nuclear cataract. *Investigative Ophthalmology & Visual Science*, 60(14):5007–5021.

Truscott, R. J. W. and Augusteyn, R. C. (1977). Changes in human lens proteins during nuclear cataract formation. *Experimental Eye Research*, 24(2):159–170.

Tsai, C. M. (2020). Aqf026 may act as a cancer therapeutic agent via inducing cancer cell oncosis. *Med Hypotheses*, 140:109685.

Tsukaguchi, H., Shayakul, C., Berger, U. V., Mackenzie, B., Devidas, S., Guggino, W. B., and Hediger, M. A. (1998). Molecular characterization of a broad selectivity neutral solute channel. *J Biol Chem*, 273(38):24737–24743.

Unakar, N. J. and Tsui, J. Y. (1980). Sodium-potassium-dependent atpase. i. cytochemical localization in normal and cataractous rat lenses. *Invest Ophthalmol Vis Sci*, 19(6):630–641.

Urban, R. C. and Cotlier, E. (1986). Corticosteroid-induced cataracts. *Survey of Ophthalmology*, 31(2):102–110.

Uzura, R., Takahashi, K., Saito, S., Tominaga, M., and Ohta, T. (2020). Reduction of extracellular sodium evokes nociceptive behaviors in the chicken via activation of trpv1. *Brain Research*, 1747:147052.

Vaghefi, E. and Donaldson, P. J. (2018). The lens internal microcirculation system delivers solutes to the lens core faster than would be predicted by passive diffusion. *Am J Physiol Regul Integr Comp Physiol*, 315(5):R994–R1002.

Vanhoudt, J., Aerts, T., Abgar, S., and Clauwaert, J. (1998). Quaternary structure of bovine alpha-crystallin: influence of temperature. *International Journal of Biological Macromolecules*, 22(3–4):229–237.

Varadaraj, K., Kumari, S., Shiels, A., and Mathias, R. T. (2005). Regulation of aquaporin water permeability in the lens. *Invest Ophthalmol Vis Sci*, 46(4):1393–1402.

Varadaraj, K. and Kumari, S. S. (2020). Lens aquaporins function as peroxiporins to facilitate membrane transport of hydrogen peroxide. *Biochem Biophys Res Commun*, 524(4):1025–1029.

Veldhuis, N., Lew, M., Abogadie, F. C., Poole, D. P., McIntyre, P., and Bunnett, N. W. (2012). N-glycosylation determines ionic permeability and desensitization of the TRPV1 capsaicin receptor. *Journal of Biological Chemistry*, 287(29):24143–24158.

Verbavatz, J. M., Brown, D., Sabolić, I., Valenti, G., Ausiello, D. A., Van Hoek, A. N., and Verkman, A. S. (1993). Tetrameric assembly of chip28 water channels in liposomes and cell membranes: A freeze-fracture study. *J Cell Biol*, 123(3):605–618.

Villandre, J., White, V., Lear, T. B., Chen, Y., Tuncer, F., Vaiz, E., Tuncer, B., Lockwood, K., Camarco, D., Liu, Y., Chen, B. B., and Evankovich, J. (2022). A repurposed drug screen for compounds regulating aquaporin 5 stability in lung epithelial cells. *Frontiers in Pharmacology*, 13:828643.

Vincent, F., Acevedo, A., Nguyen, M. T., Bayan, J., Gaster, D., Pastor, R., Marugán, J., Silverman, J., and Duncton, M. A. J. (2009). Identification and characterization of novel TRPV4 modulators. *Biochemical and Biophysical Research Communications*, 389(3):490–494.

Vitari, A. C., Thastrup, J., Rafiqi, F. H., Deak, M., Morrice, N. A., Karlsson, H. K., and Alessi, D. R. (2006). Functional interactions of the spak/osr1 kinases with their upstream activator wnk1 and downstream substrate nkcc1. *Biochem J*, 397(1):223–231.

von Helmholtz, H. (1925). *Helmholtz's Treatise on Physiological Optics*, volume 3. The Optical Society of America, Rochester, NY. Edited and translated by J. P. C. Southall.

Vriens, J., Owsianik, G., Hofmann, T., Philipp, S. E., Stab, J., Chen, X., and Voets, T. (2011). Trpm3 is a nociceptor channel involved in the detection of noxious heat. *Neuron*, 70(3):482–494.

Vriens, J., Watanabe, H., Janssens, A., Droogmans, G., Voets, T., and Nilius, B. (2004). Cell swelling, heat, and chemical agonists use distinct pathways for the activation of the cation channel TRPV4. *Proceedings of the National Academy of Sciences*, 101(1):396–401.

Wagner, T. F., Loch, S., Lambert, S., Straub, I., Mannebach, S., Mathar, I., and Oberwinkler, J. (2008). Transient receptor potential m3 channels are ionotropic steroid receptors in pancreatic beta cells. *Nat Cell Biol*, 10(12):1421–1430.

Wallick, E. T., Lane, L. K., and Schwartz, A. (1979). Biochemical mechanism of the sodium pump. *Annu Rev Physiol*, 41:397–411.

Walls, G. L. (1942). *The Vertebrate Eye and Its Adaptive Radiation*. Hafner Publishing.

Wang, K., Gu, S., Yin, X., Weintraub, S. T., Hua, Z., and Jiang, J. X. (2012). Developmental truncations of connexin 50 by caspases adaptively regulate gap junctions/hemichannels and protect lens cells against ultraviolet radiation. *Journal of Biological Chemistry*, 287(19):15786–15797.

Wang, L.-f., Christensen, B. N., Bhatnagar, A., and Srivastava, S. K. (2001). Role of calcium-dependent protease(s) in globulization of isolated rat lens cortical fiber cells. *Investigative Ophthalmology & Visual Science*, 42(1):194–199.

Wang, X., Jaisser, F., and Horisberger, J. D. (1996). Role in cation translocation of the n-terminus of the alpha-subunit of the na(+)-k+ pump of bufo. *J Physiol*, 491(Pt 3):579–594.

Wang, Z., Friedrich, M. G., Truscott, R. J. W., and Schey, K. L. (2025). Identification of age- and cataract-related changes in high-density lens protein aggregates. *Invest Ophthalmol Vis Sci*, 66(5):34.

Warwick, R. (1954). The ocular parasympathetic nerve supply and its mesencephalic sources. *Journal of Anatomy*, 88(1):71–93.

Weale, R. A. (1962). Presbyopia. *Br J Ophthalmol*, 46(11):660–668.

Wen, X. P. and Wan, Q. Q. (2021). Regulatory effect of insulin on the structure, function and metabolism of na. *Exp Ther Med*, 22(5):1243.

Westheimer, G. (1964). Pupil size and visual resolution. *Vision Research*, 4:39–45.

Westheimer, G. and Blair, S. M. (1973). The parasympathetic pathways to internal eye muscles. *Investigative Ophthalmology & Visual Science*, 12(3):193–197.

White, J. P., Cibelli, M., Urban, L., Nilius, B., McGeown, J. G., and Nagy, I. (2016). Trpv4: Molecular conductor of a diverse orchestra. *Physiol Rev*, 96(3):911–973.

White, T. W., Goodenough, D. A., and Paul, D. L. (1998). Targeted ablation of connexin50 in mice results in microphthalmia and zonular pulverulent cataracts. *J Cell Biol*, 143(3):815–825.

Wickham, H., Averick, M., Bryan, J., Chang, W., McGowan, L. D., François, R., Grolemund, G., Hayes, A., Henry, L., Hester, J., Kuhn, M., Pedersen, T. L., Miller, E., Bache, S. M., Müller, K., Ooms, J., Robinson, D., Seidel, D. P., Spedalieri, V., Takahashi, K., Vaughan, D., Wilke, C., Woo, K., and Yutani, H. (2019). Welcome to the Tidyverse. *Journal of Open Source Software*, 4(43):1686.

Wilmarth, P. A., Taube, J. R., Riviere, M. A., Duncan, M. K., and David, L. L. (2004). Proteomic and sequence analysis of chicken lens crystallins reveals alternate splicing and translational forms of beta b2 and beta a2 crystallins. *Investigative Ophthalmology & Visual Science*, 45:2705–2715.

Wistow, G. and Piatigorsky, J. (1988a). Lens crystallins: the evolution and expression of proteins for a highly specialized tissue. *Annual Review of Biochemistry*, 57:479–504.

Wistow, G. J. and Piatigorsky, J. (1988b). Lens crystallins: the evolution and expression of proteins for a highly specialized tissue. *Annual Review of Biochemistry*, 57:479–504.

Wistrand, P. J. (1984). The use of carbonic anhydrase inhibitors in ophthalmology and clinical medicine. *Annals of the New York Academy of Sciences*, 429(1):609–619.

Won, G.-J., Fudge, D. S., and Choh, V. (2015). The effects of actomyosin disruptors on the mechanical integrity of the avian crystalline lens. *Molecular Vision*, 21:98–109.

Wyckelsma, V. L. and McKenna, M. J. (2016). Effects of age on na(+),k(+)-atpase expression in human and rodent skeletal muscle. *Front Physiol*, 7:316.

Xia, C. H., Liu, H., Cheung, D., Cheng, C., Wang, E., Du, X., and Gong, X. (2006). Diverse gap junctions modulate distinct mechanisms for fiber cell formation during lens development and cataractogenesis. *Development*, 133(10):2033–2040.

Xu, Q., Lin, X., Andrews, L., Patel, D., Lampe, P. D., and Veenstra, R. D. (2013). Histone deacetylase inhibition reduces cardiac connexin43 expression and gap junction communication. *Frontiers in Pharmacology*, 4:44.

Yang, F., Kawedia, J., and Menon, A. (2003). Cyclic amp regulates aquaporin 5 expression at both transcriptional and post-transcriptional levels through a protein kinase a pathway. *Journal of Biological Chemistry*, 278(33):32173–32180.

Yang, F., Ma, L., Cao, X., Wang, K., and Zheng, J. (2014). Divalent cations activate trpv1 through promoting conformational change of the extracellular region. *J Gen Physiol*, 143(1):91–103.

Yang, F. and Zheng, J. (2017). Understand spiciness: Mechanism of trpv1 channel activation by capsaicin. *Protein Cell*, 8(3):169–177.

Yool, A. J., Brokl, O. H., Pannabecker, T. L., Dantzler, W. H., and Stamer, W. D. (2002). Tetraethylammonium block of water flux in aquaporin-1 channels expressed in kidney thin limbs of henle's loop and a kidney-derived cell line. *BMC Physiology*, 2(1):4.

Yool, A. J., Morelle, J., Cnops, Y., Verbavatz, J. M., Campbell, E. M., Beckett, E. A., and Devuyst, O. (2013). Aqf026 is a pharmacologic agonist of the water channel aquaporin-1. *J Am Soc Nephrol*, 24(7):1045–1052.

Young, T. (1801). The bakerian lecture: on the mechanism of the eye. *Philosophical Transactions of the Royal Society of London*, 91:23–88.

Yu, X. S. and Jiang, J. X. (2004). Interaction of major intrinsic protein (aquaporin-0) with fiber connexins in lens development. *Journal of Cell Science*, 117(6):871–880.

Zaytseva, A. K., Kulichik, O. E., Kostareva, A. A., and Zhorov, B. S. (2024). Biophysical mechanisms of myocardium sodium channelopathies. *Pflugers Arch*, 476:735–753.

Zhai, K., Liskova, A., Kubatka, P., and Büsselberg, D. (2020). Calcium entry through trpv1: A potential target for the regulation of proliferation and apoptosis in cancerous and healthy cells. *International Journal of Molecular Sciences*, 21(11):4177.

Zhang, M., Ma, Y., Ye, X., Zhang, N., Pan, L., and Wang, B. (2023). Trp (transient receptor potential) ion channel family: Structures, biological functions and therapeutic interventions for diseases. *Signal Transduct Target Ther*, 8(1):261.

Zhang, R., van Hoek, A. N., Biwersi, J., and Verkman, A. S. (1993). A point mutation at cysteine 189 blocks the water permeability of rat kidney water channel chip28k. *Biochemistry*, 32(12):2938–2941.

Zhou, Y., Bennett, T. M., Ruzycki, P. A., Guo, Z., Cao, Y. Q., Shahidullah, M., and Shiels, A. (2024). A cataract-causing mutation in the trpm3 cation channel disrupts calcium dynamics in the lens. *Cells*, 13(3):257.

Zigman, S. and Lerman, S. (1964). A cold precipitable protein in the lens. *Nature*, 203(4945):662–663.

Zinn, J. G. (1755). *Descriptio anatomica oculi humani iconibus illustrata*. Vandenhoeck.

Appendix

Appendix A

Supplementary Data

A.1 Linear relationship between coefficients

For all analyzed lenses, the fitting parameters of the exponential equation ($y = y_0 + ae^{bx}$) exhibited strong linear interdependencies that were preserved across treatments. The a-coefficient showed a negative linear relationship with both the b-coefficient (Fig. A.1) and y_0 value (Fig. A.2), meaning that larger a-coefficient values are associated with smaller b-coefficients and y_0 values. Conversely, y_0 value and the b-coefficient showed a positive linear relationship (Fig. A.3), indicating that larger y_0 values are associated with larger b-coefficient values.

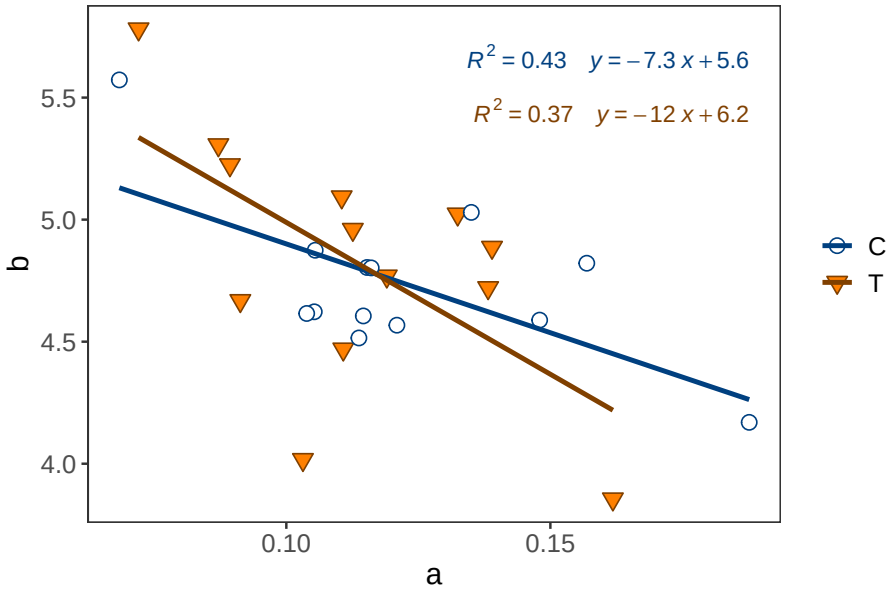


Figure A.1: Linear regression between the a-coefficient and b-coefficient for control and treated lenses. A negative linear relationship was observed in both groups, indicating that larger a-coefficients correspond to lower b-coefficients. C=control; T=treated

.

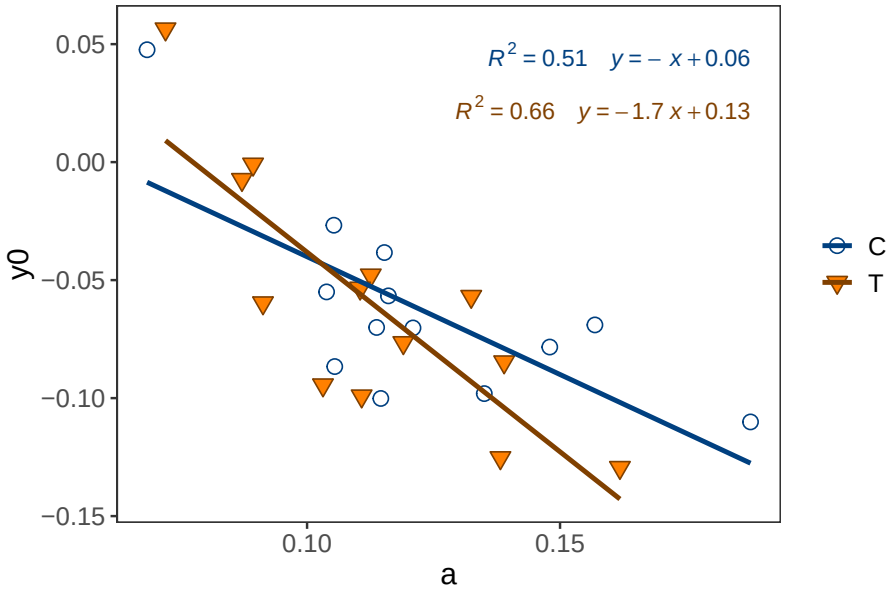


Figure A.2: Linear regression between the a-coefficient and y_0 for control and treated lenses. A negative linear relationship was observed in both groups, indicating that larger a-coefficient values are associated with lower y_0 values. C=control; T=treated

.

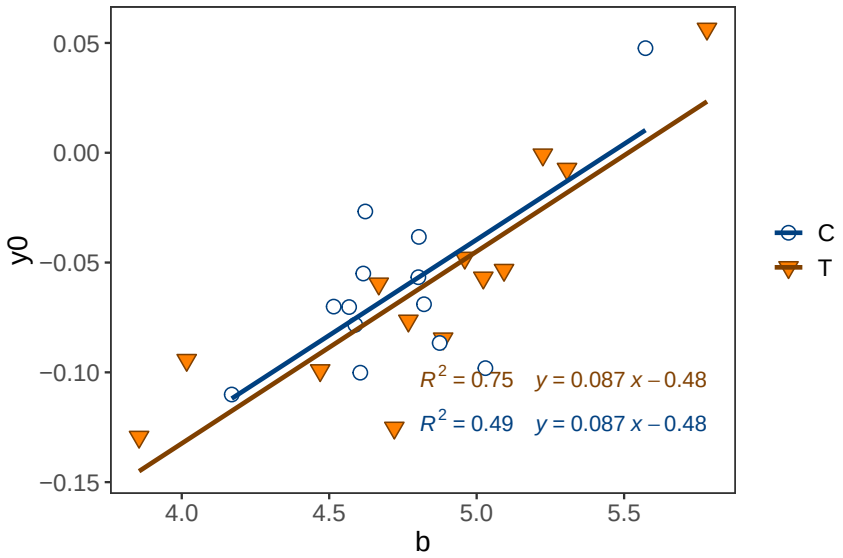


Figure A.3: Linear regression between the b-coefficient and y_0 for control and treated lenses. A positive linear relationship was observed in both groups, indicating that larger a-coefficient values are associated with larger y_0 values. C=control; T=treated

A.2 Coefficients of lenses

We found that the treatment with zinc (Fig. A.4), an agonist of AQP0, showed no significant change (p-value = 0.863) in the a-coefficient between treated (0.340 ± 0.234) and contralateral control lenses (0.348 ± 0.124). Similarly, no significant change (p-value = 0.367) was observed in the y_0 value of treated lenses (-0.254 ± 0.241) compared to control lenses (-0.301 ± 0.130). R^2 values were 0.999 ± 0.002 for control lenses and 0.998 ± 0.003 for treated lenses (p-value = 0.192).

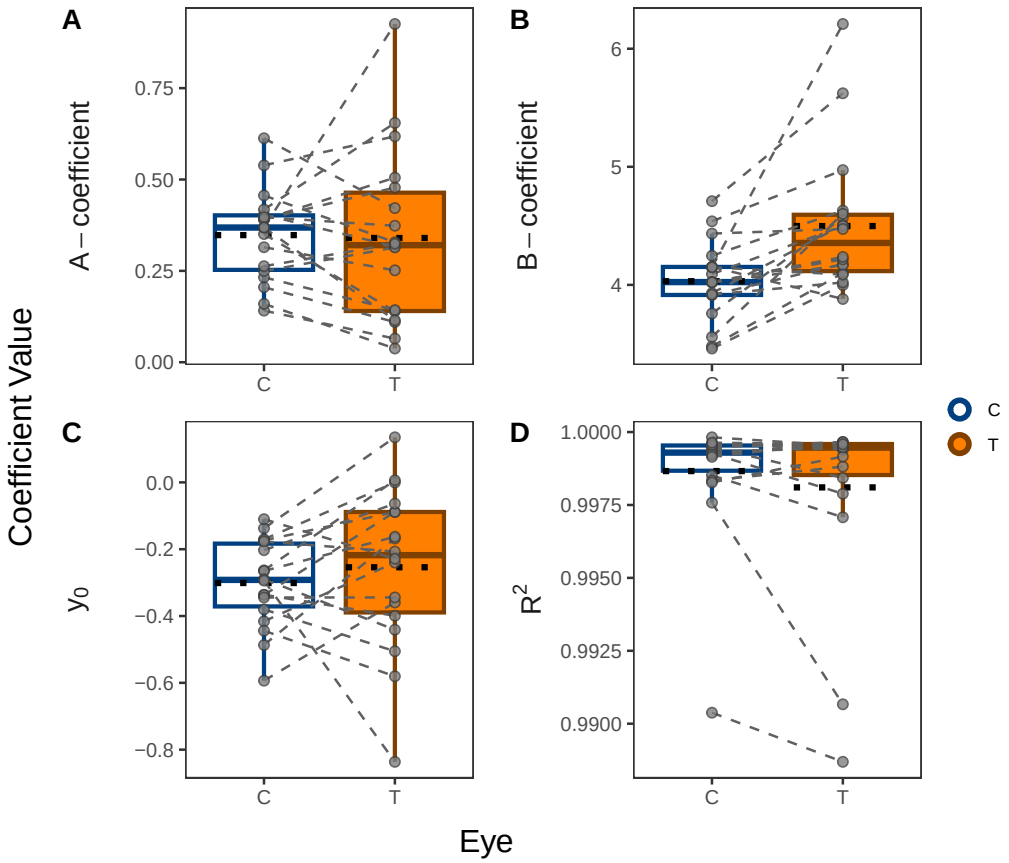


Figure A.4: Box plots of coefficients of the lenses treated with zinc and Tyrode's solution at room temperature. (A) shows the a-coefficient (p-value = 0.863); (B) shows the b-coefficient (p-value = 0.001), (C) shows the baseline force value: y_0 (p-value = 0.367) and (D) shows the R^2 values (p-value = 0.192). C=control; T=treated

.

Conversely, treatment of lenses with Ht31 (Fig. A.5), an inhibitor of AQP0-calmodulin binding, resulted in a significant increase (p-value = 0.011) in the a-coefficient, with treated lenses demonstrating a mean of 0.313 ± 0.243 relative to the control 0.132 ± 0.243. Similarly, significant change (p-value = 0.005) was observed in the y_0 value of treated lenses (-0.266 ± 0.239) compared to control lenses (-0.083 ± 0.065). R^2 values were 0.997 ± 0.002 for control lenses and 0.999 ± 0.001 for treated lenses (p-value = 0.030).

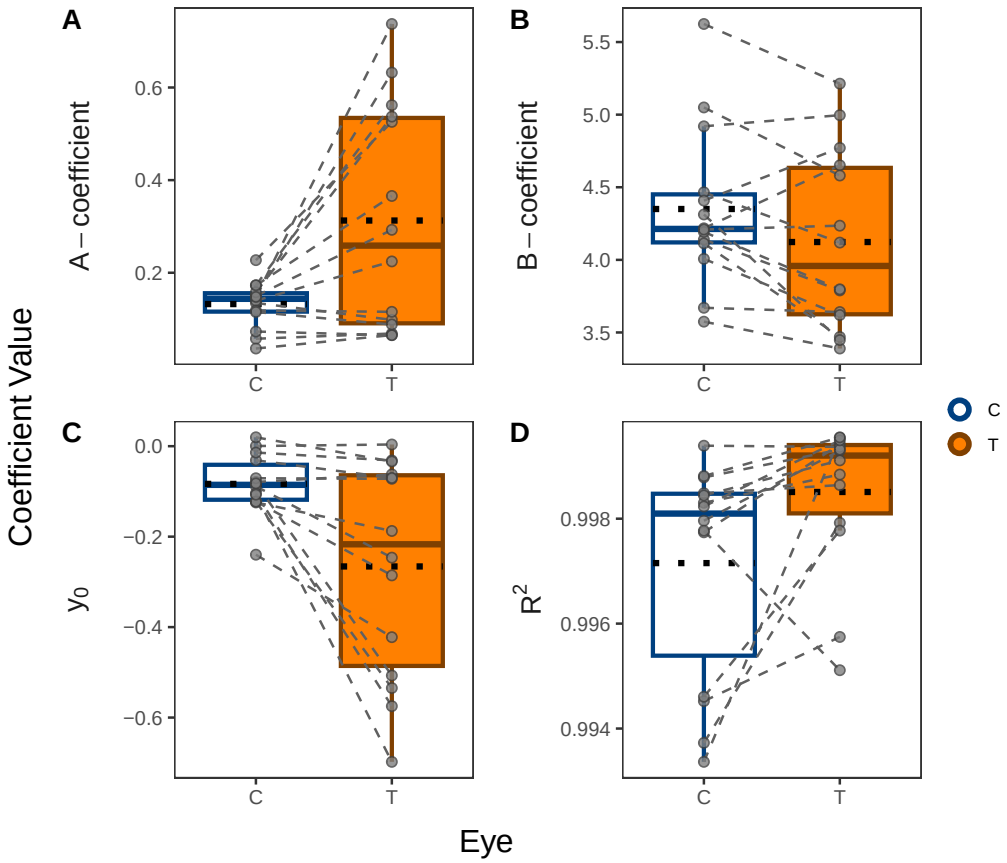


Figure A.5: Box plots of coefficients of the lenses treated with Ht31 and Tyrode's solution at room temperature. (A) shows the a-coefficient (p-value = 0.011), (B) shows the b-coefficient (p-value = 0.037), (C) shows the baseline force value: y_0 (p-value = 0.005), and (D) shows the R^2 values (p-value = 0.030). C=control; T=treated

.

Next, we target the NKA pump with insulin (Fig. A.6), which is the agonist of the NKA pump. We found no significant change in whole lens biomechanics. No significant shifts were detected in the a-coefficient (p-value = 0.430; treated: 0.228 ± 0.092, control: 0.252 ± 0.010) or in the y_0 value (p-value = 0.927) of treated lenses (-0.195 ± 0.096) compared to control lenses (-0.198 ± 0.108). R^2 values were 0.999 ± 0.002 for control lenses and 0.999 ± 0.001 for treated lenses (p-value = 0.870).

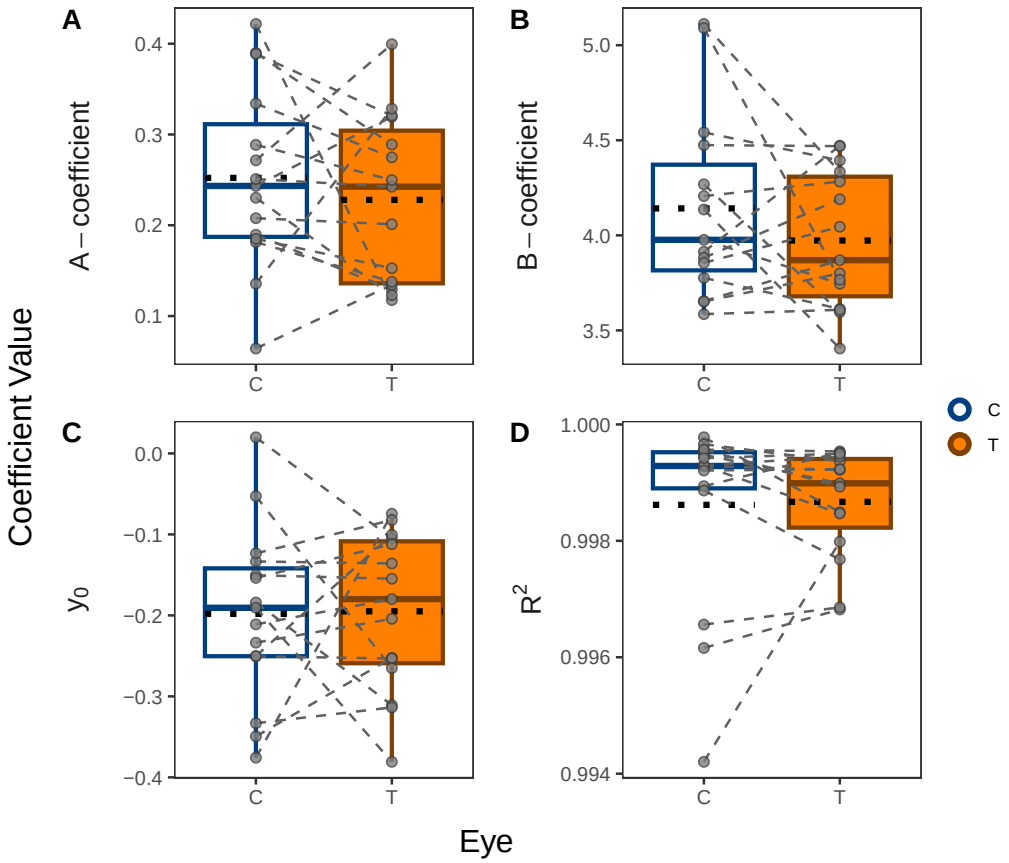


Figure A.6: Boxplot of coefficients of the lenses treated with insulin (100 nM) and Tyrode's solution at room temperature. (A) shows the a-coefficient, (B) shows the b-coefficient (p-value = 0.214), (C) shows y_0 (p-value = 0.927), and (D) shows the R^2 values (p-value = 0.870). C=control; T=treated

.

To assess potential synergistic interaction between zinc and insulin, lenses were treated with a combination of zinc and insulin (Fig. A.7). We found no significant deviation (p-value = 0.737) in the a-coefficient (treated: 0.199 ± 0.087; control: 0.212 ± 0.131) or in the y_0 value (p-value = 0.781) of treated lenses (-0.188 ± 0.091) compared to control lenses (-0.178 ± 0.129). R^2 values were 0.997 ± 0.002 for control lenses and 0.997 ± 0.004 for treated lenses (p-value = 0.901).

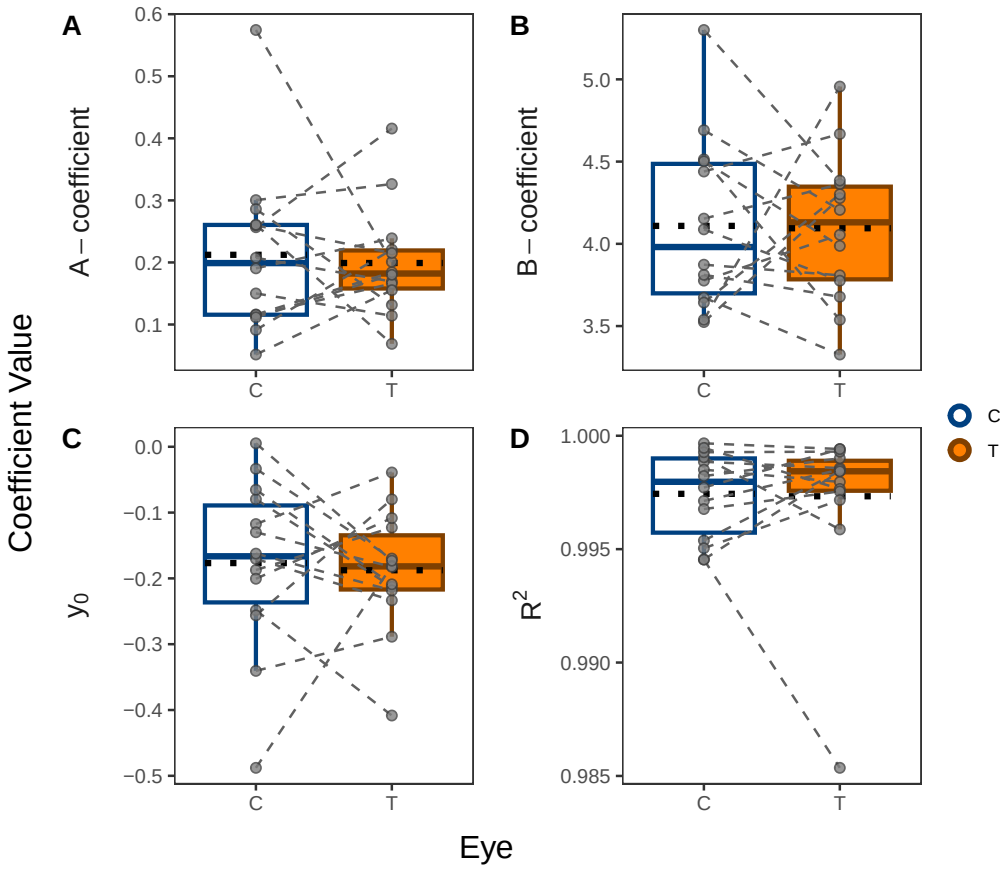


Figure A.7: Boxplot of coefficients of the lenses treated with the combination of zinc and insulin and control lenses with Tyrode's solution at room temperature. (A) shows the a-coefficient (p-value = 0.737), (B) shows the b-coefficient (p-value = 0.937), (C) shows y_0 (p-value = 0.781), and (D) shows the R^2 values (p-value = 0.901). C=control; T=treated

.

The treatment with ouabain, an inhibitor of the NKA pump, likewise did not significantly affect lens biomechanics (Fig. A.8). There was no change in the a-coefficient (p-value = 0.591; treated: 0.269 ± 0.152, control: 0.250 ± 0.152) or in the y_0 value (p-value = 0.514) of treated lenses (-0.230 ± 0.163) compared to control lenses (-0.205 ± 0.145). R^2 values were 0.998 ± 0.002 for control lenses and 0.999 ± 0.002 for treated lenses (p-value = 0.029).

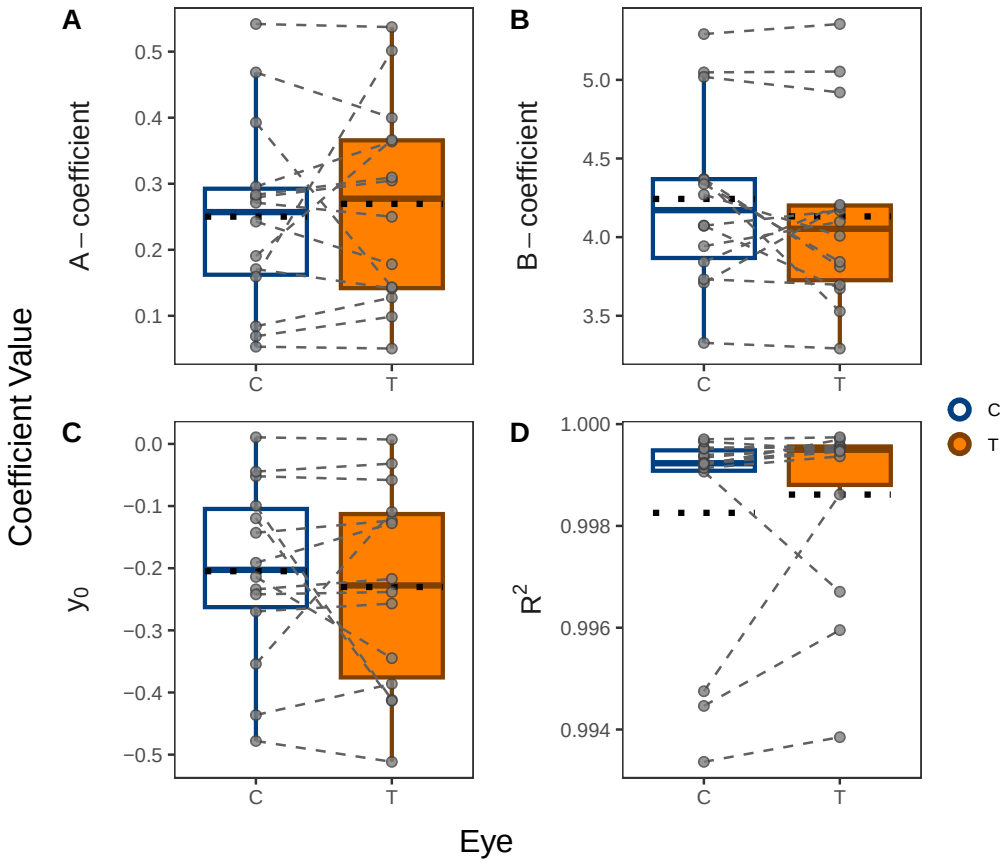


Figure A.8: Boxplot of coefficients of the lenses treated with ouabain and Tyrode's solution at room temperature. (A) shows the a-coefficient (p-value = 0.591), (B) shows the b-coefficient (p-value = 0.274), (C) shows y_0: the baseline force value (p-value = 0.514), and (D) shows the R^2 values (p-value = 0.029). C=control; T=treated

.

When the zinc + ouabain treatment group was compared to ouabain-alone controls (Fig. A.9), the a-coefficient remained comparable (p = 0.495; treated: 0.322 ± 0.118, control: 0.344 ± 0.190). Similarly, no significant change (p-value = 0.333) was observed in the y_0 value of treated lenses (-0.267 ± 0.119) compared to control lenses (-0.304 ± 0.193). R^2 values were 0.999 ± 0.001 for control lenses and 0.999 ± 0.001 for treated lenses (p-value = 0.764).

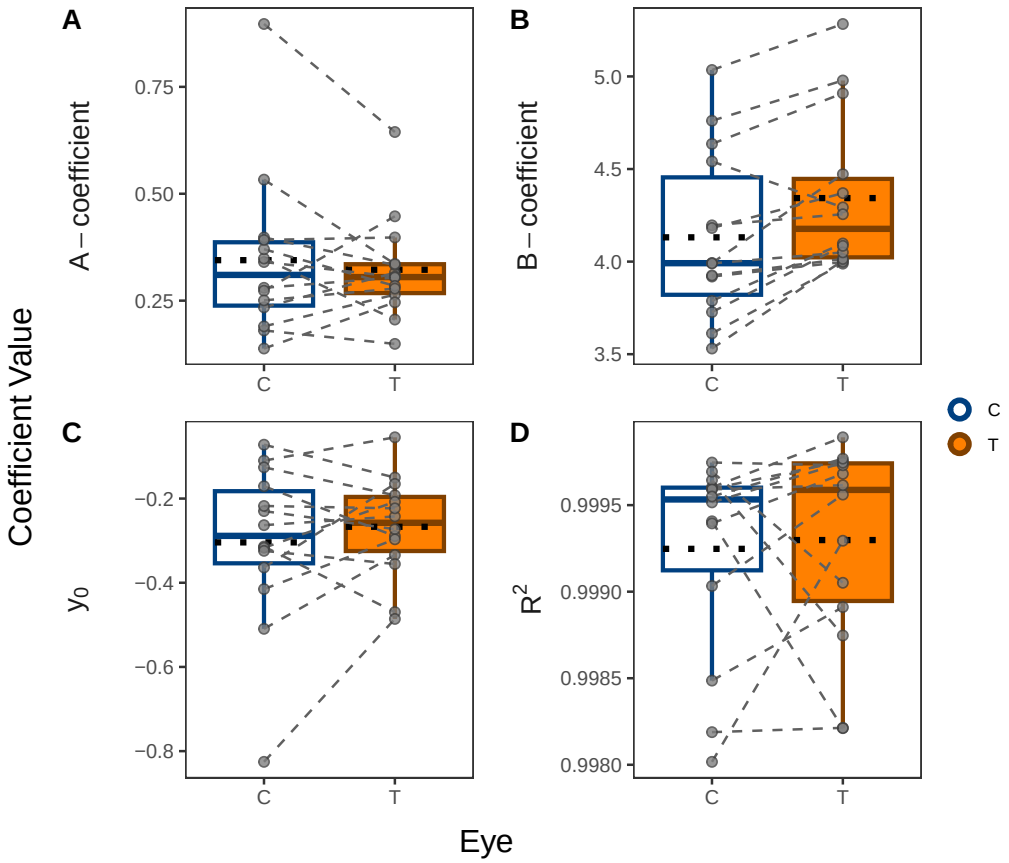


Figure A.9: Box plot of coefficients of the lenses treated with the combination of zinc and ouabain and control lenses with ouabain only at room temperature. (A) shows the a-coefficient (p-value = 0.495), (B) shows the b-coefficient (p-value = 0.001), (C) shows y_0 (p-value = 0.333), and (D) shows the R^2 values (p-value = 0.764). C=control; T=treated

.

However, when the zinc + ouabain group was compared to zinc-alone controls (Fig. A.10), a significant shift emerged in the a-coefficient (p = 0.045; treated: 0.335 ± 0.098, control: 0.275 ± 0.102). However, no significant change (p-value = 0.056) was observed in the y_0 value of treated lenses (-0.288 ± 0.088) compared to control lenses (-0.236 ± 0.090). R^2 values were 0.999 ± 0.001 for control lenses and 0.999 ± 0.000 for treated lenses (p-value = 0.169).

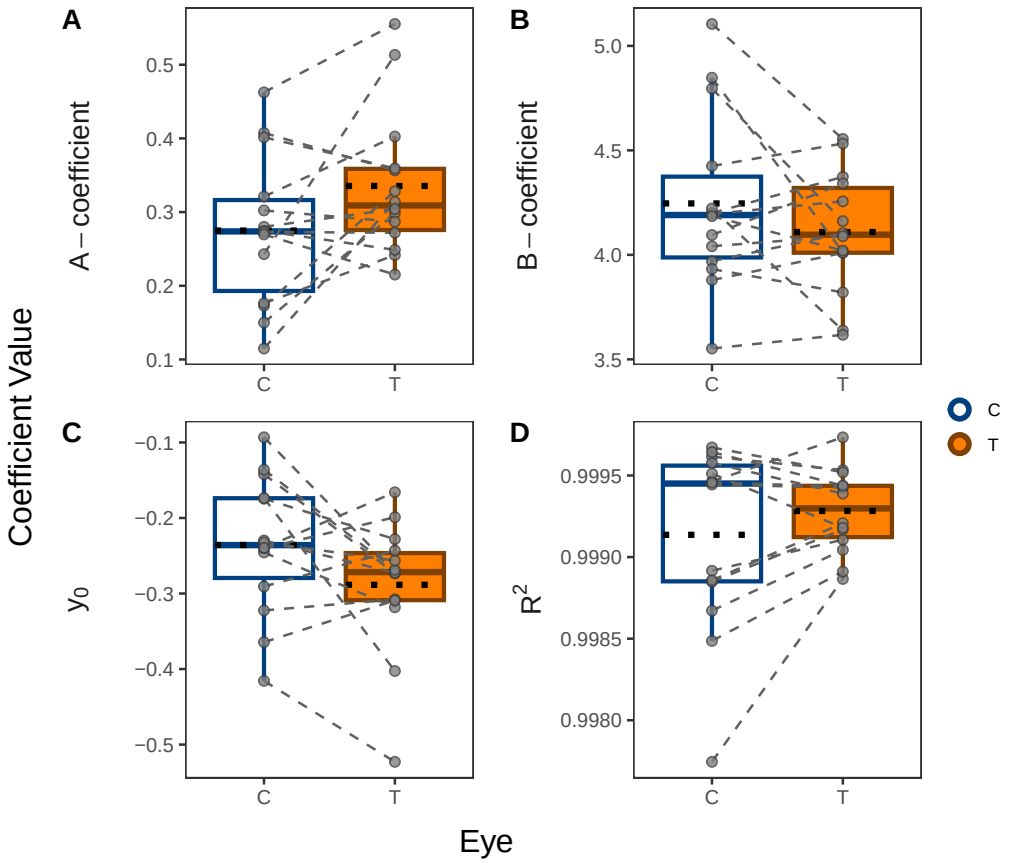


Figure A.10: Boxplots of coefficients of the lenses treated with the combination of zinc and ouabain and control lenses with zinc only at room temperature. (A) shows the a-coefficient (p-value = 0.045), (B) shows the b-coefficient (p-value = 0.177), (C) shows y_0 (p-value = 0.056), and (D) shows the R^2 values (p-value = 0.169). C=control; T=treated

.

Treatment of lenses with TRPV4 agonists, GSK1016790A, at room temperature did not show any significant change (Fig. A.15) in the a-coefficient (p = 0.654; treated: 0.161 ± 0.089, control: 0.153 ± 0.065) or y_0 value (p = 0.307; treated: -0.135 ± 0.134, control: -0.102 ± 0.074). R^2 values were 0.997 ± 0.002 for control lenses and 0.994 ± 0.005 for treated lenses (p-value = 0.085).

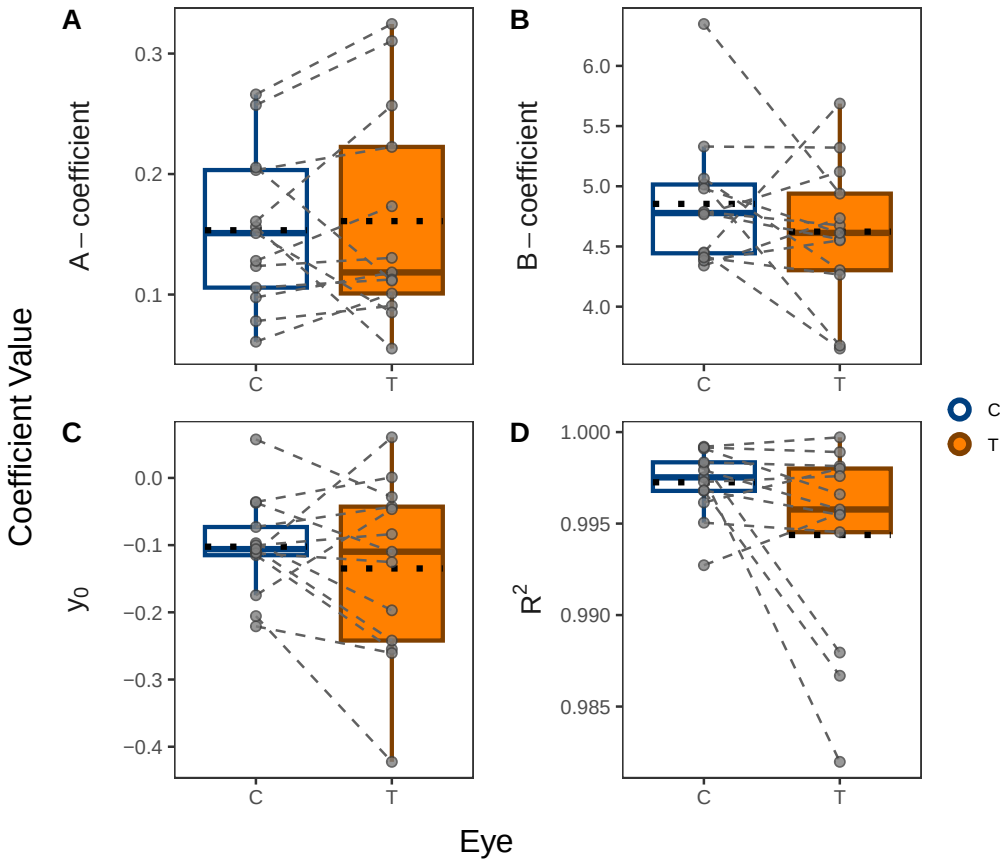


Figure A.11: Boxplots of coefficients of the lenses treated with GSK1016790A and Tyrode's solution at room temperature. (A) shows the a-coefficient (p = 0.654), (B) shows the b-coefficient (p = 0.275), (C) shows y_0 (p = 0.307), and (D) shows the R^2 values (p = 0.0852). C=control; T=treated

.

Targeted inhibition of TRPV4 using the antagonist RN 1734 at room temperature yielded comparable results (Fig. A.12), showing no significant shifts in either the a-coefficient (0.166 ± 0.060 vs. control: 0.150 ± 0.060; p = 0.482) or y_0 value (p = 0.750; treated: -0.114 ± 0.091, control: -0.010 ± 0.010). R^2 values were 0.997 ± 0.004 for control lenses and 0.998 ± 0.001 for treated lenses (p-value = 0.147).

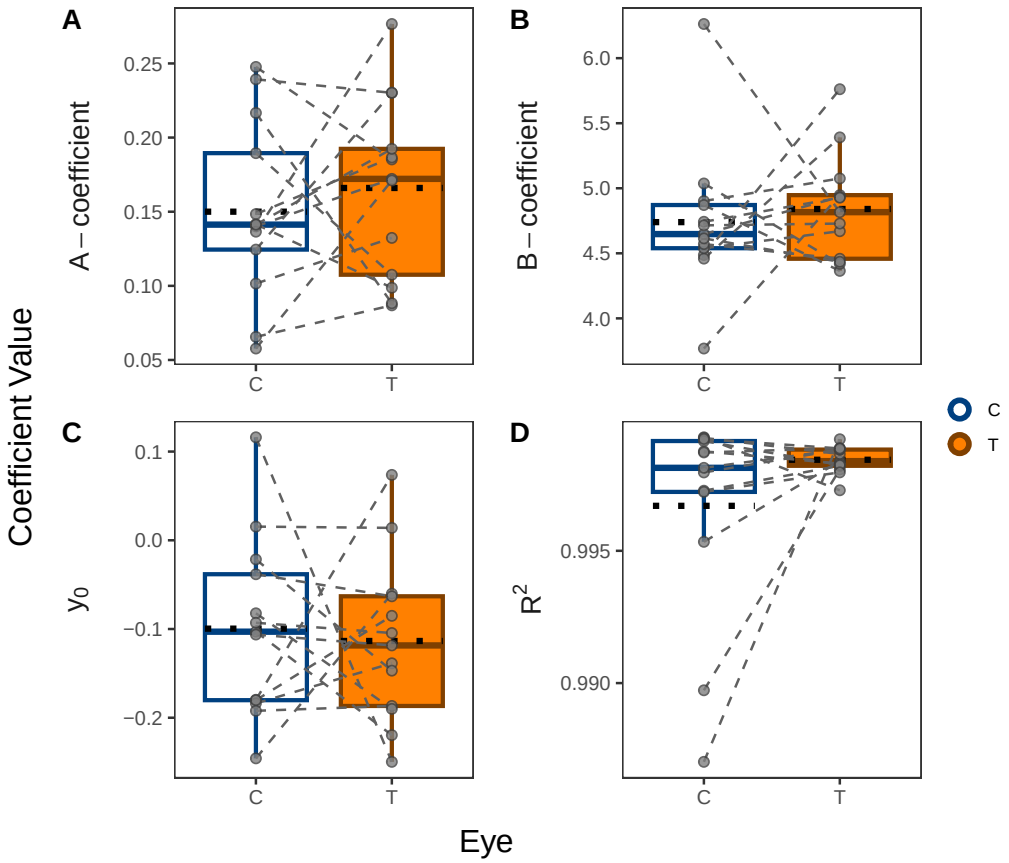


Figure A.12: Boxplots of coefficients of the lenses treated with RN 1734 and Tyrode's solution at room temperature. (A) shows the a-coefficient (p-value = 0.482), (B) shows the b-coefficient (p-value = 0.635), (C) shows y_0 (p-value = 0.750), and (D) shows the R^2 values (p-value = 0.147). C=control; T=treated

.

Parallel experiments targeting the TRPV1 channel at room temperature reveal a similar lack of mechanical responsiveness (Fig. A.13). The TRPV1 agonist capsaicin induced no significant changes in the a-coefficient (0.154 ± 0.071 vs. control: 0.176 ± 0.053; p = 0.444) or y_0 value (p = 0.615; treated: -0.125 ± 0.085 vs. control: -0.108 ± 0.071). R^2 values were 0.999 ± 0.000 for control lenses and 0.999 ± 0.000 for treated lenses (p-value = 0.314).

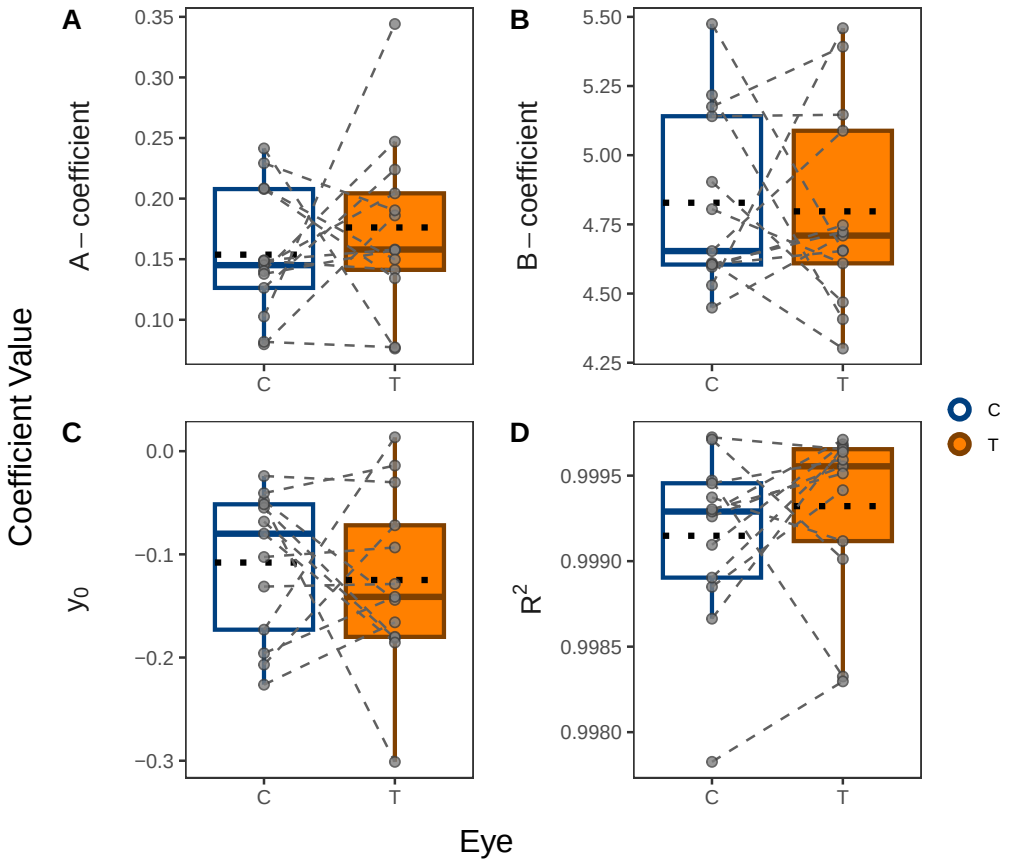


Figure A.13: Boxplots of coefficients of the lenses treated with capsaicin (5 μM) and Tyrode's solution at room temperature. (A) shows the a-coefficient (p-value = 0.444), (B) shows the b-coefficient (p-value = 0.822), (C) shows y_0 (p-value = 0.615), and (D) shows the R^2 values (p-value = 0.314). C=control; T=treated

.

Furthermore, treating lenses with TRPV1 antagonist, AMG 9810, failed to elicit any significant deviations (Fig. A.14) in the a-coefficient (0.152 ± 0.057 vs. control: 0.139 ± 0.037; p = 0.495) or y_0 value (p = 0.541; treated: -0.075 ± 0.068, control: -0.060 ± 0.057). R^2 values were 0.999 ± 0.001 for control lenses and 0.999 ± 0.001 for treated lenses (p-value = 0.769).

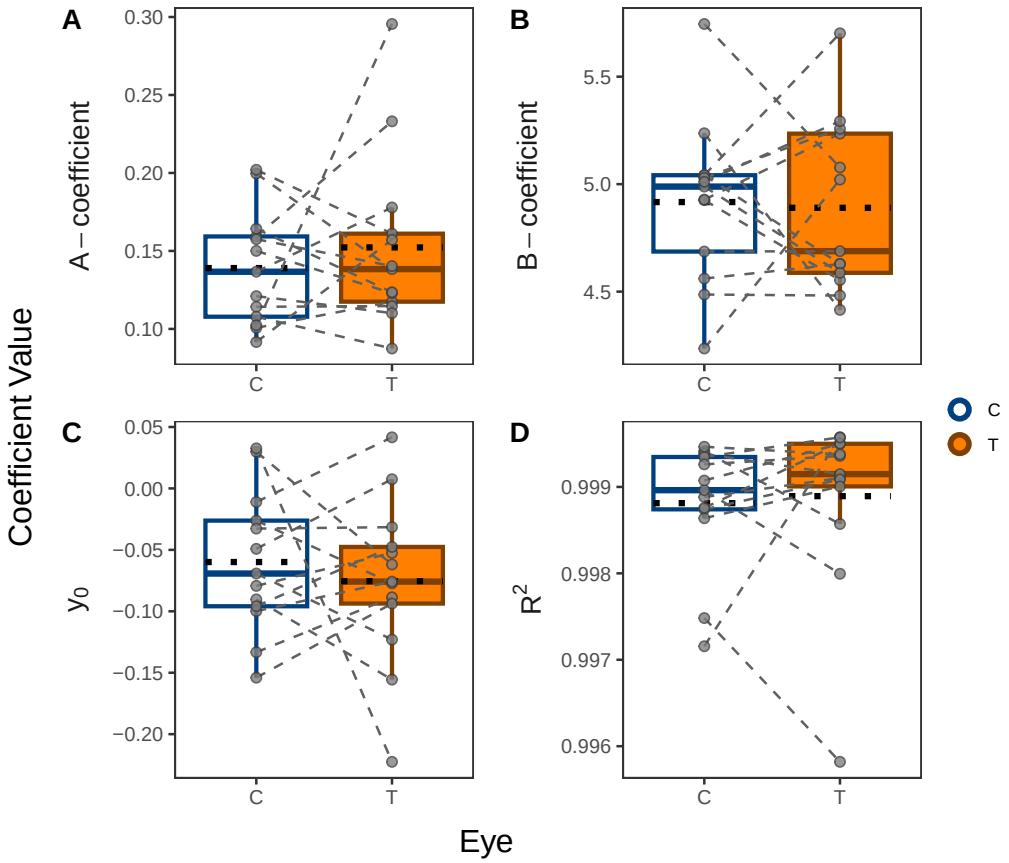


Figure A.14: Boxplots of coefficients of the lenses treated with AMG 9810 (10 μM) and Tyrode's solution at room temperature. (A) shows the a-coefficient (p-value = 0.495), (B) shows the b-coefficient (p-value = 0.847), (C) shows y_0 (p-value = 0.541), and (D) shows the R^2 values (p-value = 0.769). C=control; T=treated

.

When incubated at physiological temperature, TRPV4 activation via GSK1016790A did not change (Fig. A.15) the a-coefficient (0.112 ± 0.011 vs. control: 0.118 ± 0.074; p = 0.693) or the y_0 value (p = 0.403; treated: -0.063 ± 0.059, control: -0.079 ± 0.059). R^2 values were 0.998 ± 0.001 for control lenses and 0.997 ± 0.002 for treated lenses (p-value = 0.307).

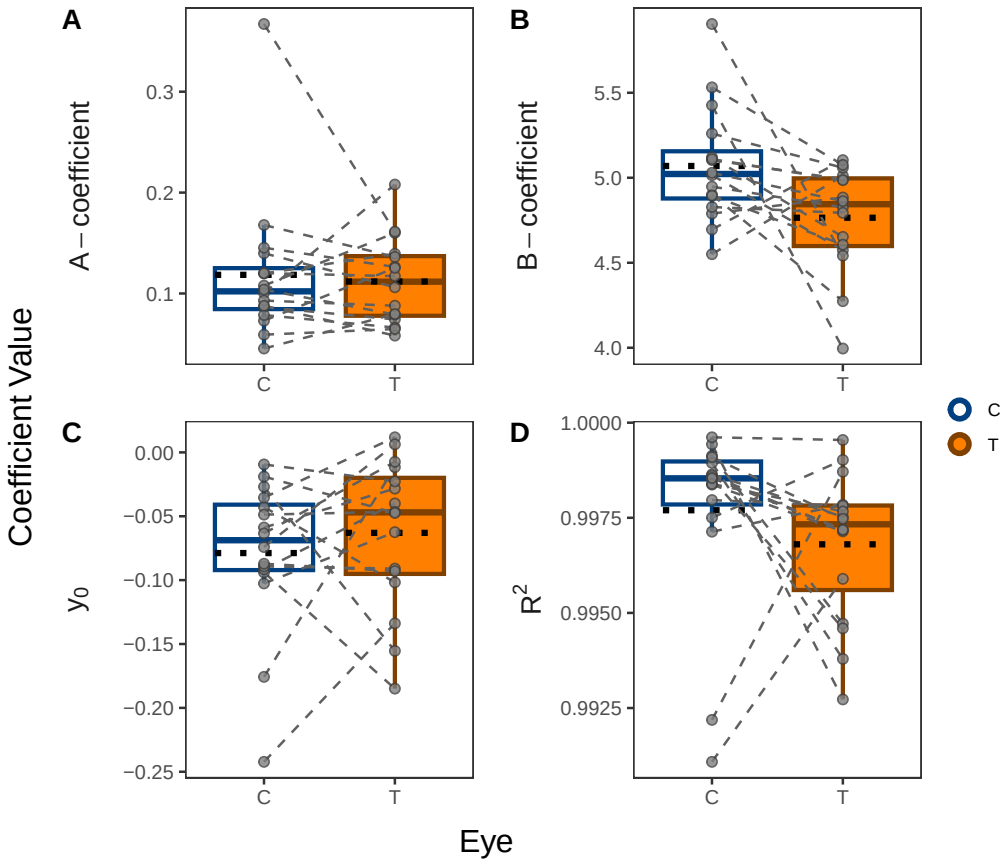


Figure A.15: Boxplots of coefficients of the lenses treated with GSK1016790A (100 nM) and Tyrode's solution at physiological temperature. (A) shows the a-coefficient (p-value = 0.693), (B) shows the b-coefficient (p-value = 0.033), (C) shows y_0 (p-value = 0.403), and (D) shows the R^2 values (p-value = 0.307). C=control; T=treated

.

Conversely, TRPV4 inhibition via the antagonist RN-1734 (Fig. A.16) left the a-coefficient unaffected (0.090 ± 0.027 vs. control: 0.095 ± 0.028; p = 0.552). Similarly, no significant change (p-value = 0.506) was observed in the y_0 value of treated lenses (-0.026 ± 0.058) compared to control lenses (-0.038 ± 0.051). R^2 values were 0.994 ± 0.005 for control lenses and 0.996 ± 0.002 for treated lenses (p-value = 0.144).

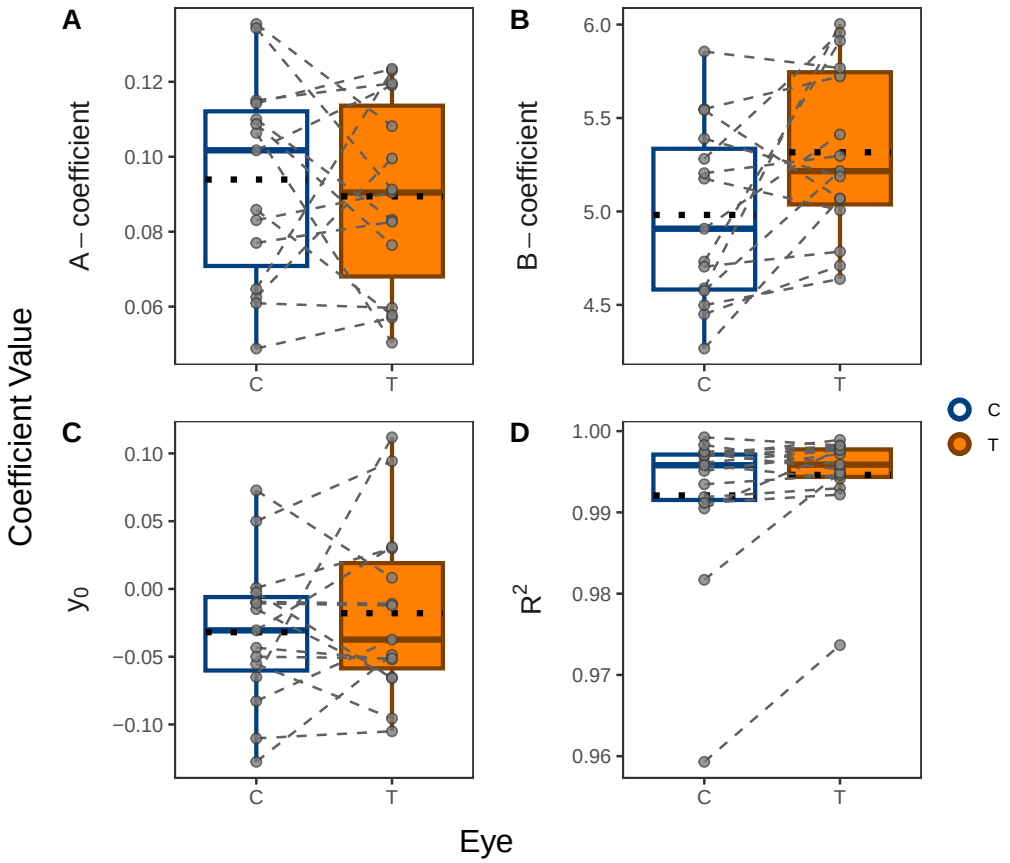


Figure A.16: Boxplots of coefficients of the lenses treated with RN 1734 and Tyrode's solution at physiological temperature. (A) shows the a-coefficient (p-value = 0.552), (B) shows the b-coefficient (p-value = 0.020), (C) shows y_0 (p-value = 0.506), and (D) shows the R^2 values (p-value = 0.144). C=control; T=treated

.

Unlike the changes observed within the TRPV4 channel, the TRPV1 channel remained unresponsive at physiological temperature (Fig. A.17). Exposure to the TRPV1 agonist capsaicin induced no significant changes in the a-coefficient (0.110 ± 0.030 vs. control: 0.121 ± 0.035; p = 0.192) or the y_0 value (p = 0.264; treated: -0.049 ± 0.051, control: -0.068 ± 0.051). R^2 values were 0.998 ± 0.001 for control lenses and 0.997 ± 0.002 for treated lenses (p-value = 0.130).

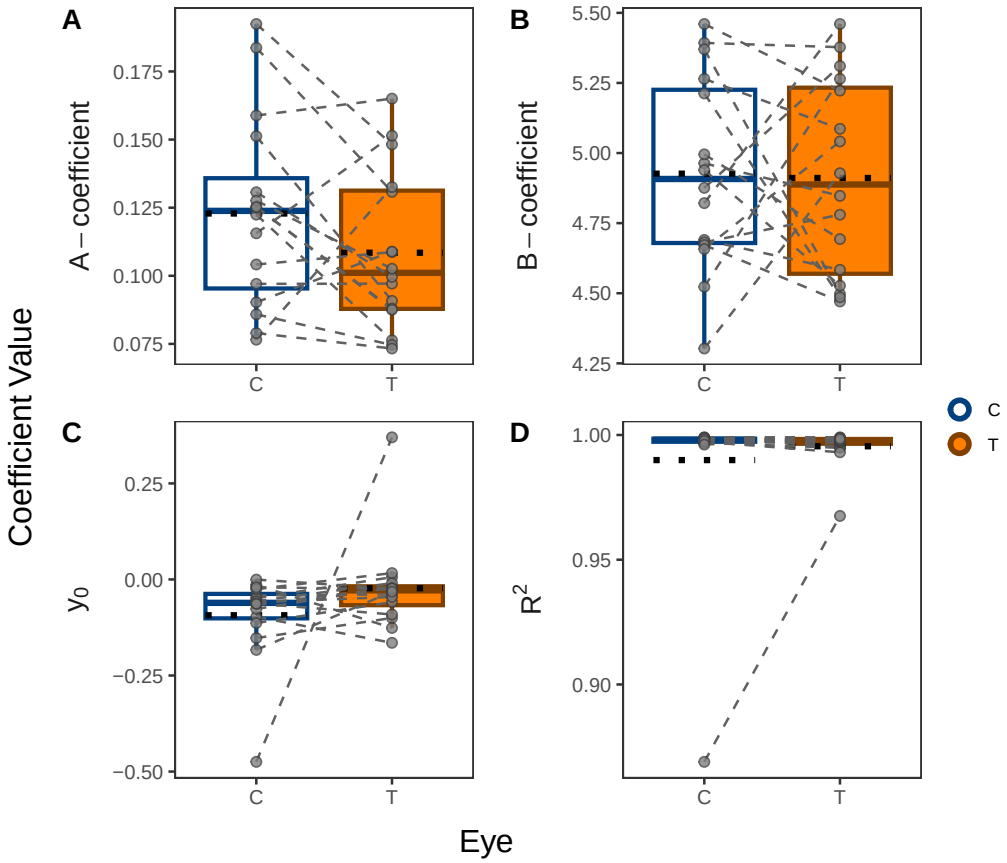


Figure A.17: Boxplots of coefficients of the lenses treated with capsaicin (5 μM) and Tyrode's solution at physiological temperature. (A) shows the a-coefficient (p-value = 0.192), (B) shows the b-coefficient (p-value = 0.576), (C) shows y_0 (p-value = 0.264), and (D) shows the R^2 values (p-value = 0.130). C=control; T=treated

.

Similarly, the treatment with the TRPV1 antagonist AMG 9810 failed to elicit any statistically significant (Fig. A.18) changes (Fig. 4.9) in the a-coefficient (0.113 $\pm$ 0.025 vs. control: 0.122 $\pm$ 0.029; p = 0.214) or the y_0 value (p = 0.884; treated: -0.060 $\pm$ 0.052, control: -0.062 $\pm$ 0.041). R^2 values were 0.998 $\pm$ 0.001 for control lenses and 0.998 $\pm$ 0.003 for treated lenses (p-value = 0.901).

To assess the impact of temperature on lens biomechanics, the compression parameters of paired contralateral lenses were compared under room-temperature and physiological-temperature conditions (Fig. A.19). A paired t-test revealed a statistically significant

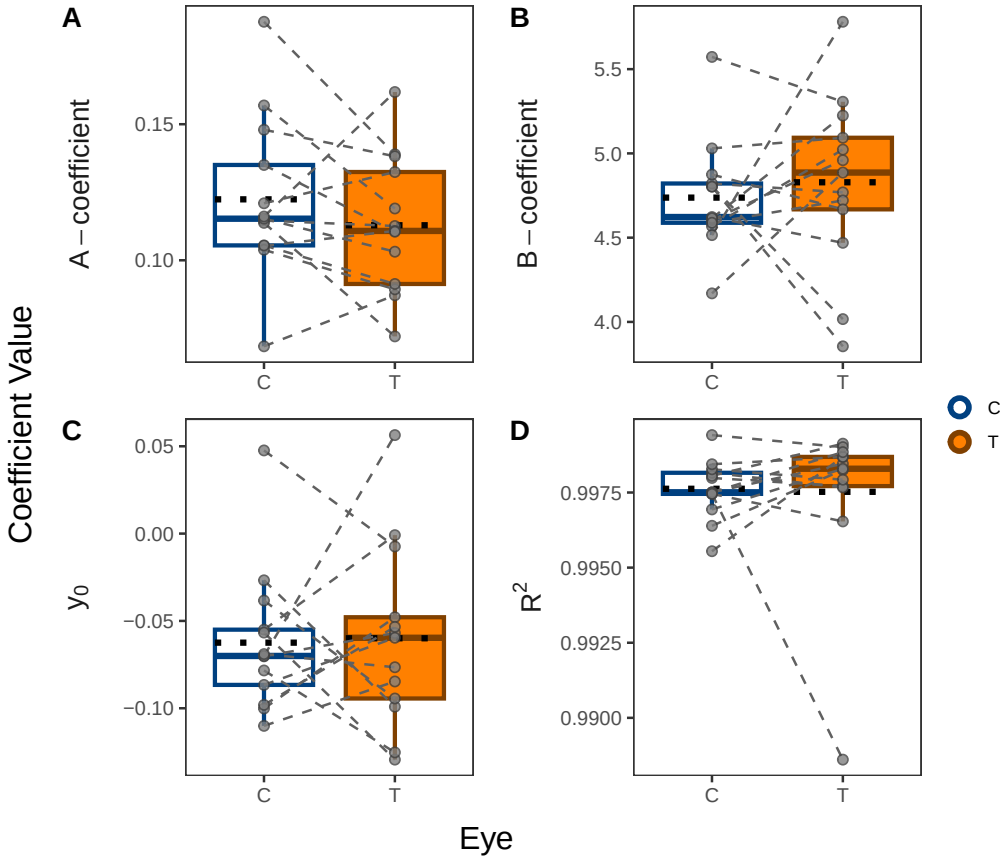


Figure A.18: Boxplots of coefficients of the lenses treated with AMG 9810 (10 μM) and Tyrode's solution at physiological temperature. ((A) shows the a-coefficient (p-value = 0.214), (B) shows the b-coefficient (p-value = 0.597), (C) shows y_0 (p-value = 0.884), and (D) shows the R^2 values (p-value = 0.901). C=control; T=treated

.

reduction in the a-coefficient at physiological temperature (0.078 ± 0.017) compared to room temperature (0.175 ± 0.081; p = 0.001). Similarly, a significant change was observed in the y_0 value (p = 0.000; treated: -0.020 ± 0.045, control: -0.107 ± 0.069). R^2 values were 0.999 ± 0.000 for control lenses and 0.998 ± 0.001 for treated lenses (p-value = 0.000).

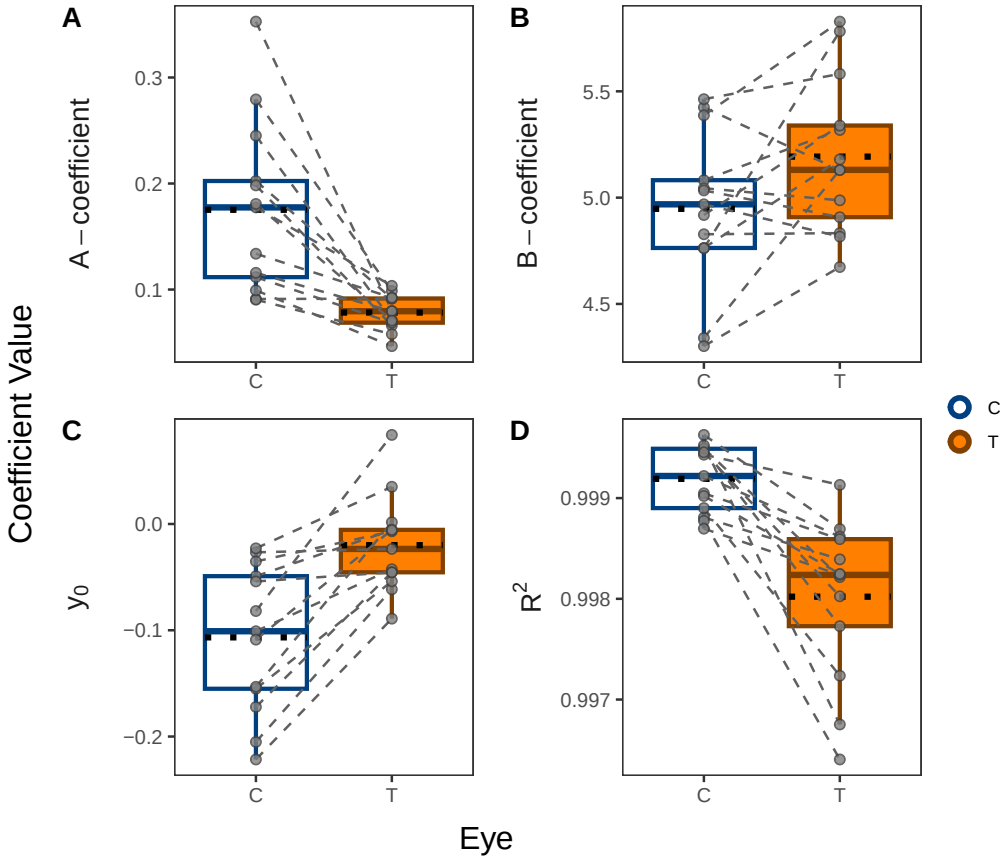


Figure A.19: Boxplots of coefficients of the lenses incubated in Tyrode's solution at room versus physiological temperature. (A) shows the a-coefficient (p-value = 0.001), (B) shows the b-coefficient (p-value = 0.040), (C) shows y_0 (p-value = 0.000), and (D) shows the R^2 values (p-value = 0.000). C=control; T=treated

.

To evaluate the effects of AQP0 activation at physiological temperature, lenses were treated with AQP0 agonist zinc (Fig. A.20). Zinc treatment resulted in a statistically significant increase in the a-coefficient (0.305 ± 0.1087) compared to contralateral controls (0.235 ± 0.076; p = 0.016). Similarly, a significant change was observed in the y_0 value (p

= 0.032; treated: -0.222 ± 0.111, control: -0.166 ± 0.080). R^2 values were 0.999 ± 0.001 for control lenses and 0.999 ± 0.001 for treated lenses (p-value = 0.897).

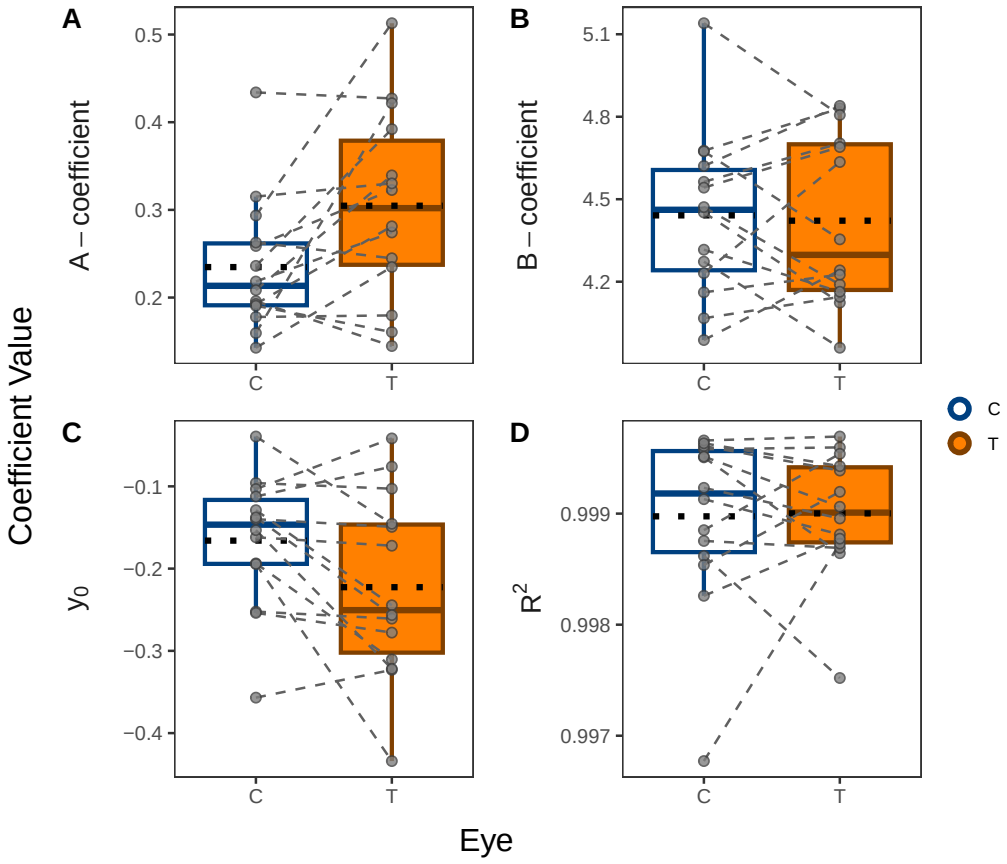


Figure A.20: Boxplots of coefficients of the lenses treated with zinc (80 μg/mL) and Tyrode's solution at physiological temperature. (A) shows the a-coefficient (p-value = 0.016), (B) shows the b-coefficient (p-value = 0.785), (C) shows y_0 (p-value = 0.032), and (D) shows the R^2 values (p-value = 0.897). C=control; T=treated

.

Targeted inhibition of AQP0 using the antagonist did not yield statistically significant alterations in lens biomechanics at physiological temperatures (Fig. A.21). The a-coefficient showed a marginal, non-significant trend toward an increase in HT31-treated lenses (0.290 ± 0.075) relative to controls (0.232 ± 0.068; p = 0.059). However, a significant change was observed in the y_0 value (p = 0.046; treated: -0.216 ± 0.083, control: -0.159 ± 0.079). R^2

values were 0.999 ± 0.000 for control lenses and 0.999 ± 0.000 for treated lenses (p-value = 0.549).

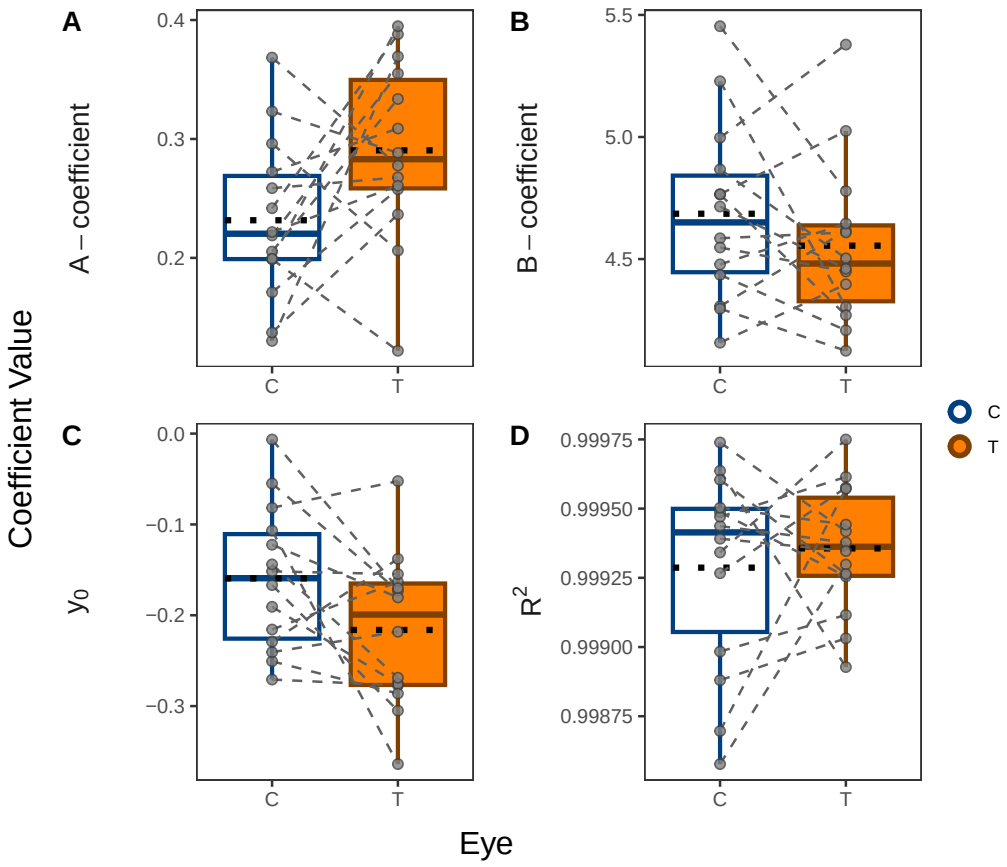


Figure A.21: Boxplots of coefficients of the lenses treated with Ht31 (10 μM) and Tyrode's solution at physiological temperature. (A) shows the a-coefficient (p-value = 0.059), (B) shows the b-coefficient (p-value = 0.234), (C) shows y_0 (p-value = 0.046), and (D) shows the R^2 values (p-value = 0.549). C=control; T=treated

.

Stimulation of NKA pump activity with insulin did not significantly modify any of the evaluated biomechanical properties at physiological temperature (Fig. A.22). The a-coefficient for insulin-treated lenses was 0.247 ± 0.313, which did not differ significantly from vehicle-treated controls (0.375 ± 0.452; p = 0.414; p = 0.150). Similarly, no significant change was observed in the y_0 value (p = 0.112; treated: -0.176 ± 0.300, control: -0.303 ±

0.429). R^2 values were 0.995 ± 0.008 for control lenses and 0.996 ± 0.004 for treated lenses (p-value = 0.288).

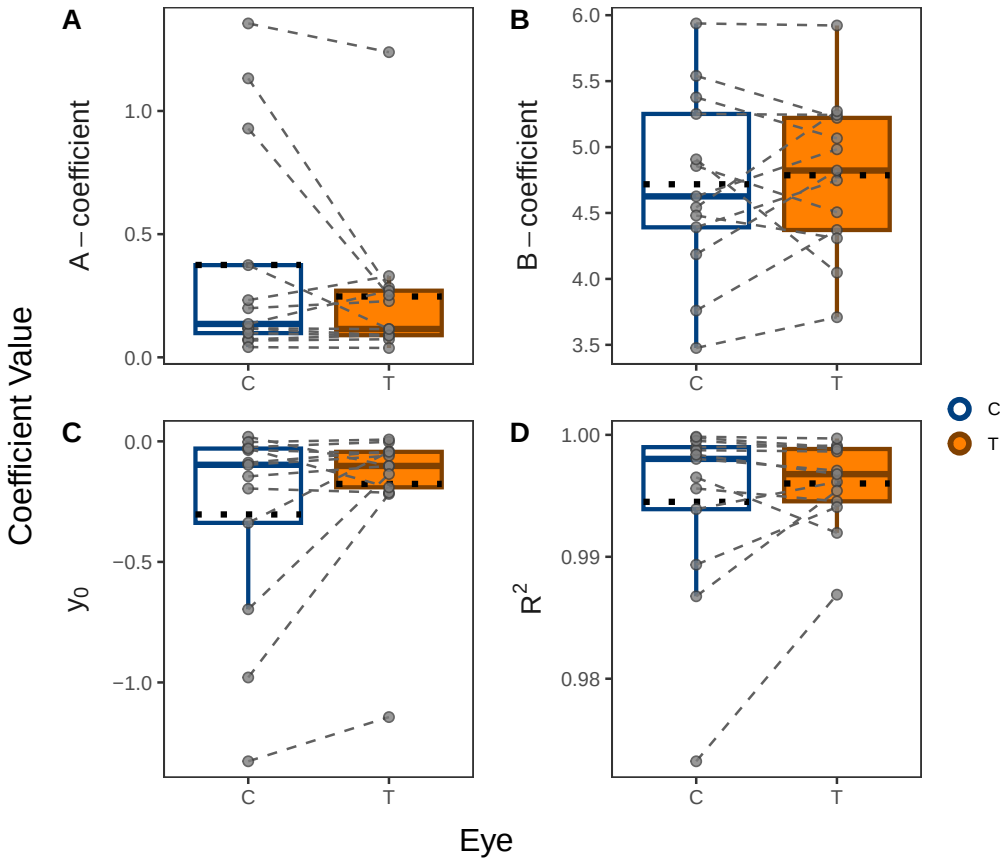


Figure A.22: Boxplots of coefficients of the lenses treated with insulin and Tyrode's solution at physiological temperature. (A) shows the a-coefficient (p-value = 0.150), (B) shows the b-coefficient (p-value = 0.610), (C) shows y_0 (p-value = 0.112), and (D) shows the R^2 values (p-value = 0.288). C=control; T=treated

.

Inhibition of the NKA pump using ouabain similarly failed to induce significant biomechanical changes at physiological temperature (Fig. A.23). The a-coefficient remained the same between the ouabain-treated and control lenses (0.117 ± 0.030 vs. 0.117 ± 0.035, respectively; p = 0.997). Similarly, no significant change was observed in the y_0 value (p = 0.183; treated: -0.119 ± 0.060, control: -0.083 ± 0.067). R^2 values were 0.994 ± 0.005 for control lenses and 0.993 ± 0.005 for treated lenses (p-value = 0.455).

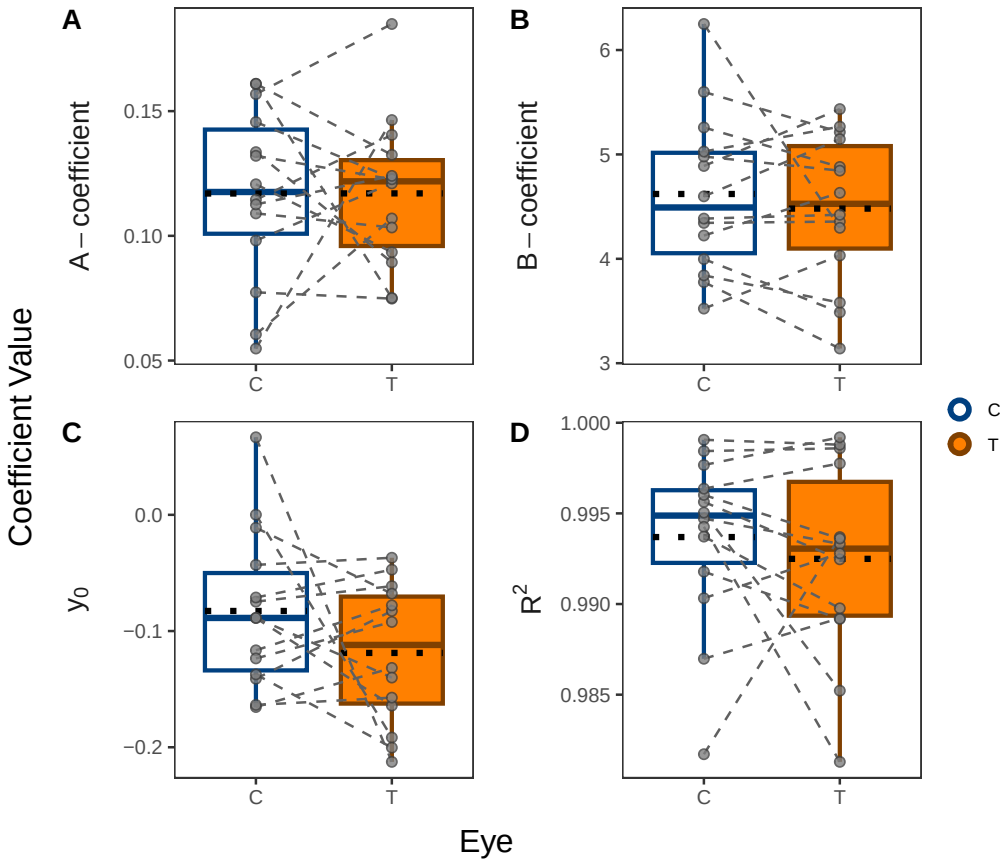


Figure A.23: Boxplots of coefficients of the lenses treated with ouabain and Tyrode's solution at physiological temperature. (A) shows the a-coefficient (p-value = 0.997), (B) shows the b-coefficient (p-value = 0.442), (C) shows y_0 (p-value = 0.183), and (D) shows the R^2 values (p-value = 0.455). C=control; T=treated

.

A.3 Force decay slope during the 5-second hold phase

During the 5-second hold phase under constant displacement, the negative force slope reflects the lens's intrinsic viscoelastic properties. A steeper negative slope indicates that the lens dissipates internal stress more rapidly through viscoelastic relaxation (Table A.1).

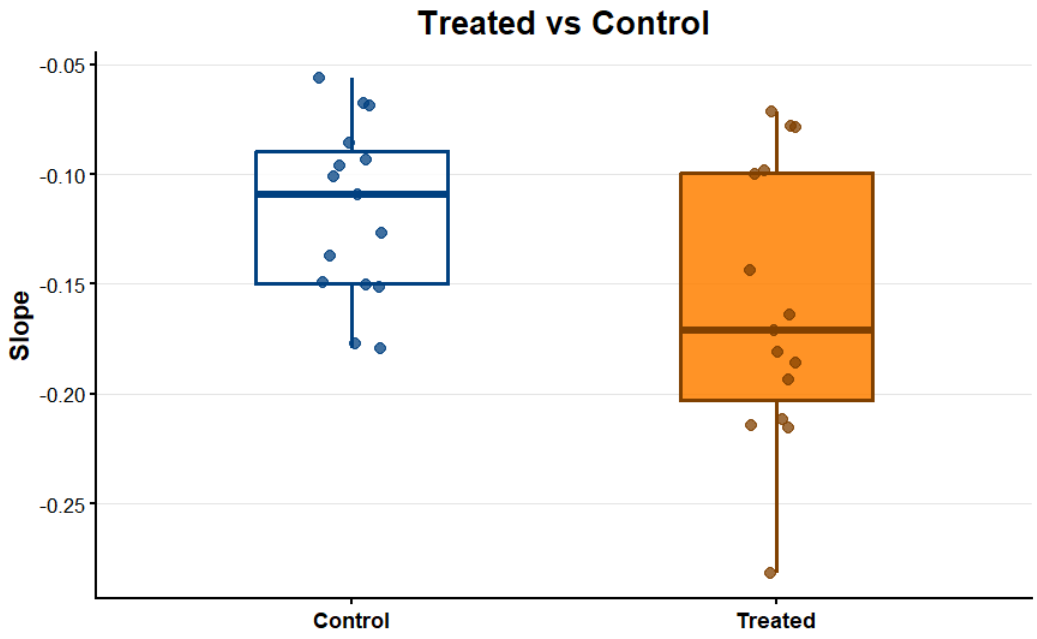


Figure A.24: Boxplots of the force decay during the 5-second hold phase under constant displacement for lenses treated with RN 1734 and Tyrode's solution at physiological temperature. Lenses treated with RN 1734 exhibited a significant increase in the slope magnitude compared to control lenses (p-value = 0.037). C=control; T=treated

.

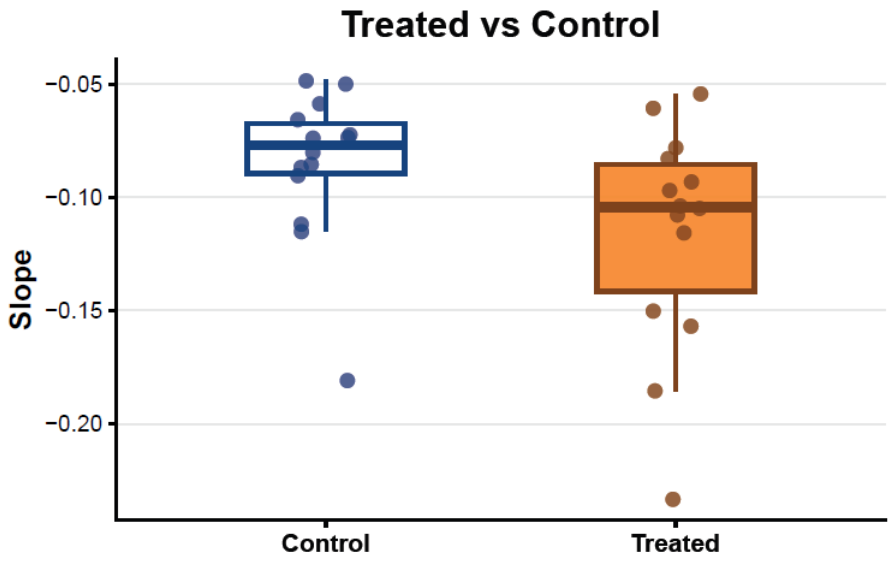


Figure A.25: Boxplots of the force decay during the 5-second hold phase under constant displacement for lenses treated with a combination of zinc and insulin and Tyrode's solution at room temperature. Lenses treated with the combination of zinc and insulin exhibited a significant increase in the slope magnitude compared to control lenses (p-value = 0.049). C=control; T=treated

.

Table A.1: Summary of the hold-phase relaxation slopes under room and physiological temperatures (↑ indicates increase, ↓ indicates decrease, and = indicates no change)

Channel/target	**Temp**	**Modulator**	**Slope of hold**	***p*-value**
Aquaporin 0 (AQP0)	20–22 °C	Zinc	=	0.318
		Ht31	=	0.114
Sodium–potassium ATPase pump (NKA)	20–22 °C	Insulin	=	0.227
		Ouabain	=	0.399
Transient receptor potential vanilloid 1 (TRPV1)	20–22 °C	Capsaicin	=	0.146
		AMG 9810	=	0.370
Transient receptor potential vanilloid 4 (TRPV4)	20–22 °C	GSK1016790A	=	0.058
		RN 1734	=	0.524
AQP0 + NKA	20–22 °C	Zinc + insulin	↑	0.049
		Zinc + ouabain vs. ouabain	=	0.528
		Zinc + ouabain vs. zinc	=	0.053
TRPV1	36–37 °C	Capsaicin	=	0.134
		AMG 9810	=	0.643
TRPV4	36–37 °C	GSK1016790A	=	0.524
		RN 1734	↑	0.037
AQP0	36–37 °C	Zinc	=	0.172
		Ht31	=	0.228
NKA	36–37 °C	Insulin	=	0.477
		Ouabain	=	0.426